
FINAL TECHNICAL REPORT

DOE AWARD NUMBER: DE-FC07-97ID13537

AWARDEE: AUDREY ZINK-SHARP, VIRGINIA TECH DEPARTMENT OF WOOD SCIENCE AND FOREST PRODUCTS, BLACKSBURG, VA 24060

PROJECT TITLE: MOISTURE DISTRIBUTION AND FLOW DURING DRYING OF WOOD AND FIBER

PROJECT DIRECTOR: AUDREY ZINK-SHARP, VIRGINIA TECH, BLACKSBURG, VA

TEAM MEMBERS: ROBERT B. HANNA, STATE UNIVERSITY OF NEW YORK, SYRACUSE, NY

DISTRUBITION LIMITATIONS: NONE

EXECUTIVE SUMMARY

New understanding, theories, and techniques for moisture flow and distribution were developed in this research on wood and wood fiber.

Improved understanding of the mechanisms of flake drying has been provided. Observations of flake drying and drying rate curves revealed that rate of moisture loss consisted of two falling rate periods and no constant rate drying period was observed. Convective heat transfer controls the first period, and bound water diffusion controls the second period.

Influence of lower drying temperatures on bending properties of wood flakes was investigated. Drying temperature was found to have a significant influence on bending stiffness and strength.

A worksheet for calculation of the energy required to dry a single strandboard flake was developed but has not been tested in an industrial setting yet.

A more complete understanding of anisotropic transverse shrinkage of wood is proposed based on test results and statistical analysis. A simplified model of a wood cell's cross-section was drawn for calculating differential transverse shrinkage. The model utilizes cell wall thickness and microfibrillar packing density and orientation. In spite of some phenomena of cell wall structure not yet understood completely, the results might explain anisotropic transverse shrinkage to a major extent.

Boundary layer theory was found useful for evaluating external moisture resistance during drying. Simulated moisture gradients were quite comparable to the actual gradients in dried wood. A mathematical procedure for determining diffusion and surface emission coefficients was also developed. Thermal conductivity models of wood derived from its anatomical structure were created and tested against experimental values. Model estimations provide insights into changes in heat transfer parameters during drying.

Two new techniques for measuring moisture gradients created in wood during drying were developed. A new technique that utilizes optical properties of cobalt chloride was developed for nondestructive determination of surface moisture content.

Fundamental new understanding of drying characteristics in wood and fiber has been provided that can be used by researchers to improve drying of wood and fiber. The three techniques for measuring moisture content and gradients provided in this study are efficient, practical, and economical - easy to apply by industry and researchers. An energy consumption worksheet is provided as a first step toward reducing energy consumed during drying of lumber and strandboard flakes. However, it will need additional verification and testing.

COMPARISON OF ACCOMPLISHMENTS WITH OBJECTIVES

Objectives of this project were to determine flow rate and direction, location, concentration, and gradient character of moisture in solid wood, OSB flakes, and wood fiber using four experimental approaches and then apply this understanding to increase the efficiency and quality of industrial drying of lumber, wafers, and wood fiber.

Flow rate and direction of OSB flakes as influenced by lower drying temperatures was investigated. The influence of lower flake drying temperatures on final products has not been determined in industrial drying. Location, concentration, and gradient character of moisture in solid wood was determined using the new techniques, models, and theories as developed in this study. However, quantification of moisture distribution has eluded analysis of MRI scans so far. Heat and mass transfer models provided additional results not originally planned. The models have yet to be applied to industrial drying of lumber and wafers. Drying characteristics of wood fiber was not satisfactorily determined due to unexpected equipment limitations and unexplainable behavior. An energy consumption worksheet was developed but has not been tested in an industrial setting. Basically, fundamental information has been discovered but not applied to industrial drying as yet.

Specific Accomplishments include the following:

Summary

1 M.S. Thesis, 3 PhD dissertations, and 7 journal articles were completed.

Two new techniques for measuring moisture content were contributed and are described in the following manuscript summaries.

Two new models for heat and mass transfer in wood were designed as described below.

Research results are presented in seven journal manuscripts, two published, two accepted, and three submitted.

A worksheet for calculation of the energy required to dry a single OSB flake is appended to this report.

Research in developing the colorimetric technique was awarded 1st Place in the 2001 Wood Award competition. This award is given annually by the Forest Products Society for outstanding graduate student research in the field of forest products research.

Details

MS thesis:

"Moisture Gradient Measurement during Kiln Drying of Red Oak", Hong-mei Gu, September, 1997, Virginia Tech, Blacksburg, VA

PhD dissertations completed:

"Evaluation of Mass Transfer in Wood Utilizing a Colorimetric Technique", Hwanmyeong Yeo, Spring 2001, State University of New York, Syracuse, NY

"Structure-Based, Two-Dimensional Anisotropic, Transient Heat Conduction Model for Wood," Hongmei Gu, August, 2001, Virginia Tech, Blacksburg, VA

"Mechanism of Flake Drying and its Correlation to Quality", Edgar Deomano, July 2001, Virginia Tech, Blacksburg, VA

Seven journal manuscripts have been prepared, two have been published, two have been accepted, and three have been submitted. Summaries of these manuscripts follows, and full papers are appended to this report.

MEASUREMENT OF MOISTURE GRADIENTS IN WOOD

Forest Products Journal 49(4):77-86

Gu, H.-M. and A. Zink-Sharp

Summary

Moisture gradients in red oak were measured through four different techniques--bandsaw slicing, Forstner bit layering, flaking, and razor blade slicing. The first two techniques were found in the literature. The last two were developed in this study. The results obtained with these four techniques on five different drying days were compared, and it was found that the two newly developed techniques could get moisture gradients that were less affected by cutting and environmental conditions. Using the two new techniques, an optimum slice or flake thickness was determined for wood products industries and research studies.

ROLE OF CELL WALL STRUCTURE

IN TRANSVERSE DIFFERENTIAL SHRINKAGE OF WOOD

Holz als Roh- und Werkstoff 56(6):436-442
Hongmei Gu, Audrey Zink-Sharp, Jürgen Sell

Summary

The cell wall thickness under dry and wet conditions and the cellulose fibril arrangement on transverse fracture surface of the S2 layer of the tangential and radial walls were examined from SEM images and ESEM images, respectively. A hypothesis for explaining the anisotropic transverse shrinkage of wood was proposed based on the test results and statistical analysis. A simplified model of a tracheid's cross-section was drawn for calculating the differential transverse shrinkage. Results of this study indicate that the radial cell wall of Scots pine latewood is about 25 percent thicker than the tangential wall. Earlywood does not show such a difference. Furthermore, there is a significant tendency of a preferential orientation (i.e. packing density) of the fibrils on the tangential and radial walls in the overall tangential direction. Despite some phenomena of the cell wall structure not yet understood clearly, this might explain the anisotropic transverse shrinkage of wood to a major extent.

MASS TRANSFER IN WOOD EVALUATED WITH A COLORIMETRIC TECHNIQUE AND NUMERICAL ANALYSIS

accepted for publication in Wood and Fiber Science
Hwanmyeong Yeo, William B. Smith, and Robert B. Hanna

Summary

A colorimetric Co Cl_2 treated wood technique was used for determining surface moisture content of wood nondestructively and continuously during unsteady state desorption conditions. Utilizing these surface moisture data, diffusion and surface emission coefficients have been determined simultaneously and continuously during drying. The conversion method which has been developed to facilitate making comparison between mass transfer coefficients in this study has proven that the boundary layer theory is useful for evaluating the external moisture resistance during wood drying. The moisture profiles simulated by the finite difference method were quite comparable to the actual moisture profiles in dried wood, which substantiates the high credibility of using the colorimetric technique for determining surface moisture content and a mathematical procedure for determining the diffusion and surface emission coefficient.

DETERMINATION OF SURFACE MOISTURE CONTENT OF WOOD UTILIZING A COLORIMETRIC TECHNIQUE

accepted for publication in Wood and Fiber Science

Hwanmyeong Yeo, William B. Smith, and Robert B. Hanna

Summary

Optical properties of cobalt chloride (Co Cl_2) hydrate, whose color changes with surrounding humidity, were used to develop a colorimetric technique for determining surface moisture content of wood nondestructively. The colorimetric Co Cl_2 treated wood technique for determining surface moisture content through color degree change in CIE $L^*a^*b^*$ color space has been experimentally verified with high resolution.

BENDING PROPERTIES OF WOOD FLAKES

submitted to Wood and Fiber Science
Edgar C. Deomano and Audrey Zink-Sharp

Summary

This research focuses on experimental investigations of the bending properties of wood flakes. Modulus of elasticity (MOE), modulus of rupture (MOR), and strength at proportional limit (SPL) of flakes were measured based on Methods of Testing Small Clear Specimens of Timber (ASTM D143-94) using a miniature material tester. Effect of species, cutting direction, and temperature were evaluated. Bending properties were found to vary between and within the three species. Southern yellow pine had the lowest bending stiffness and strength followed by sweetgum while yellow-poplar had the highest bending properties. Radially-cut specimens were found to have lower MOE, MOR, and SPL than tangentially-cut specimens. Drying temperature was also found to have a significant effect on bending stiffness and strength. A decreasing trend in bending properties was observed when drying temperature was increased.

MECHANISM OF FLAKE DRYING

submitted to Wood and Fiber Science
Edgar C. Deomano and Audrey Zink-Sharp

Summary

This research focuses on experimental investigations of the drying properties of wood flakes. Three species (southern yellow pine, sweetgum, and yellow-poplar) were tested. Experiments on flake drying and effect of flake properties (cutting direction and dimension) and an external factor (temperature) were used to evaluate the flake drying process. Observation on drying and drying rate curves revealed that the rate of moisture loss consists of two falling rate periods; no constant rate drying period was observed. The first falling rate drying period is controlled by convective heat transfer. Bound water diffusion controls the second falling rate drying period. Species, cutting direction, dimension, and temperature were found to have a significant effect on drying rate of wood flakes.

GEOMETRIC MODELING OF WOOD TRANSVERSE THERMAL CONDUCTIVITY FOR SOFTWOOD SPECIES

submitted to Wood Science and Technology
Hongmei Gu and Audrey Zink-Sharp

Summary

Thermal conductivity of wood is the important parameter for measuring heat transfer rate in wood. The accuracy and consistency for the values of thermal conductivity of wood with a wide range of moisture content are required for the drying model development and industry operations. Wood material properties are structure dependent. Thermal conductivity of wood derived from the anatomical structure was proposed and examined in this research for softwood species. Geometric models for predicting thermal conductivity in radial and tangential directions were developed. The models were generated from wood anatomical structure observation and measurements. Structure observation was made under the Scanning Electron Microscope and Environmental Scanning Electron Microscope and measurements were preformed with the help of image analysis. Modeling the effective thermal conductivity in radial and tangential direction is helpful to understand the heat transfer mechanism in the two directions and predict the values in a wide range when the practical experiments for obtaining those values are hard to make.

Model estimations provide insights for changes of the heat transfer parameters -- thermal conductivity, with the independent variables used in the model. Theoretical estimations for the radial thermal conductivity of softwood species is greater than the tangential thermal conductivity for moisture content below FSP due to the structure difference in the two directions. A linear relationship was found between moisture content (in the range of 0%-30%) and the radial thermal conductivity, but a less significant linear relationship is shown between moisture content and the tangential thermal conductivity. Both radial and tangential thermal conductivity are increasing with the increase of latewood percentage in wood. When MC is above FSP with free water appears in wood samples, tangential and radial thermal conductivity increase dramatically with moisture content changes. No significant difference was found between the radial and tangential thermal conductivity. The geometric difference in the two directions has little affect on the resulted thermal conductivities when free water takes part of the cell lumen.

SUMMARY OF PROJECT ACTIVITIES

1. Approach Changes

Research on moisture distribution and gradient character in wood fiber using the confocal scanning laser microscope (CSLM) was attempted at Virginia Tech rather than at SUNY-ESF, Syracuse. Examination of drying behavior of individual wood fibers was conducted in the environmental scanning electron microscope (ESEM) at SUNY-ESF, Syracuse rather than Virginia Tech. Neither approach provided the information expected from initial pilot studies. Wood fiber proved very difficult to work with in the microscopes for a variety of reasons from the simple handling of a very small, delicate wood cell to obscure microscope chamber conditions causing freeze drying rather than controlled drying.

Magnetic resonance imaging was conducted at the local hospital imaging facility rather than at the private company originally contracted. Technical understanding of the underlying principals of MRI and their applications to wood was superior at the private company and this lack lead to incomplete understanding and conclusion of this component of the research. While a disappointment certainly, it does not leave a significant gap in obtaining original objectives.

Drying defects and anisotropic shrinkage in small wood specimens were examined in a field emission scanning electron microscope (SEM) in cooperation with the Swiss Federal Lab for Materials Testing and Research, in Dubendorf, Switzerland, instead of with a conventional SEM. The field emission microscope offered the possibility of examination at low beam voltage which produces less specimen damage. This approach change lead to much better visualization and understanding of anisotropic shrinkage – long an unexplained phenomenon in wood.

Low temperature drying of oriented strandboard (OSB) flakes took place at 150, 200, and 250 deg. C instead of 100, 200, and 300 due to equipment limitations. These temperatures are all much lower than the current rotary dryers and not very practical in an industrial setting. They represent a first attempt at approaching the concept and determining significance of the variables.

Atomic force microscopy did not prove to be effective for measurement of surface forces associated with drying and was not pursued. Surfaces forces associated with drying were not determined but surface emission coefficients were determined using mathematical theory instead.

Mill trials at Georgia-Pacific, Skippers, VA, were not warranted and did not take place. Dry kiln experimental runs at Weyerhaeuser, Tacoma, WA, also were not warranted and did not take place. Application of laboratory research with industrial colleagues is a very important component and should be pursued vigorously in future projects.

2. Performance Variances and Problems

Performance variances

Early delays were caused by a faulty dry kiln at Virginia Tech, the unexpected late arrival of one of the student researchers, and the need to coordinate with the hospital's imaging schedule.

Further delays and complications were caused by unexpected and, as yet, unexplainable behavior of individual wood fibers in the environmental scanning electron microscope.

A numerical model of the relationship between the MRI scan brightness and moisture content or moisture amount has not been found.

The energy consumption worksheet was completed in year 4 rather than year 3.

Project spanned 4 years rather than 3.

Problems

Correlation of MRI brightness with moisture distribution, measurement of S_2 cell wall microfibril angle with the confocal laser scanning microscope, and characterizing wood fiber drying in the ESEM are still illusive and all relate to unexpected equipment limitations and problems with handling individual wood fibers.

Products Developed and Technology Transfer Activities

No products, patent applications, or licensing agreements were developed.

Technology transfer is through journal publications as follows:

Measurement of Moisture Gradients in Wood. 1999. Forest Products Journal 49(4):77-86.

Hypothesis on the Role of Cell Wall Structure in Transverse Differential Shrinkage of Wood. 2001. Holz als Roh- und Werkstoff 56(6):436-442.

Mass Transfer in Wood Evaluated with a Colorimetric Technique and Numerical Analysis.
Accepted by Wood and Fiber Science

Determination of surface moisture content of wood utilizing a colorimetric technique. Accepted by Wood and Fiber Science

Bending properties of wood flakes. Submitted to Wood and Fiber Science

Mechanism of flake drying. Submitted to Wood and Fiber Science

Geometric modeling of wood transverse thermal conductivity for softwood species. In revision, to be submitted to Holzforschung.

Description of Attachments

1. Manuscript accepted by *Wood and Fiber Science* "Mass transfer in wood evaluated with a colorimetric technique and numerical analysis"
2. Manuscript accepted by *Wood and Fiber Science* "Determination of surface moisture content of wood utilizing a colorimetric technique"
3. Manuscript submitted to *Wood and Fiber Science* "Bending properties of wood flakes"
4. Manuscript submitted to *Wood and Fiber Science* "Mechanism of flake drying"
5. Manuscript submitted to *Wood Science and Technology* "Geometric modeling of wood transverse thermal conductivity for softwood species"
6. Energy Worksheet

Attachment 1

**MASS TRANSFER IN WOOD EVALUATED WITH
A COLORIMETRIC TECHNIQUE AND NUMERICAL ANALYSIS***

Hwanmyeong Yeo

Research Associate

William B. Smith

Professor

Faculty of Wood Products Engineering

and

Robert B. Hanna

Director

Center for Ultrastructure Studies

College of Environmental Science and Forestry

State University of New York, Syracuse, NY 13210

* This paper presents research results for which Dr. Yeo received the Forest Products Society Wood Award, First Place 2001. The authors wish to acknowledge the financial support of U.S. Department of Energy (DOE) project -DE-FC07-97ID13537- Moisture Distribution and Flow During Drying of Wood and Fiber.

ABSTRACT

A colorimetric CoCl_2 treated wood technique was used for determining surface moisture content of wood nondestructively and continuously during unsteady state desorption conditions. Utilizing these surface moisture data, diffusion and surface emission coefficients have been determined simultaneously and continuously during drying. The conversion method, which has been developed to facilitate making comparison between mass transfer coefficients in this study, has proven that the boundary layer theory is useful for evaluating the external moisture resistance during wood drying. The moisture profiles simulated by finite difference method were quite comparable to the actual moisture profiles in real dried wood, which substantiates the high credibility of using the colorimetric technique for determining surface moisture content and mathematical procedure for determining the diffusion and surface emission coefficient.

KEYWORDS

Mass transfer, diffusion, surface emission, boundary layer theory, finite difference method, colorimetric technique

INTRODUCTION

Moisture movement in wood during drying is constrained by two resistances. The internal resistance due to wood itself can be described by the diffusion coefficient. Second is an external resistance to moisture leaving the wood surface and being transferred to the ambient drying air. This external resistance can be described by the mass transfer coefficient. Solutions of Fick's law and boundary layer theory have been widely applied to determine the diffusion and mass transfer coefficients, respectively (Crank 1975, Geankoplis 1993). However, a fully reliable method to determine these coefficients for a hygroscopic material simultaneously and continuously over the entire moisture content range has not yet been developed. A primary reason is the difficulty of determining wood surface moisture concentration nondestructively and continuously in unsteady state drying conditions. This difficulty results in most mathematical approaches for determining the diffusion coefficient using an improper assumption that the surface moisture concentration is at equilibrium with the surrounding air as soon as the drying process starts. Due to this difficulty theoretically calculated mass transfer coefficients have not been well proved by experimental results (Siau 1995).

Accurate and continuous measurement of surface moisture concentration in wood in unsteady state drying conditions can increase credibility of methods for determining the coefficients. In this study, color change on wood surfaces treated with CoCl_2 according to humidity has been used for determining surface moisture content (SMC) nondestructively and continuously during drying. Utilizing surface moisture data, diffusion and mass transfer coefficients have been determined. Also, using these coefficients and numerical analysis with the finite difference method, a computer simulation program was developed to predict 2-dimensional moisture profiles in wood during drying.

MATERIALS AND METHODS

Determination of diffusion and mass transfer coefficients

Completely water soaked cubes of hard maple (*Acer saccharum* Marsh), red oak (*Quercus rubra* L.), and southern pine (*Pinus* spp.), with 20mm longitudinal, radial and tangential dimension

were manufactured. Four side walls of each cubic specimen were wrapped with rubber tape (Magic Wrap, Glasgow Mfg. Ltd.), leaving open the two opposite surfaces of interest, to provide one dimensional moisture flow for drying. Six replicates, to determine the mass transfer coefficient based on moisture concentration at wood surface, also called the surface emission coefficient, and the diffusion coefficient in each orientation, longitudinal, radial, and tangential, were prepared.

SURFACE AND AVERAGE MOISTURE CONTENT

Using the recently developed colorimetric technique (Yeo 2001) and oven drying, surface moisture content (SMC) and average moisture content (AMC) changes were determined, respectively, during drying at 25%RH and both 30 and 50°C. Saturated CoCl₂ solution, approximately 5μL, was dropped on the exposed surface area of three of those six replicates for each orientation, and spread with the tip of a dispensing micropipette. The surface spectral reflectance was measured with a portable spectrophotometer (Microflash 200d, manufactured by DataColor International) during drying at 25%RH and both 30 and 50°C, and then CIE L*a*b* color values were calculated on the basis of CIE (Commission Internationale de l'Eclairage) standards (CIE 1986). Using surface color differences (dE_{mc-eq}) between moist wood and wood equilibrated at 25%RH, surface moisture content of each species were determined.

$$dE_{mc-eq} = \sqrt{(L^*_{mc} - L^*_{eq})^2 + (a^*_{mc} - a^*_{eq})^2 + (b^*_{mc} - b^*_{eq})^2} \quad (1)$$

where, L^*_{mc} , a^*_{mc} , b^*_{mc} : L*, a*, and b* values on the CoCl₂ treated surfaces equilibrated at any %RH

L^*_{eq} , a^*_{eq} , b^*_{eq} : L*, a*, and b* values on the CoCl₂ treated surfaces equilibrated at 25%RH

Also, three untreated specimens were used as controls to prove the drying rate of treated wood to be similar to that of untreated wood.

SPECIFIC GRAVITY

Specific gravities of moist wood (G_{MC}) were not measured directly during drying because of the excessive time required to make many measurements. This likely would have decreased the efficiency of the method for determining the diffusion and surface emission coefficients. Instead of direct measurement, G_{MC} was approximated by linear interpolation between oven-dry specific gravity and green specific gravity.

DIFFUSION COEFFICIENT

A new analytical solution was derived to determine the diffusion coefficient when surface moisture contents were varied. The experimentally measured surface moisture content (SMC), average moisture content (AMC), the half thickness of specimen (L), drying time (t), initial moisture content in each drying time interval (IMC_i), and specific gravity of moist wood were used for determining the three directional diffusion coefficients. The analytical solution of the unsteady state

diffusion equation was obtained by separation of variables for the constant diffusion coefficient case with the following initial and boundary conditions.

Initial condition: $C = C(x,0)$ at $x = x$ and $t = 0$

1st boundary condition: $C = C(0,t) = C_s(t)$ at $x = 0$ and $t = t$

2nd boundary condition: $C = C(2L,t) = C_s(t)$ at $x = 2L$ and $t = t$

Where, C = moisture concentration, kg/m^3 , $C(x,t)$ = concentration in any location and at any time, kg/m^3 , $C_s(t)$ = surface moisture concentration at any time, kg/m^3 , L = half thickness of specimen, m , t = drying time, sec , x = a space of the geometry, m .

Assumptions used in deriving the solution are that dimensional change in the moisture movement direction does not occur, and that the diffusion coefficient is constant in each drying time interval. By redefining the fractional change in moisture concentration (E) as $E = \frac{C(x,t) - C_s(t)}{C(x,0) - C_s(t)}$, the

unsteady state diffusion equation $\frac{\partial C}{\partial t} = D \cdot \frac{\partial^2 C}{\partial x^2}$ can be expressed as $\frac{\partial E}{\partial t} = D \cdot \frac{\partial^2 E}{\partial x^2}$. The solution can be obtained by the separation of variables method.

$$E = \frac{C(x,t) - C_s(t)}{C(x,0) - C_s(t)} = \sum_{n=0}^{\infty} \frac{4}{(2n+1) \cdot \pi} \cdot \sin\left(\frac{(2n+1)\pi}{2L} \cdot x\right) \cdot \exp\left(-\frac{(2n+1)^2 \pi^2}{(2L)^2} Dt\right) \quad (2)$$

By integration of equation (2) over the half thickness from 0 to L , the fractional change in the average moisture concentration (\bar{E}) becomes;

$\bar{E} = \frac{C_{\text{AVG}}(t) - C_s(t)}{C_{\text{IMC}_i} - C_s(t)} = \frac{8}{\pi^2} \cdot \sum_{n=0}^{\infty} \frac{1}{(2n+1)^2} \cdot \exp\left(-\frac{(2n+1)^2 \pi^2}{(2L)^2} Dt\right)$, where, $C_{\text{AVG}}(t)$ = average moisture concentration in wood, kg/m^3 , and C_{IMC_i} = initial moisture concentration in wood in each drying time interval, kg/m^3 . Because water concentration in wood can be presented by $C(x,t) = \frac{G_{\text{MC}} \cdot \rho_w \cdot \text{MC}(x,t)}{100}$, where, G_{MC} = specific gravity of moist wood, ρ_w = water density, kg/m^3 , and MC = %moisture content, the diffusion coefficient (D) in each drying time interval can be calculated as follows;

$$D = -\frac{4 \cdot L^2}{\pi^2} \cdot \left(\frac{G_i \text{IMC}_i - G_s \text{SMC}(t)}{G_A \text{AMC}(t) - G_s \text{SMC}(t)} \right) \cdot \left(\frac{1}{G_i \text{IMC}_i - G_s \text{SMC}(t)} \cdot \frac{dG_A \text{AMC}(t)}{dt} + \frac{(-G_i \text{IMC}_i + G_A \text{AMC}(t))}{(G_i \text{IMC}_i - G_i \text{SMC}(t))^2} \cdot \frac{dG_s \text{SMC}(t)}{dt} \right) \quad (3)$$

where, IMC_i = %initial moisture content in each drying time interval, SMC and AMC = %surface and %average moisture content, G_i , G_s , and G_A = specific gravity of wood at IMC_i , SMC , and AMC .

MASS TRANSFER COEFFICIENTS

The surface emission coefficients, which can explain an external resistance including surface resistance on the moisture-evaporating rate, were experimentally determined by

$$S_{\text{exp}} = \frac{J}{(C_{s,\text{wood}} - C_{e,\text{wood}})} = \frac{\Delta W / (A \cdot \Delta t)}{G_s \cdot \rho_w \cdot \text{SMC} / 100 - G_E \cdot \rho_w \cdot \text{EMC} / 100} \quad (4)$$

where, S_{exp} = experimentally determined surface emission coefficient, m/s, J = moisture flux from surface to air, kg/s m², $C_{s,\text{wood}}$ = moisture concentration at wood surface, kg/m³, $C_{e,\text{wood}}$ = moisture concentration in wood at equilibrium with surrounding condition, kg/m³, W = mass of evaporated moisture, kg, A = surface area of specimen, m², EMC = %equilibrium moisture content, and G_E = specific gravity of wood at EMC. The S_{exp} were compared with mass transfer coefficients calculated by boundary layer theory (h_{air}).

$$h_{\text{air}} = \frac{0.66 \cdot D_{\text{H}_2\text{O},\text{air}} \text{Re}^{1/2} \text{Sc}^{1/3}}{L_s} \quad (\text{for laminar flow}), \quad (5)$$

where, h_{air} = mass transfer coefficient based on moisture concentration in air, m/s, $D_{\text{H}_2\text{O},\text{air}}$ = diffusion coefficient of water vapor in air = $2.2 \cdot 10^{-5} \left(\frac{1.013 \cdot 10^5}{P} \right) \left(\frac{T}{273} \right)^{1.75}$, m²/s, P = total pressure of air and water vapor, Pa, T = temperature, K, Re = Reynolds number = $\frac{L_s \cdot v \cdot \rho_a}{\mu}$, Sc = Schmidt numbers = $\frac{\mu}{\rho_a D_{\text{H}_2\text{O},\text{air}}}$, L_s = length of surface along which convection occurs, m, v = air velocity, m/sec, ρ_a = density of air, kg/m³, and μ = dynamic viscosity of air, Pa·s.

Because S_{exp} is based on the moisture concentration in wood, and h_{air} is based on the moisture concentration in air, a conversion method from h_{air} to surface emission coefficient is required to facilitate making comparisons to each other. Siau (1995) believed water vapor pressure on the surface of wood (p_s) in the hygroscopic range could be determined by multiplying the saturated vapor pressure of water at dry bulb temperature ($p_{o,\text{dry}}$) by relative humidity at the surface (RH_s). This calculation, however, resulted in large deviations between experimental and theoretical surface emission coefficients. Siau's method overestimates the p_s because when very wet wood surfaces are being dried to the fiber saturation point (FSP), the p_s is close to the saturated vapor pressure at wet bulb temperature ($p_{o,\text{wet}}$) not $p_{o,\text{dry}}$. And when the surface is being dried from FSP to EMC in the hygroscopic range, the p_s might decrease from $p_{o,\text{wet}}$ to vapor pressure equilibrated to ambient air (p_e), which can be determined by multiplying $p_{o,\text{dry}}$ by environmental relative humidity (RH_e). Using

this concept, a new conversion method between mass transfer coefficients can be developed. p_s can be determined, using the relationship of $\frac{p_{o,wet} - p_s}{p_{o,wet} - p_e} = \frac{100 - RH_s}{100 - RH_e}$, as

$$p_s = p_{o,wet} - \left(\frac{p_{o,wet} - p_e}{100 - RH_e} \right) \cdot (100 - RH_s) = p_{o,wet} - \left(\frac{p_{o,wet} - p_{o,dry} \cdot \left(\frac{RH_e}{100} \right)}{100 - RH_e} \right) \cdot (100 - RH_s) \quad (6)$$

where, p_s and p_e = water vapor pressure in air adjacent to surface of wood and in ambient air, Pa, $p_{o,wet}$ and $p_{o,dry}$ = saturated water vapor pressure at wet bulb and at dry bulb temperature, Pa, and RH_s and RH_e = %relative humidity of air adjacent to surface of wood and of ambient air.

Moisture concentration in air adjacent to a wood surface ($C_{s,air}$) and moisture concentration in ambient air ($C_{e,air}$) can be calculated by the gas law. $C_{s,air} = \frac{M_{H_2O} \cdot p_s}{R \cdot T_s}$, and $C_{e,air} = \frac{M_{H_2O} \cdot p_e}{R \cdot T_{dry}}$,

where, M_{H_2O} = water molecular weight, 18 kg/kgmol., R = gas law constant, 8314 m³Pa/kgmol K, and T_s and T_{dry} = temperature in air adjacent to surface and in ambient air, K. Finally, surface emission coefficient can be theoretically converted from h_{air} by the equation,

$$\begin{aligned} S_{theo} &= h_{air} \cdot \frac{(C_{s,air} - C_{e,air})}{(C_{s,wood} - C_{e,wood})} = h_{air} \cdot \frac{\frac{M_{H_2O} \cdot p_s}{R \cdot T_s} - \frac{M_{H_2O} \cdot p_e}{R \cdot T_{dry}}}{G_s \cdot \rho_w \cdot \frac{SMC}{100} - G_E \cdot \rho_w \cdot \frac{EMC}{100}} \\ &= h_{air} \cdot \frac{\frac{M_{H_2O}}{R \cdot T_s} \left(p_{o,wet} - \left(\frac{p_{o,wet} - p_{o,dry} \cdot \left(\frac{RH_e}{100} \right)}{100 - RH_e} \right) \cdot (100 - RH_s) \right) - \frac{M_{H_2O}}{R \cdot T_{dry}} \left(p_{o,dry} \cdot \left(\frac{RH_e}{100} \right) \right)}{G_s \cdot \rho_w \cdot \frac{SMC}{100} - G_E \cdot \rho_w \cdot \frac{EMC}{100}} \end{aligned} \quad (7)$$

MOISTURE CONTENT PROFILES IN WOOD

Actual MC profiles

Fully saturated maple, oak, and pine specimens with 200 (longitudinal) x 50 (radial) x 50 (tangential) mm dimensions were wrapped in plastic at 30 and 50°C to assure isothermal conditions prior to drying. Also, prior to each drying experiment, the specimens were end coated with a fibered asphalt compound (St. Louis Paint Mfg. Co.) to provide 2-dimensional only, radial and tangential, moisture flow. MC profiles in each specimen were measured by the slicing method, with 7 sections each in the radial and tangential directions cut and MCs of those sections determined by oven drying.

Simulated MC profiles

2-dimensional MC profiles in wood during drying were simulated by the finite difference method (FDM). The computer simulation program utilized DELPHI updated PASCAL program language. Moisture concentration equations in this program were solved by implicit formulation and Gauss-Seidel iteration.

RESULTS

Colorimetric technique

Surfaces of CoCl_2 treated wood exhibit a light yellow-red color at high MC, which changes to a dark green-blue color at low MC. Spectral reflectance from the surfaces was measured with the spectrophotometer. Surfaces of treated wood at higher MC reflected particularly well longer wavelength light. Using reflectance data and wood hygroscopicity, color value change on the CoCl_2 treated moist wood surface could be plotted in CIE $L^*a^*b^*$ color space. L^* , a^* and b^* values continuously decrease over the high to low MC range.

Surface and Average MC and specific gravity

Using the colorimetric technique and oven drying, SMC and AMC were determined, respectively, during drying at 25%RH and both 30 and 50°C (Figure 1). Green specific gravity of hard maple, red oak, and southern pine were 0.47, 0.56, and 0.44, and their oven-dry specific gravities were 0.53, 0.64, and 0.50, respectively. Specific gravity of moist wood that was approximated by linear interpolation between green and oven-dry specific gravity has been used to determine diffusion and surface emission coefficients.

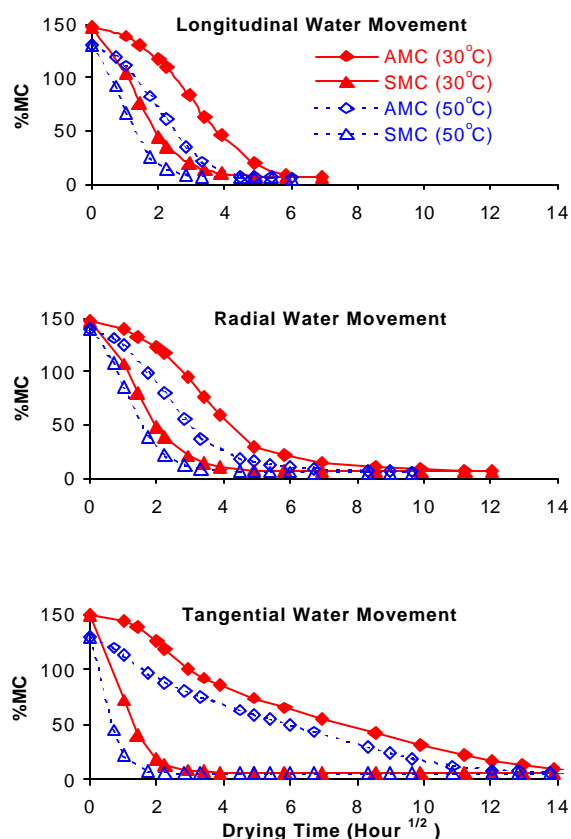


Figure 1. Average and surface moisture contents of hard maple whose moisture movement is constrained to either longitudinal, radial, or tangential directions during drying at 25%RH and 30°C or 50°C.

Diffusion coefficient

During drying at 30°C and 25%RH, the diffusion coefficients in the longitudinal direction of each species remained constant in the range from maximum MC to 30%AMC, and then decreased to EMC (Figure 2). These results might indicate that continuity of liquid water exists in the longitudinal direction from initial moisture content to 30%AMC, and that the longitudinal movement of moisture in that range is by capillary action. The diffusion coefficient in the transverse direction for each species, except the radial direction with hard maple, decreased from over 100%AMC to EMC. This could indicate that continuity of liquid water in the radial direction of red oak and southern pine and the tangential direction of each species was broken at the very beginning of the drying process. Major resistance to water movement in this case might be evaporation and condensation of moisture in wood and so governed by water vapor pressure and bound water gradients. The diffusion coefficient in the radial direction of hard maple remained constant to about 60%AMC, and then decreased to EMC. In this case continuity of liquid water exists in the radial direction to about 60%AMC. This result might be due to the anatomical structure of hard maple where ray cells may support continuous free water movement relatively well in the radial direction. Over the entire AMC range diffusion coefficients decreased during drying, which means that internal resistance increased. Although the data is not presented, diffusion coefficients determined during drying at 50°C and 25%RH condition were twice as high as those determined during drying at 30°C and 25%RH.

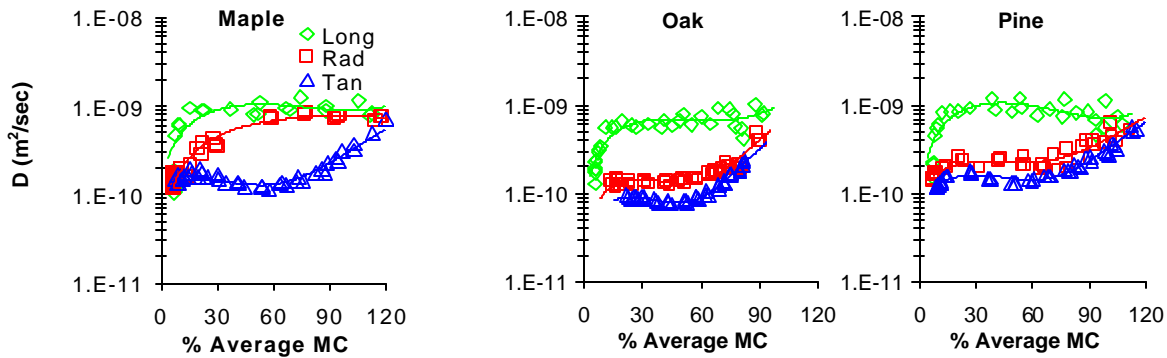


Figure 2. Diffusion coefficients in three orientations for maple, oak and southern pine at 30°C.

Mass transfer coefficient

Experimentally determined surface emission coefficients (S_{exp})

Relationships between S_{exp} and SMC of maple, oak, and pine were observed while drying at 30°C and 50°C with 25%RH (Figure 3). As drying progressed, the coefficients slightly increased when above the FSP range and then rapidly increased from FSP to EMC. Also, a positive effect of temperature on the surface emission coefficient was found, as the coefficient values at 50°C were greater than those at 30°C. These results show that surface emission coefficients were strongly dependent upon the SMC and air temperature as well as air velocity, which is known as a critical factor.

Mass transfer coefficient calculated by boundary layer theory (h_{air})

After the physical properties of air, such as velocity, density, and viscosity were measured and surveyed, mass transfer coefficients were calculated by boundary layer theory (h_{air}). Air velocities in the environmental chambers used for drying were 1m/sec, measured with a hot wire anemometer. Airflow direction was parallel to exposed wood surfaces. The surface lengths of specimens along which convection occurs were 0.02m. Air densities at 30°C (303K) and 50°C (323K) were 1.167 and 1.096 kg/m³, respectively. Air viscosities at 30°C and 50°C were 1.87 x10⁻⁵ and 1.96 x10⁻⁵ Pa·s, respectively. Based on those data, diffusion coefficients of water vapor in air ($D_{H_2O,air}$, 2.64x10⁻⁵ m²/s at 30°C and 2.95x10⁻⁵ m²/s at 50°C), Reynolds number (Re, 1248 at 30°C and 1118 at 50°C) and Schmidt number (Sc, 0.6069 at 30°C and 0.6062 at 50°C) were determined. Using those values, mass transfer coefficients (h_{air}) were determined to be 0.026 and 0.028 m/s at 30 and 50°C, respectively.

Surface emission coefficient theoretically converted from h_{air} (S_{theq})

The h_{air} were converted to surface emission coefficients using the previously developed conversion method with drying condition and the physical properties of each species. For example, with hard maple dried at 30°C and 25%RH, the wet bulb temperature is 16.8°C (290K), 140%, 29%, and 6.2%MC were used for initial surface moisture content, fiber saturation point, and equilibrium moisture content, 0.47 and 0.53 were used for green and oven-dry specific gravity, and 1923Pa ($p_{o,wet}$) and 4249Pa ($p_{o,dry}$) were used for the saturated vapor pressure of water in air at wet bulb temperature 16.8°C and dry bulb temperature 30°C, respectively. Since RH_e was 25%RH, water vapor pressure in ambient air (p_e) was 1062Pa = 4249·(25/100).

Using those values, h_{air} were converted to surface emission coefficients. These theoretically converted surface emission coefficients (S_{theo}) were quite close to S_{exp} (Figure 3). This proves that boundary layer theory is useful for evaluating the external moisture resistance during drying.

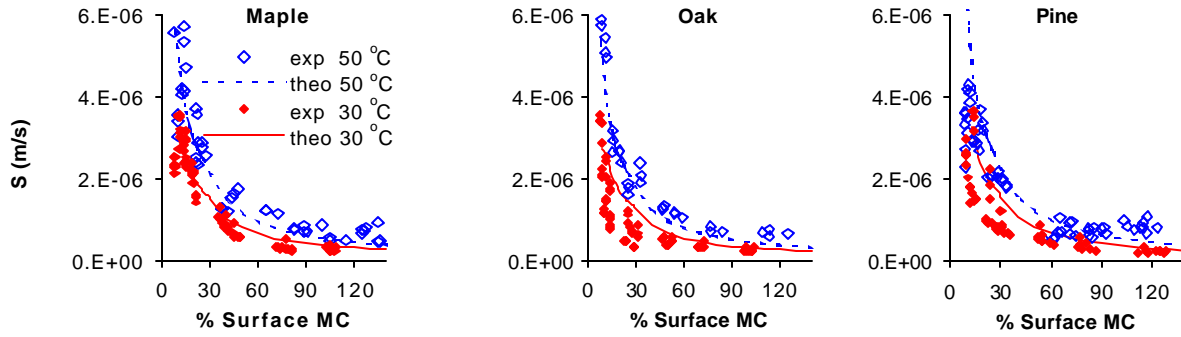


Figure 3. Experimentally determined surface emission coefficient (S_{exp}) and surface emission coefficient theoretically converted from mass transfer coefficient calculated by boundary layer theory (S_{theo}).

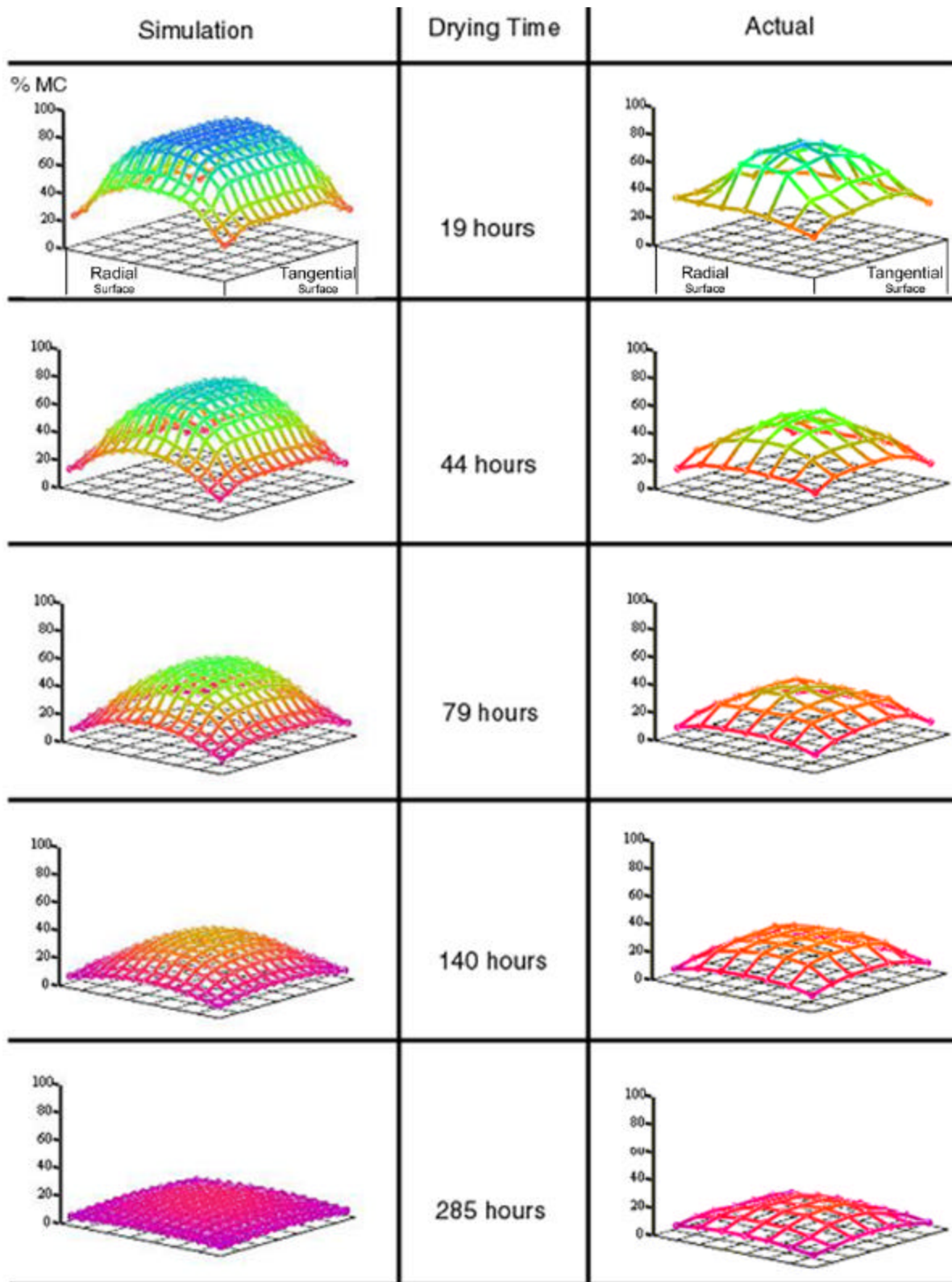


Figure 4. Simulated and actual MC profiles in hard maple during drying at 30°C and 25%RH.

Moisture profiles in wood

Overall, the moisture profiles simulated by finite difference method were quite comparable to the actual moisture profiles in real dried wood. Results for maple at 30°C are illustrated in Figure 4. This substantiates the high credibility of using the colorimetric technique for determining surface moisture content and mathematical procedure for determining the diffusion and surface emission coefficient.

CONCLUSIONS

Use of the colorimetric CoCl₂ treated wood technique for determining surface moisture content of wood nondestructively and continuously in unsteady state drying conditions could increase the credibility of methods for calculating the internal and external resistances for moisture movement in, and surface evaporation from, wood.

The decrease of diffusion coefficient determined in these experiments proves the increase of internal resistance during drying of wood. Experimental results showed that diffusion coefficients were dependent upon the temperature and average moisture content in wood. Also, the surface emission coefficients were shown to strongly depend on the surface moisture content of wood and air temperature as well as air velocity, which has been known as a critical factor.

The mass transfer coefficient conversion method developed using surface moisture data in this study has proven that the boundary layer theory is useful for evaluating the external resistance during wood drying. Due to this proof, the external resistance for wooden surfaces can be theoretically described in dynamic drying situations.

The moisture profiles simulated by finite difference method were quite comparable to the actual moisture profiles in real dried wood, which substantiates the credibility of using the colorimetric technique for determining surface moisture content and mathematical procedure for determining the diffusion and surface emission coefficient.

REFERENCES

- CIE. 1986, Colorimetry. 2nd Edition. CIE Pub. No. 15.2. Commission Internationale de l'Eclairage, Vienna. 74pp.
- Crank, J. 1975: The Mathematics of Diffusion. 2nd Edition. Clarendon press, Oxford. 414pp.
- Geankoplis, C. J. 1993: Transport Process and Unit Operations. 3rd Edition. Prentice Hall Inc., Englewood Cliffs, New Jersey. 921pp.
- Siau, J. F. 1995. Wood: Influence of moisture on physical properties. Dept. of Wood Sci. and For. Prod., Virginia Tech. 227pp.
- Yeo, H. 2001. Evaluation of Mass Transfer in Wood Utilizing a Colorimetric Technique and Numerical Analysis. Ph.D. thesis. SUNY-ESF, Syracuse, New York. 200pp.

Attachment 2

**DETERMINATION OF SURFACE MOISTURE CONTENT OF WOOD UTILIZING A
COLORIMETRIC TECHNIQUE***

Hwanmyeong Yeo

Research Associate

William B. Smith

Professor

Faculty of Wood Products Engineering

and

Robert B. Hanna

Director

Center for Ultrastructure Studies

College of Environmental Science and Forestry

State University of New York, Syracuse, NY 13210

* The authors wish to acknowledge the financial support of U.S. Department of Energy (DOE) project –DE–FC07–97ID13537– Moisture Distribution and Flow During Drying of Wood and Fiber.

ABSTRACT

Optical properties of cobalt chloride (CoCl_2) hydrate, whose color changes with surrounding humidity, were used to develop a colorimetric technique for determining surface moisture content of wood nondestructively. The colorimetric CoCl_2 treated wood technique for determining surface moisture content through color degree change in CIE $L^*a^*b^*$ color space has been experimentally verified.

KEYWORDS

Cobalt chloride (CoCl_2) hydrate, colorimetric technique, surface moisture content, CIE $L^*a^*b^*$, spectrophotometer

INTRODUCTION

Though the determination of surface moisture content (SMC) is important in the study of stress development and preventing surface checking of wood during drying, methods to measure SMC have not yet been well developed. This paper will introduce a colorimetric technique for determining surface moisture content utilizing the optical properties of CoCl_2 hydrate and a color-measuring instrument. Wood surfaces exhibit different color values when exposed under different circumstances. For example, the surface of wet wood is usually relatively dark, while dried surfaces are a lighter color. It is difficult, however, to determine specific moisture content by color change of wood specimens when there is little variation or change with incremental moisture content, especially when below the fiber saturation point. To address this problem wood specimens were treated with CoCl_2 hydrate, a compound whose color depends upon and changes with relative humidity (RH) and temperature. CoCl_2 hydrate is shown to exhibit a reddish color that then changes to a bluish color, over the high to low humidity range, respectively. In the 1930's Rother developed a wood hygrometer using paper test strips treated with CoCl_2 . Estimation of moisture content in the range from 6 to 23% in steps of 3% was possible by comparing the color of the test strip with a color scale (cited by Kollmann and Cote 1968). The method is cheap and quick. The results, however, are influenced by variation in lighting conditions and the personal element in visual observations. Due to these disadvantages, this optical method could not practically be used to determine moisture content before development of a method and instrument for expressing color numerically. Recently, using optical fiber and color value change of CoCl_2 hydrate according to humidity and temperature, fiber optic humidity and temperature sensors have been developed to detect relative humidity and temperature in air (Otsuki and Adachi 1993, Kharaz and Jones 1995, Hyspser and Wierzba 1997, Kawamura et al. 1999, Dybko et al. 1999, Coera et al. 2000). In this study, the surface of wood was treated with CoCl_2 and the color changes were measured using a spectrophotometer at various surrounding humidity conditions. The measured color was shown numerically in the CIE $L^*a^*b^*$ color space, available to present all visible color, and based on the daylight 6500K degree color temperature.

Colorimetry

Colorimetry is the technique of color measurement, and is based on a mechanism of human visual perception. In 1931, an international organization concerned with light and color, the Commission Internationale de l'Eclairage (CIE, International Commission on Illumination), defined CIE XYZ tristimulus values, which are now used throughout the world for color communication. Based on these CIE XYZ tristimulus values, the CIE $L^*a^*b^*$ color space was devised in 1976 to provide more uniform color differences in relationship to visual differences (CIE 1986).

CIE XYZ

To measure the color of a specimen, each of three parameters must be analyzed. The first parameter is the spectral energy distribution of the light source ($S(\lambda)$), the second is the reflectance from the specimen ($R(\lambda)$) and the third is the spectral sensitivity ($x(\lambda)$, $y(\lambda)$, $z(\lambda)$) of the observer (Crisment 1998). The concept for the XYZ tristimulus values is based on the three-component theory of color vision, which states that the eye possesses receptors for three primary colors (red, green, and blue) and that all colors are seen as mixtures of these three primary colors. The values of X, Y, and Z are calculated according to the formulas below:

$$X = K \int_{380}^{780} S(\lambda) R(\lambda) x(\lambda) d\lambda, \quad Y = K \int_{380}^{780} S(\lambda) R(\lambda) y(\lambda) d\lambda, \quad Z = K \int_{380}^{780} S(\lambda) R(\lambda) z(\lambda) d\lambda \quad (1)$$

where $K = 100 / \int_{380}^{780} S(\lambda) y(\lambda) d\lambda$

λ : wavelength (nm)

$S(\lambda)$: relative spectral energy distribution of light source

$R(\lambda)$: spectral reflectance of specimen

$x(\lambda)$, $y(\lambda)$, $z(\lambda)$: spectral sensitivity corresponding to the human eye

CIE L*a*b*

The tristimulus values XYZ are useful for defining a color, but the results are not easily visualized. Because of this the CIE also defined CIE L*a*b* color space in 1976 for graphing color. The L*a*b* color space is presently one of the most popular color spaces for measuring object color and is widely used in virtually all fields. The values of L*, a*, and b* are calculated according to the formulas below:

$$L^* = 116 (Y/Y_n)^{1/3} - 16, \quad (2)$$

$$a^* = 500 [(X/X_n)^{1/3} - (Y/Y_n)^{1/3}],$$

$$b^* = 200 [(Y/Y_n)^{1/3} - (Z/Z_n)^{1/3}]$$

where X, Y, Z : Tristimulus values XYZ of the specimen

X_n , Y_n , Z_n : Tristimulus values XYZ of a perfect reflection

If X/X_n , Y/Y_n , or Z/Z_n is less than 0.008856,

$(X/X_n)^{1/3}$ is replaced by $7.787(X/X_n) + 16/116$

$(Y/Y_n)^{1/3}$ is replaced by $7.787(Y/Y_n) + 16/116$

$(Z/Z_n)^{1/3}$ is replaced by $7.787(Z/Z_n) + 16/116$

In this color space, L^* indicates lightness, and a^* and b^* are the chromaticity coordinates. a^* and b^* values indicate color directions: $+a^*$ is the red direction, $-a^*$ is the green direction, $+b^*$ is the yellow direction, and $-b^*$ is the blue direction. The center is achromatic. As a^* and b^* values increase and the color point moves out from the center the saturation of the color increases.

MATERIALS AND METHODS

Experiments were carried out with three species, hard maple (*Acer saccharum* Marsh), red oak (*Quercus rubra* L.), and southern pine (*Pinus* spp.). Three different directional, cross, radial and tangential, sections with the dimension of 15 (length) x 15 (width) x 5 (thickness) mm were prepared and soaked in water. CoCl_2 hydrate (from Fisher Scientific Com.) was saturated in water. From this saturated CoCl_2 solution, approximately 3 μL was dropped from a dispensing micropipette on the wet surface of specimens (15 x 15mm) and spread across the surface with the pipette tip. When five specimens each were equilibrated at two different temperatures, 30 and 50°C, and five lower RH conditions, the treated surface spectral reflectance was measured with a portable spectrophotometer (Microflash 200d, DataColor International) and then CIE $L^*a^*b^*$ color values were calculated. The SMC is determined by hygroscopicity of untreated wood and surface color difference ($dE_{\text{mc-eq}}$) between treated wood at any moisture condition and treated wood equilibrated under the specified lowest RH condition. 25%RH was used as the lowest RH condition in these experiments.

$$dE_{\text{mc-eq}} = \sqrt{(L^*_{\text{mc}} - L^*_{\text{eq}})^2 + (a^*_{\text{mc}} - a^*_{\text{eq}})^2 + (b^*_{\text{mc}} - b^*_{\text{eq}})^2} \quad (3)$$

where, L^*_{mc} , a^*_{mc} and b^*_{mc} : L^* , a^* , and b^* values on the surface of treated moist wood

equilibrated at any RH.

L^*_{eq} , a^*_{eq} , and b^*_{eq} : L^* , a^* , and b^* values on the surface of treated wood

equilibrated at the lowest RH.

When making the regression functions for SMC determined with color value, as a first step, surrounding RH condition on the surface of wood was determined by the CoCl_2 treated wood color difference, then SMC of wood is determined by hygroscopicity of untreated wood. Hygroscopicity of three species, hard maple, red oak, and southern pine, was measured with 12 specimens for each species at two temperatures conditions.

RESULTS

Hygroscopicity of wood

As expected, the moisture content (MC) of wood decreased with the decrease of surrounding relative humidity, and moisture content equilibrated at low temperature was higher than MC equilibrated at high temperature for the same RH. The equilibrium moisture contents (EMC) of wood as third order functions of relative humidity are given in Table 1. These third order functions of sorption curves are well fitted for the relationship between EMC and RH over the whole RH range.

Species	Temp. (°C)	% MC = a · %RH ³ + b · %RH ² + c · %RH			r ²
		a x 10 ⁵	b x 10 ³	c x 10	
Hard maple	30	5.19	5.95	3.64	0.99
	50	5.30	5.86	3.17	0.99
Red oak	30	5.76	6.68	3.80	0.99
	50	6.11	6.99	3.46	0.99
Southern Pine	30	7.03	8.27	4.09	0.99
	50	7.11	8.33	3.79	0.99

Table.1. Equilibrium moisture content of wood as third order functions of relative humidity

Determination of surface moisture content

Spectral reflectance

The surface of treated hard maple at higher RH reflected particularly well the light with longer wavelength (Figure 1). Similar results were found with red oak and southern pine.

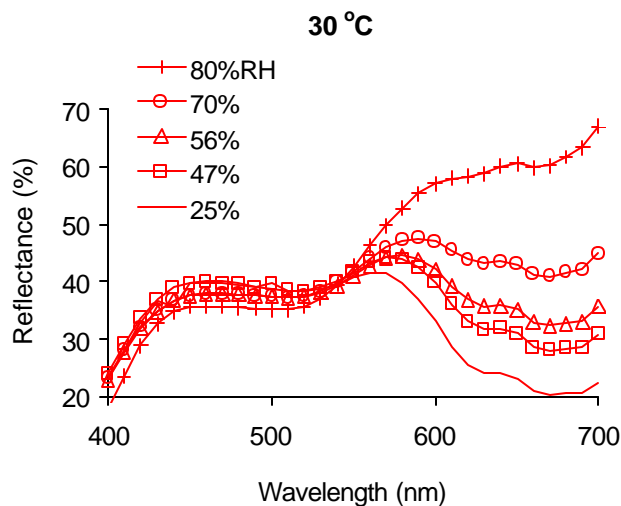


Figure 1. Spectral reflectance change on the tangential surface of treated hard maple with relative humidity at 30°C.

CIE L*a*b*

CIE L*a*b* color values were calculated using the reflectance data. Wood treated with CoCl_2 exhibits a reddish color at high RH and changes to a green-blue color at low RH. This means a^* and b^* values continuously decrease over the high to low RH range. Also, lightness (L^*) of the treated wood surface decreases with RH in the hygroscopic range.

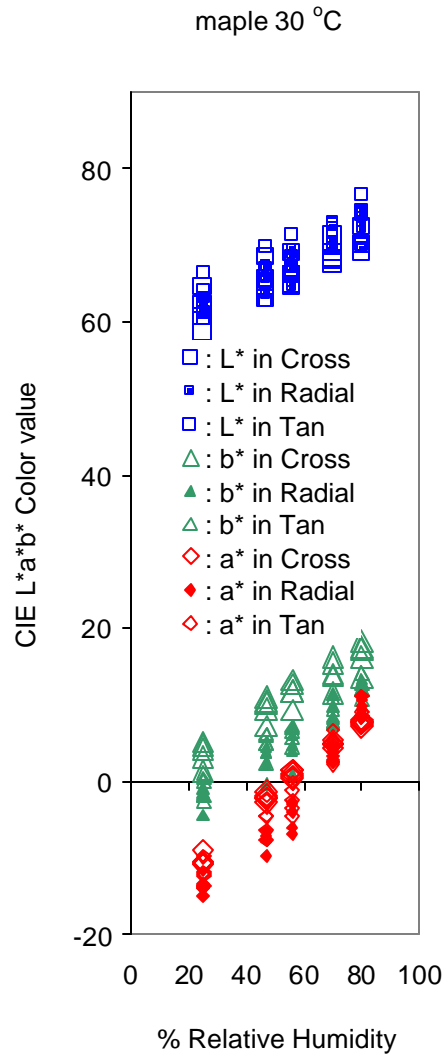


Figure 2. CIE L*a*b* values of treated hard maple specimens at different relative humidity at 30°C.

Surface moisture content

Using hygroscopicity of untreated wood, surface moisture content is predicted by dE_{mc-eq} of wood treated with $CoCl_2$. The linear relationships between surface moisture content and dE_{mc-eq} on the surface of three directional sections of each species, hard maple, red oak, and southern pine treated with $CoCl_2$ are summarized in Table 2.

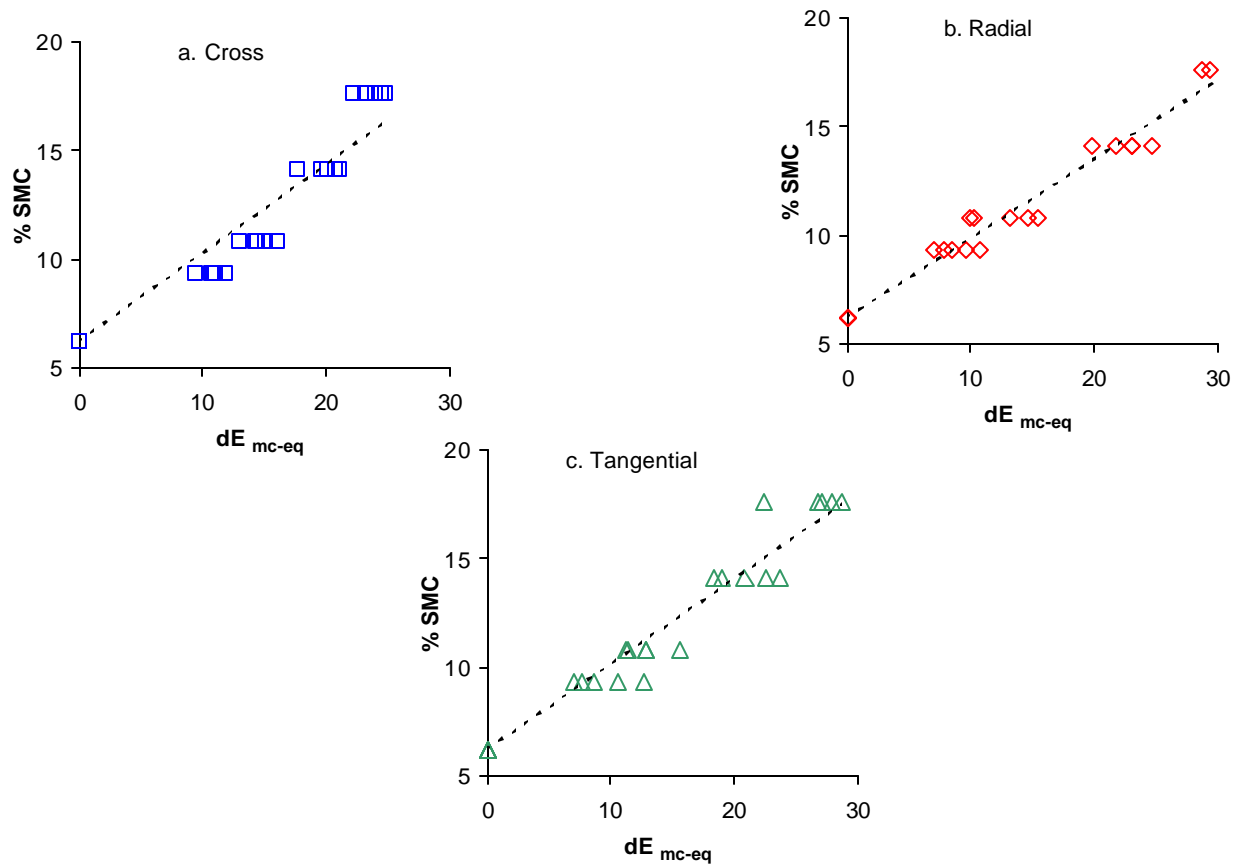


Figure 3. Relationship between surface moisture content and color difference (dE_{mc-eq}) of a. cross section, b. radial, and c. tangential surfaces of maple at 30° C. Linear regression and r^2 values are presented in Table 2.

Temp. (°C)	Species	Section	%SMC = $a \cdot dE_{mc-eq} + b$		r^2
			a	b	
30	Hard maple	Cross	0.410	6.2	0.91
		Radial	0.366	6.2	0.98
		Tangential	0.395	6.2	0.95
	Red oak	Cross	0.399	6.2	0.87
		Radial	0.338	6.2	0.97
		Tangential	0.353	6.2	0.97
	Southern pine	Cross	0.300	6.2	0.77
		Radial	0.275	6.2	0.96
		Tangential	0.275	6.2	0.96
50	Hard maple	Cross	0.513	5.1	0.93
		Radial	0.479	5.1	0.97
		Tangential	0.482	5.1	0.96
	Red oak	Cross	0.471	5.2	0.89
		Radial	0.446	5.2	0.96
		Tangential	0.428	5.2	0.97
	Southern pine	Cross	0.322	5.4	0.72
		Radial	0.312	5.4	0.83
		Tangential	0.366	5.4	0.93

Table 2. Linear relationships between surface moisture content and dE_{mc-eq} on the three different directional sections of hard maple, red oak, and southern pine treated with $CoCl_2$.

RESOLUTION OF COLORIMETRIC METHOD

The spectrophotometer detector consists of a 128-element diode array. Following the study of Hill (1997), CIE $L^*a^*b^*$ optimal color space is arrayed within the limits $0 < L^* < 100$, $-166 < a^* < 141$, $-132 < b^* < 147$. Since the spectrophotometer might divide the lightness (L^*) range 0 to 100, the a^* value range -166 to 141, and the b^* value range -132 to 147 by the 128 diodes, the spectrophotometer can measure approximately 0.78 of lightness difference (ΔL^*), 2.40 of a^* value difference (Δa^*), and 2.18 of b^* value difference (Δb^*), respectively. Because color difference (dE) is defined as $dE = \sqrt{\Delta L^{*2} + \Delta a^{*2} + \Delta b^{*2}}$, the spectrophotometer can measure 3.33 of dE . Results from this experiment showed that average maximum dE_{mc-eq} of treated wood between 80%RH and 25%RH was about 30. Therefore, the %RH difference determined by the spectrophotometer can be calculated as $(80\%RH - 25\%RH) \times (3.33 / 30) = 6.1\%RH$. Since EMC of wood at 80%RH is about 18%MC and EMC at 25%RH is about 6%MC, %MC difference determined by the spectrophotometer can be calculated as $(18\%MC - 6\%MC) \times (3.33 / 30) = 1.3\%MC$.

CONCLUSIONS

The colorimetric $CoCl_2$ treated wood technique, which has been developed for determining surface moisture content through color degree change in CIE $L^*a^*b^*$ space while drying, has been experimentally

verified. The good linear relationship between SMC and dE_{mc-eq} has shown that surface moisture content can be determined by this colorimetric method.

Because this colorimetric technique has the advantage of freedom from electromagnetic interference and offers the prospect of remote monitoring of surface moisture content, a number of useful applications of this technique might be possible. Examples include surface moisture content sensing of wood and other hygroscopic particle and powder materials in bulk storage, and humidity monitoring through industrial drying systems to optimize use of energy.

Also, because the color value measured by this technique is representative as a standard color value for determining the surface MC of wood, if there is good color space conversion from CIE $L^*a^*b^*$ to other color spaces, especially the RGB that is used in image capture devices (scanners and digital camera), surface moisture content and geometrical information can be simultaneously determined in pixel units. This might encourage better analysis in studies on various hygroscopic materials' physical properties related to moisture.

REFERENCES

- Chrisment, A. 1998. Color and Colorimetry. Editions 3C Conceil, Paris. 30pp.
- CIE. 1986. Colorimetry. CIE Publication No 15.2. 2nd Edition. Commission Internationale de l'Eclairage, Vienna. 74pp.
- Coera, F.P., A. Gaston, and J. Sevilla. 2000 May. Relative humidity sensor based on side-polished fiber optic. Proceedings of 17th IEEE Instrumentation and Measurement Technology Conference. Baltimore, MD, USA.1:17-22.
- Dybko, A., W. Wroblewski, E. Rozniecka, J. Maciejewski, and Z. Brzozka. 1999. Comparision of two thermochromic solutions for fiber optic temperature probes. Sensors and Actuators A (Physical). A76:203-207.
- Hill, B., T. Roger, and F. W. Vorhagen. 1997. Comparative analysis of the quantization of color spaces on the basis of the CIE LAB color-difference formula. ACM Transactions on graphics. 16(2):109-154.
- Hypszter, R. and H. J. Wierzba. Fiber optic technique for relative humidity sensors. 1997. Proceeding of SPIE – Int. Society for Optical Engineering. 3054:145-150.
- Kawamura, M., T. Takeuchi, H. Faud, and S. Sato. 1999. Feb. Humidity and temperature sensing using an optical fiber and a corner cube prism. Japanese Journal of Applied Physics, Part 1. 38(2A):849-850.
- Kharaz, A., and B. E. Jones. 1995. A distributed optical-fiber sensing system for multi-point humidity measurement. Sensors and Actuators A (Physical). A46-47:491-493.
- Kollmann, F. F. P. and W. A. Cote. 1968. Principles of Wood Science and Technology. Vol. I. Solid Wood. Springer-Verlag, New York. 592pp.
- Otsuki, S. and K. Adachi. 1993. Humidity dependence of visible absorption spectrum of gelatin film coating cobalt chloride. Journal of Applied Polymer Science. 48(9):1557-1564.

Attachment 3

BENDING PROPERTIES OF WOOD FLAKES*

Edgar C. Deomano
Research Assistant

and

Audrey Zink-Sharp
Associate Professor
Department of Wood Science and Forest Products
Virginia Polytechnic Institute and State University
Blacksburg, Virginia 24061

* The authors wish to acknowledge the financial support of U.S. Department of Energy (DOE) project –DE–FC07–97ID13537– Moisture distribution and flow during drying of wood and fiber.

ABSTRACT

This research focuses on experimental investigations of the bending properties of wood flakes. Modulus of elasticity (MOE), modulus of rupture (MOR), and strength at proportional limit (SPL) of flakes were measured based on Methods of Testing Small Clear Specimens of Timber (ASTM D143-94) using a miniature material tester. Effect of species, cutting direction, and temperature were evaluated. Bending properties were found to vary between and within the three species. Southern yellow pine had the lowest bending stiffness and strength followed by sweetgum while yellow-poplar had the highest bending properties. Radially-cut specimens were found to have lower MOE, MOR, and SPL than tangentially-cut specimens. Drying temperature was also found to have a significant effect on bending stiffness and strength. A decreasing trend in bending properties was observed when drying temperature was increased.

INTRODUCTION

Quality of any wood composite material depends upon the quality of the raw materials used. Strength of Oriented Strand Board (OSB) is a function of the mechanical properties of the flakes. Knowledge of mechanical properties of flakes can lead to better strength and performance of OSB. Flakes used in manufacture of OSB are generally dried to very low moisture content using high temperature. When wood is dried below the fiber saturation point, its physical, chemical, and mechanical properties are affected. Also, temperature may have an effect on the mechanical properties of wood. Generally, wood strength decreases when the wood is heated and increases when it is cooled. There is minimal permanent strength loss when temperature does not exceed 100°C, but exposure to high temperature for long periods can cause permanent strength loss (Haygreen and Bowyer, 1996).

General discussions on temperature effect on mechanical properties of wood have been presented in the Wood Handbook (FPS, 1999) and by Haygreen and Bowyer (1996). Research on the effect of temperature on various mechanical properties of wood specimens has been performed through the years. Gerhards (1982) summarizes the relevant studies on the immediate effects of moisture content and temperature on mechanical properties of clear wood. A detailed account is given by Salaman (1969) of changes in mechanical properties from thin boards to dimension lumber of softwoods and hardwoods dried at high temperature.

The only research done on the effect of temperature on wood flakes was performed by Plagemann (1982). Red oak, white oak, and sweetgum flakes were dried at 20, 150, and 350°C and conditioned at 21.1°C (70°F) and 65% relative humidity. Small beams measuring 0.5 x 3.8 x 14.2 mm (0.02 x 0.15 x .56 in.) were tested for modulus of elasticity (MOE) and modulus of rupture (MOR) . Results of flake bending tests are presented in Table 1. Bending tests indicated a general

trend of decreased flake strength and stiffness with increased drying temperature. However, the trend toward decreasing flake bending properties associated with high temperature drying did not manifest in board properties (i.e. MOR and MOE).

Table 1. Average Flake Bending Properties at Various Dryer Temperature for Three Southern Hardwood Species (Plagemann, 1982).

SPECIES	DRYER TEMPERATURE (°C)	MOE		MOR	
		(PSI)	(N/mm ²)	(PSI)	(N/mm ²)
Red oak	20	696000	4799	14776	102
	150	750000	5171	15237	105
	350	513000	3537	12757	88
White oak	20	590000	4068	13233	91
	150	502000	3461	12023	83
	350	534000	3682	13171	91
Sweetgum	20	766000	5281	14641	101
	150	691000	4764	13401	92
	350	650000	4482	12610	87

The objective of this study is to determine the bending properties of flakes. Bending properties of southern yellow pine, sweetgum, and yellow-poplar flakes that were measured are MOE, MOR, and stress at proportional limit (SPL). The effect of species, cutting direction, and drying temperature on bending stiffness and strength were analyzed.

MATERIALS AND METHODS

Fresh, green bolts, 1.5 m and around 30 cm in diameter of southern yellow pine (*Pinus* spp.) and sweetgum (*Liquidambar styraciflua*) were obtained from Georgia Pacific OSB plant in Skippers, VA and freshly-cut yellow-poplar (*Liriodendron tulipifera*) boards 50 mm in thickness were obtained from Turman Lumber in Radford, VA. The logs and boards were transported to Blacksburg, VA. The logs were cut into 50 mm boards using a portable sawmill. Sound boards from the three species

were segregated according to type of cut: flatsawn or quartersawn. Radially- and tangentially-cut specimens were taken from the flatsawn and quartersawn boards, respectively (Figure 1). Randomly selected blocks measuring 25x152 mm were prepared from the flatsawn and quartersawn boards. Each block was properly labeled for easy identification. The blocks were placed in plastic bags segregated according to species and cutting direction and stored in a refrigerated room maintained at 2°C.

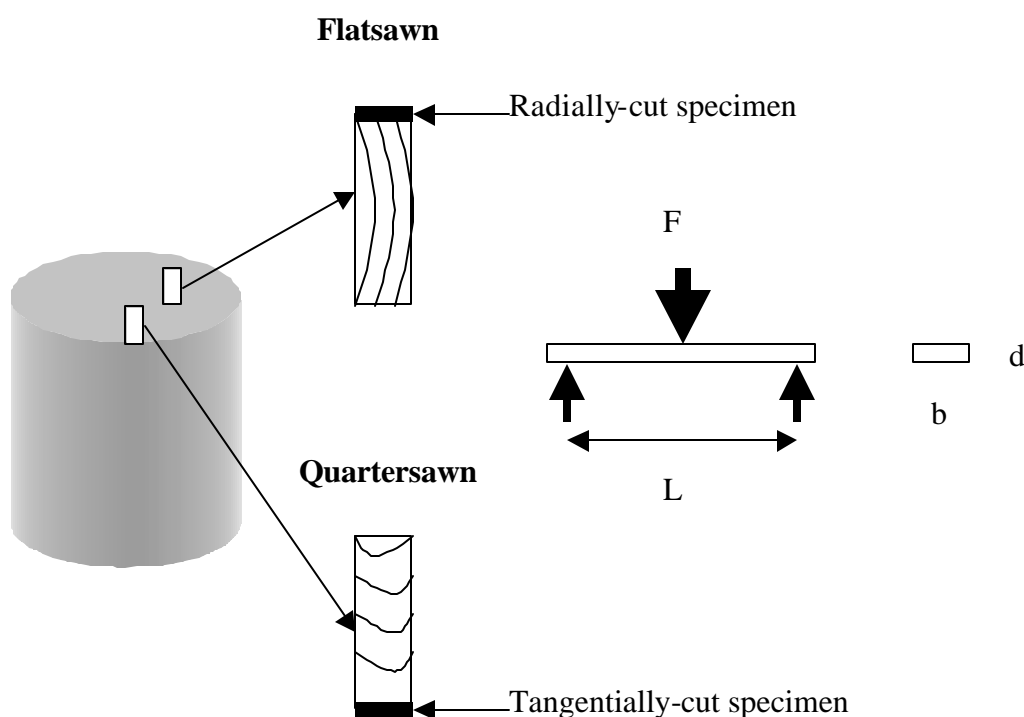


Figure 1 Cutting Diagram of Flake Bending Specimens.

A block was randomly selected for cutting of wafers and subsequently drying of the flakes. Three flakes 0.6 mm in thickness were cut from each block using a CAE flaker. One flake was dried at every drying temperature level (150, 200, and 250°C). Ten replicates were used. Total number of flakes dried in this experiment was 180. After drying, flakes were

conditioned based on ASTM D 4933-91 (ASTM, 1994). Flakes were tested for bending properties when they reached EMC (temperature and relative humidity set at 20°C and 65%, respectively).

Methods

Bending test based on Methods of Testing Small Clear Specimens of Timber ASTM D 143-94 (ASTM, 1994) was adopted. The following bending properties were measured: MOE, MOR and SPL. Static bending tests on small specimens cut from the each flake were performed. A small specimen measuring 5.0 mm (width) x 25.0 mm (length) was cut using a mounted razor blade. Bending tests were performed using a miniature material tester (Rheometric Scientific MiniMat 2000) at a cross-head speed of 2.54 mm/min. MOE, MOR, and SPL were calculated using the following equations (Bodig and Jayne, 1982; Haygreen and Bowyer, 1996):

$$\text{MOE} = P_{pl}L^3/4\Delta_{pl}bd^3 \quad (\text{Eq. 5.1})$$

$$\text{MOR} = 1.5 P_{ult}L/bd^2 \quad (\text{Eq. 5.2})$$

$$\text{SPL} = 1.5 P_{pl}L/bd^2 \quad (\text{Eq. 5.3})$$

where: P_{pl} is load at proportional limit (N)

L is span of the bending specimen (mm)

Δ_{pl} is the deflection of the bending specimen (mm)

b is the width of the bending specimen (mm)

d is the thickness of the bending specimen (mm)

P_{ult} is the ultimate load (N)

Excess material from the flake where the specimen was cut was used for moisture content and specific gravity determinations using the oven-dry (ASTM D 2395-93, 1994) and water

displacement (ASTM D 4442-92, 1994) methods, respectively. Initial weight of the flake was measured. Volume of the flake was determined by clipping one end of the flake using an alligator clip connected to a stand and immersing the flake inside a tube containing distilled water. The weight of the tube with water was determined before and after immersing the flake. The difference in weight is converted into volume of the flake. Oven-dry weight of the flake was determined by placing the flake inside an oven at $102 \pm 3^\circ\text{C}$ overnight. The moisture content for each flake was calculated using the oven-dry and initial weights. Oven-dry weight and green volume was used to calculate specific gravity. Table 2 shows the average moisture content and specific gravity of the flakes.

Table 2 Average Moisture Content and Specific Gravity of the Flakes

SPECIES	MOISTURE CONTENT (%)	SPECIFIC GRAVITY
SYP	10.3	0.58
Sweetgum	12.0	0.64
Yellow-poplar	9.5	0.58

Statistical Analyses

Multiple comparisons of bending properties between species, cutting direction, and drying temperature were done using ANOVA and Tukey's test. MOE, MOR, and SPL were compared between species, cutting direction, and drying temperature using the split-plot design (Snedecor and Cochran, 1980; Steel and Torrie, 1980). Species represented the whole plots. Cutting direction and temperature represented the sub-plots. Linear model considered for the analysis of bending properties is shown below:

$$y_{ijkl} = \mu + S_i + C_j + SC_{ij} + \epsilon_{ijk}^{(A)} + T_l + ST_{il} + CT_{jl} + SCT_{jl} + \epsilon_{ijkl}^{(B)} \quad (1)$$

where: y_{ijkl} is bending property (MOE, MOR, or SPL)

μ is mean

S_i is species effect

C_j is effect of cutting direction

SC_{ij} is interaction effect of species and cutting direction

$\epsilon^{(A)}_{ijk}$ is error

T_l is temperature effect

ST_{il} is interaction effect of species and temperature

CT_{jl} is interaction effect of cutting direction and temperature

SCT_{ijl} is interaction effect of species, cutting direction, and temperature

$\epsilon^{(B)}_{ijkl}$ is error

Means and Tukey's test were used in comparing the main parameters. Analyses were done using GLM procedure of the SAS software package

Comparison of bending properties between cutting directions and drying temperature by species was analyzed using an analysis of covariance (ANACOVA) (Ott, 1992) with specific gravity as covariate. The linear model of the split-polt design shown below was used in the analysis of the bending properties by species:

$$y_{ijk} = \mu + C_i + \epsilon^{(A)}_{ij} + T_k + CT_{ik} + \beta G_{ijk} + \epsilon^{(B)}_{ijk} \quad (2)$$

where: y_{ijk} is bending property (MOE, MOR, or SPL)

μ is mean

C_i is effect of cutting direction

$\epsilon^{(A)}_{ij}$ is error

T_k is temperature effect

CT_{ik} is interaction effect of cutting direction and temperature

β is regression coefficient

G_{ijk} is covariate (specific gravity)

$\epsilon_{ijk}^{(B)}$ is error

Treatment levels were compared using the least squares means and Tukey's test. GLM procedure of the SAS software was also used in the analyses.

RESULTS AND DISCUSSION

Bending properties of the three species, between radial and tangential cutting directions, and the effect of drying temperature and their interaction are discussed. ANOVA indicates variation of bending stiffness and strength between species, cutting direction, and drying temperature (Table 3). The analyses showed that there were highly significant differences in flake MOE, MOR, and SPL between species. There was also a highly significant difference between radial and tangential cutting directions in terms of bending properties. It is well established that there are variations between and within species in mechanical properties of wood (FPS, 1999). Interaction of species and cutting direction was not significant for all bending stiffness and strength. This means that the effect of cutting direction on flake MOE, MOR, and SPL was the same for the three species.

Table 3. P-values of MOE, MOR, and SPL.

SV	DF	MOE	MOR	SPL
S	2	<.01	<.01	<.01
C	1	<.01	<.01	<.01
S*C	2	0.47	0.28	0.18
T	2	<.01	<.01	<.01
S*T	4	0.06	0.40	0.20
C*T	2	0.82	0.53	0.35
S*C*T	4	0.93	0.57	0.51

There were highly significant differences in flake bending properties between drying temperature. However, interaction of temperature with species and with cutting direction were not

significant at $p=0.05$. This implies that the difference in bending properties caused by temperature did not depend on the species or on cutting direction. Three-way interaction among species, cutting direction, and drying temperature was also not significant.

Among the three species, southern yellow pine had the lowest average bending properties (Table 4 and Figure 2). Average MOE, MOR, and SPL of southern yellow pine were 4086.9, 66.0, and 48.1 N/mm², respectively. Sweetgum had higher bending strength and stiffness than southern yellow pine except for MOE which was not significantly different. Mean MOE, MOR, and SPL of sweetgum were 4430.6, 78.6 and 56.5 N/mm², respectively. Yellow-poplar had the highest MOR, MOE, and SPL with average values of 5829.4 N/mm², 89.0, and 66.0 N/mm², respectively.

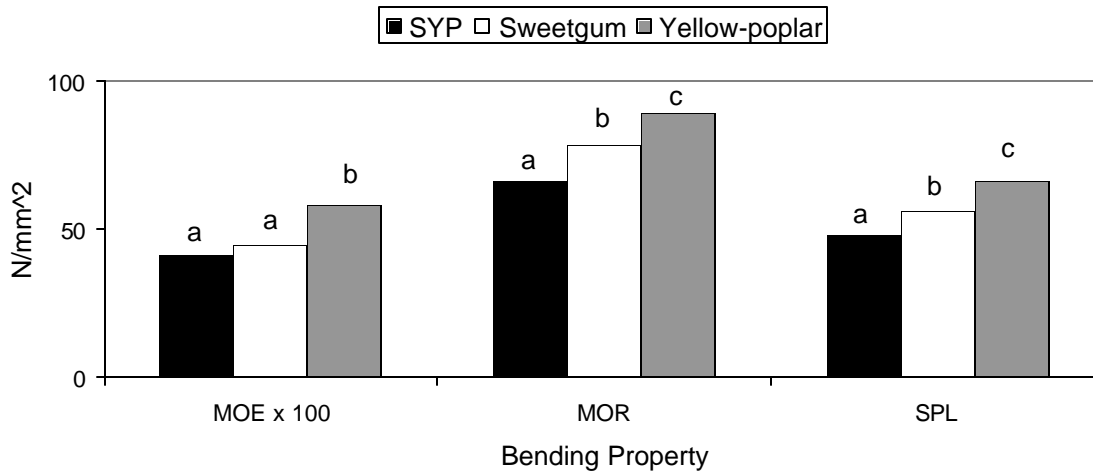
Table 4. Average Flake Bending Properties of the Three Species, Two Cutting Directions, and Three Drying Temperatures.

PARAMETER	MOE (N/mm ²)	MOR (N/mm ²)	SPL (N/mm ²)
Species			
SYP	4086.9 a	66.0 a	48.1 a
Sweetgum	4430.6 a	78.6 b	56.5 b
Yellow-poplar	5829.4 b	89.0 c	66.0 c
Cutting Direction			
Radial	4308.0 a	69.1 a	48.3 a
Tangential	5256.6 b	86.7 b	65.5 b
Temperature (°C)			
150	5401.6 a	87.7 a	64.3 a
200	4665.4 b	77.6 b	56.5 b
250	4280.3 c	68.3 c	49.6 c

Means with the same letter are not significantly different at $p=0.05$

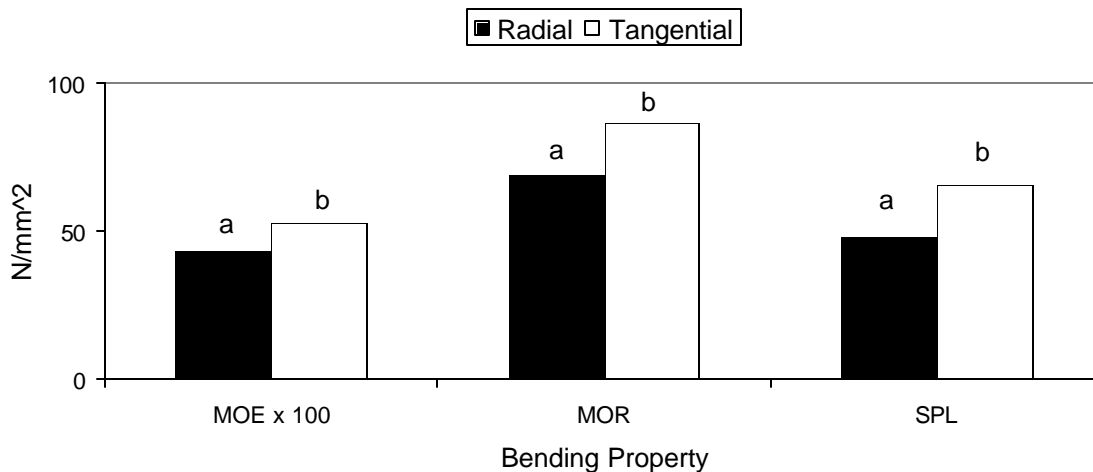
Radially-cut specimens have lower bending properties than tangentially-cut specimens (Table 4 and Figure 3). Radially-cut specimens have average values 4308.0, 69.1, and 48.3 N/mm² for

MOE, MOR, and SPL, respectively. On the other hand, tangentially-cut specimens have average values of 5256.6, 86.7, and 65.5 N/mm² for MOE, MOR, and SPL, respectively.



Note: Means with the same letter are not significantly different at $p=0.05$

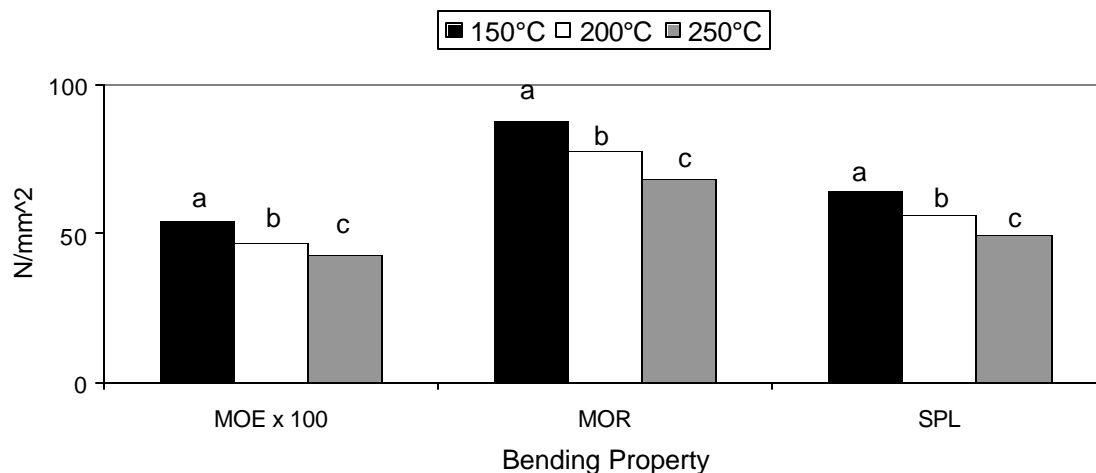
Figure 2 Average Bending Stiffness and Strength of the Three Species.



Note: Means of the same letter are not significantly different at $p=0.05$

Figure 3 Average Bending Stiffness and Strength of the Two Cutting Directions.

The effect of temperature on bending properties is also shown in Table 4 and in Figure 4. A decreasing trend in flake bending strength and stiffness with increased temperature was observed. The same trend was observed by Plagemann (1982), however, statistical analysis indicated that only MOE of flakes was significantly affected by temperature in his tests. In this experiment, the effect of temperature on MOE, MOR, and SPL were all highly significant. Specimens dried at 150°C have higher mean bending properties (MOE=5401.6 N/mm², MOR=87.7 N/mm², and SPL=64.3 N/mm²) than specimens dried at 200°C (MOE=4665.4 N/mm², MOR=77.6 N/mm², and SPL=56.5 N/mm²). Specimens dried at 250°C have the lowest mean bending stiffness and strength (MOE=4280.3 N/mm², MOR=68.3 N/mm², and SPL=49.6 N/mm²).



Note: Means with the same letter are not significantly different at $p=0.05$

Figure 4 Average Bending Stiffness and Strength of the Three Drying Temperatures

The previous discussion dealt with the ANOVA of measured bending properties of the three species combined. The succeeding discussions focus on the ANACOVA of adjusted bending strength and stiffness of each species. Specific gravity was used as covariate to compute for the adjusted means for MOE, MOR, and SPL.

Southern Yellow Pine

Bending properties of southern yellow pine are discussed. Shown in Table 5 is the ANACOVA of adjusted MOE, MOR, and SPL means of southern yellow pine using specific gravity as covariate and as influenced by cutting direction and drying temperature and their interaction. Cutting direction had a highly significant influence on all three bending properties of southern yellow pine. Effect of drying temperature was significant (at $p=0.05$) only on the MOE. Interaction of cutting direction and drying temperature was not significant. Thus, influence of drying temperature on bending properties of southern yellow pine flakes was not affected by cutting direction.

Table 5. P-values of MOE, MOR, and SPL of Southern Yellow Pine.

SV	DF	MOE	MOR	SPL
C	1	0.01	0.01	<0.01
T	2	0.02	0.10	0.24
C*T	2	0.80	0.49	0.39

Bending test results of southern yellow pine are presented in Table 6. Cutting direction had a significant effect on MOE, MOR, and SPL. Radially-cut specimens have lower bending properties than tangentially-cut specimens. Adjusted means of MOE, MOR, and SPL of radially-cut specimens were only 3030.2, 47.4, and 30.5 N/mm², respectively. Tangentially-cut specimens have higher adjusted means of MOE, MOR, and SPL calculated at 5143.6, 84.6, and 65.7 N/mm², respectively.

Table 6. Adjusted Means of Bending Stiffness and Strength of Southern Yellow Pine.

PARAMETER	SPECIFIC GRAVITY	MOE (N/mm ²)		MOR (N/mm ²)		SPL (N/mm ²)	
		MEAN	ADJ	MEAN	ADJ	MEAN	ADJ
Cutting Direction							
Radial	0.61	3469.9	3030.2 a	55.2	47.4 a	36.7	30.5 a
Tangential	0.54	4710.8	5143.6 b	76.9	84.6 b	59.5	65.7 b
Temperature (°C)							
150	0.60	5206.9	4940.1 a	79.3	74.5 a	55.3	51.4 a
200	0.56	3772.6	3959.6 ab	65.4	68.7 a	49.0	51.6 a
250	0.57	3281.1	3360.9 b	53.4	54.8 a	40.0	41.2 a

Means with the same letter are not significantly different at $p=0.05$

A decreasing trend in bending properties was observed when drying temperature increased (Table 6). However, statistical analyses showed that drying temperature only had a significant effect on MOE of southern yellow pine. Specimens dried at 150 (4940.1 N/mm²) and 200°C (3959.6 N/mm²) was significantly different from specimens dried at 250°C (3360.9 N/mm²). Also, specimens dried at 200 and 250°C have lower MOE than specimens dried at 150°C. Drying temperature was found to have no significant effect on MOR and SPL. Adjusted MOR means were 74.5, 68.7, and 54.8 N/mm² for specimens dried 150, 200, and 250°C, respectively. Adjusted means of SPL were 51.4, 51.6, and 41.2 N/mm² for specimens dried at 150, 200, and 250°C, respectively.

Sweetgum

ANACOVA (Table 7) of bending stiffness and strength of sweetgum is discussed. Effect of cutting direction was highly significant for all bending properties. Effect of temperature was also highly significant on MOE, MOR, and SPL. Interaction of cutting direction and drying temperature was not significant, similar to southern yellow pine. Thus, influence of temperature on bending properties of sweetgum was not affected by cutting direction.

Table 7. P-values of MOE, MOR, and SPL of Sweetgum.

SV	DF	MOE	MOR	SPL
C	1	<.01	<.01	<.01
T	2	<.01	<.01	<.01
C*T	2	0.65	0.40	0.50

Table 8 shows the bending test results of sweetgum. Cutting direction had a significant effect on adjusted means of MOR, MOE, and SPL. Similar to southern yellow pine, radially-cut specimens consistently have lower bending strength and stiffness than tangentially-cut specimens. Adjusted MOE, MOR, and SPL of 4135.2, 67.6, and 47.3 N/mm², respectively were calculated for specimens cut radially. On the other hand, specimens that were cut tangentially have adjusted MOR, MOE, and SPL means of 4726.1, 89.6, and 65.8 N/mm², respectively.

Table 8. Adjusted Means of Bending Stiffness and Strength of Sweetgum.

PARAMETER	SPECIFIC GRAVITY	MOE (N/mm ²)		MOR (N/mm ²)		SPL (N/mm ²)	
		MEAN	ADJ	MEAN	ADJ	MEAN	ADJ
Cutting Direction							
Radial	0.64	4153.4	4135.2 a	67.9	67.6 a	47.4	47.3 a
Tangential	0.63	4707.9	4726.1 b	89.2	89.6 b	65.6	65.8 b
Temperature (°C)							
150	0.61	4912.2	5012.2 a	90.7	92.6 a	69.4	70.1 a
200	0.66	4205.0	4144.6 b	75.9	74.7 b	52.2	51.8 b
250	0.65	4174.7	4135.1 b	69.2	68.4 b	48.0	47.7 b

Means with the same letter are not significantly different at p=0.05

Similar to southern yellow pine, a decreasing trend in bending properties when drying temperature increased was also observed in sweetgum (Table 8). Drying temperature had a significant effect on all bending properties of sweetgum, unlike in southern yellow pine wherein only MOE was affected. Specimens dried at 150°C were significantly different from specimens dried at 200 and 250°C. Bending properties of specimens dried at 200 and 250°C were no longer statistically significant. Adjusted MOR values of 5012.2, 4144.6, and 4135.1 N/mm² were calculated for

specimens dried at 150, 200, and 250°C, respectively. Adjusted means of MOE for specimens dried at 150, 200, and 250°C were 92.6, 74.7 and 68.4 N/mm², respectively. Adjusted SPL values for specimens dried at 150, 200, and 250°C were 70.1, 51.8, and 47.7 N/mm², respectively.

Yellow-poplar

ANACOVA of the bending properties of yellow-poplar is shown in Table 9. Effect of cutting direction on bending properties of yellow-poplar was not significant. Among the three species, only yellow-poplar had an insignificant effect of cutting direction on bending stiffness and strength. Temperature effect was significant on MOR but not significant on MOE and SPL at $p=0.05$. Cutting direction and drying temperature interaction was again insignificant, similar to southern yellow pine and sweetgum. Therefore, influence of temperature on bending properties of yellow-poplar was not affected by cutting direction.

Table 9. P-values of MOE, MOR, and SPL of Yellow-poplar.

SV	DF	MOE	MOR	SPL
C	1	0.17	0.22	0.10
T	2	0.07	0.02	0.06
C x T	2	0.94	0.96	0.90

Presented in Table 10 is the bending test results of yellow-poplar. Radially-cut specimens consistently have lower bending properties than tangentially-cut specimens, similar with southern yellow pine and sweetgum. However, the effect of cutting direction on bending properties of yellow-poplar was shown to be statistically insignificant. Adjusted means of MOE, MOR, and SPL were 5365.3, 85.3, and 61.6 N/mm², respectively for radially-cut specimens. MOE, MOR, and SPL adjusted values were 6293.5, 92.8, and 70.5 N/mm², respectively for tangentially-cut specimens.

Table 10 also shows the influence of drying temperature on bending properties of yellow-poplar. Drying temperature only had a significant effect on MOR wherein specimens dried at 150

(93.1 N/mm²) and 200°C (92.1 N/mm²) have higher bending strength than specimens dried at 250°C (82.0 N/mm²). Decreasing MOE and SPL at higher temperature was observed but found to be statistically not significant. Adjusted MOE of 6080.0, 6043.1, and 5364.4 N/mm² for specimens dried 150, 200, and 250°C, respectively were calculated. SPL adjusted values of 69.2, 68.6, and 60.4 N/mm², respectively were calculated for specimens dried 150, 200, and 250°C.

Table 10. Adjusted Means of Bending Stiffness of Yellow-poplar.

PARAMETER	SPECIFIC GRAVITY	MOE (N/mm ²)		MOR (N/mm ²)		SPL (N/mm ²)	
		MEAN	ADJ	MEAN	ADJ	MEAN	ADJ
Cutting Direction							
Radial	0.60	5307.8	5365.3 a	84.1	85.3 a	60.8	61.6 a
Tangential	0.55	6351.0	6293.5 a	94.0	92.8 a	71.2	70.5 a
Temperature (°C)							
150	0.58	6085.6	6080.0 a	93.2	93.1 a	69.2	69.2 a
200	0.58	6017.6	6043.1 a	91.6	92.1 a	68.3	68.6 a
250	0.59	5385.1	5364.4 a	82.4	82.0 b	60.6	60.4 a

Means with the same letter are not significantly different at p=0.05

Results of flake bending properties of the three species were compared with MOE and MOR of clear wood specimens taken from the Wood Handbook (FPS, 1999). Adjusted means of the bending properties of flakes were compared to bending properties of clear wood specimens dried at 12%. Variations between species and differences between flakes and clear wood specimens on bending stiffness and strength were observed. Table 11 clearly shows that flakes dried at high temperature have lower bending stiffness and strength compared to clear wood specimens dried conventionally. The reduction in bending properties was affected by high temperature. Exposure to high temperature for long periods causes permanent strength loss (Haygreen and Bowyer, 1996). This strength loss is a permanent effect due to degradation of wood substance (FPS, 1999).

Southern yellow pine had the greatest loss on MOE followed by sweetgum then yellow-poplar. Southern yellow pine remained to have the highest MOR loss followed by sweetgum. Clear

wood specimens of southern yellow pine have the highest bending properties but southern yellow pine flakes have the lowest bending properties. On the other hand, clear wood specimens of yellow-poplar have the least MOE and MOR but yellow-poplar flakes have the highest MOE and MOR. Apparently high temperature drying has a greater effect on the bending properties of southern yellow pine than on yellow-poplar.

Table 11. Comparison of Bending Properties Between Flake and Clear Wood Specimens.

SPECIES	FLAKE			CLEAR WOOD		
	SPECIFIC GRAVITY	MOE (N/mm²)	MOR	SPECIFIC GRAVITY	MOE (N/mm²)	MOR
Southern yellow pine	0.58	4067	66	0.51	12300	88
Sweetgum	0.64	4431	79	0.52	11300	86
Yellow-poplar	0.58	5829	89	0.42	10900	70

Differences in bending properties observed between species can be related to differences in specific gravity. Approximate relationship between various mechanical properties and specific gravity for clear straight-grained wood of hardwoods and softwoods are given as power functions (FPS, 1999). In the case of flakes, the coefficients must be changed so that the equations can be applied to bending properties of flakes dried at high temperature.

Even with equal average values of specific gravity, southern yellow pine had lower MOE and MOR than yellow-poplar. Yellow-poplar had a lower average specific gravity than sweetgum but yellow-poplar had better bending properties than sweetgum. Other than specific gravity, many factors may also be considered like anatomical differences, moisture content, and relative size of the test specimens, among others to account for the differences in bending properties between species.

Cutting direction had a significant effect on bending properties. Analyses by species revealed that effect of cutting direction was only significant on southern yellow pine and sweetgum but not on yellow-poplar. Radially-cut specimens consistently had lower MOE, MOR, and SPL than

tangentially-cut specimens. This was expected since force applied on radially-cut specimens was directed along the tangential axis of the flake specimens while force applied on tangentially-cut specimens is directed along the radial axis. Elastic behavior of wood along the tangential axis is always lower than elastic behavior along the radial axis. This is due to the fact that wood is an orthotropic material: i.e. it has unique and independent mechanical properties along the three mutually independent axes: longitudinal, radial, and tangential. Elastic ratios vary within species. This ratio also varies with specific gravity and moisture content.

Comparisons of the E_R/E_T ratio of the flakes and of clear wood specimens (FPS, 1999) show big differences (Table 12). Difference in elastic ratio between flake and clear wood can be attributed to the effect of high temperature on the bending properties of flakes. It is either the radial elasticity is greatly reduced in the case of sweetgum and yellow-poplar or the tangential elasticity is affected in the case of southern yellow pine.

Table 12. Comparison of Radial/Tangential Elasticity Ratio (E_R/E_T) of Flake and Clear Wood Specimens.

SPECIES	FLAKE	CLEAR WOOD
Southern yellow pine	1.7	1.4
Sweetgum	1.1	2.3
Yellow-poplar	1.2	2.1

A general trend of decreasing bending properties for increasing drying temperature was observed. Although significant differences were only detected on the MOE of SYP, on MOE, MOR, and SPL of sweetgum, and on MOR of yellow-poplar, the trend was consistently observed on all bending properties of the three species. Plagemann (1982) observed the same trend in his flake bending tests however, only MOE was found to be affected by dryer temperature while MOR was not affected. The decrease in bending properties as influenced by dryer temperature can be easily attributed to thermal degradation of the wood components when exposed at high temperature.

Haygreen and Bowyer (1996) stated that wood subjected to high temperature lead to permanent strength loss. The strength loss is a permanent effect due to degradation of the wood.

CONCLUSIONS

Bending properties of flakes differed between and within the three species. Yellow-poplar had the highest bending properties followed by sweetgum and southern yellow pine had the lowest bending stiffness and strength. The effect of cutting direction was similar on the three species. Radially-cut specimens were found to have lower MOE, MOR, and SPL than tangentially-cut specimens. Drying temperature was also found to have a significant effect on the bending properties of flakes. Effect of temperature was similar for the three species and did not depend on the cutting direction. A decreasing trend was observed for flakes dried at higher temperature.

Correlation between bending properties and specific gravity was analyzed by species. Measured bending properties were adjusted using specific gravity as covariate. This lead to a slight change in least square means of the MOE, MOR, and SPL of all three species. Bending properties were determined to be significantly different between radial and tangential cutting directions on southern yellow pine and sweetsgum but not on yellow-poplar. Significant difference caused by drying temperature was only detected on MOE of southern yellow pine; MOE, MOR, and SPL of sweetgum; and only MOR of yellow-poplar.

Drying of flakes at high temperature resulted in a dramatic decrease in bending properties when compared to clear wood specimens dried conventionally. MOE and MOR decreased by as much as 67% as in the case of southern yellow pine. The reduction of flake bending stiffness and strength was attributed to the thermal degradation. Wood subjected to high temperature lead to permanent strength loss and this loss is a permanent effect due to degradation of the wood substance.

Relative to OSB production, it would be ideal to use yellow-poplar or more of it in combination with other species and dried at lower temperature due to better bending properties as gleaned from the results of the flake bending experiments. Since southern yellow pine is the species predominantly used in OSB production, it may be an advantage to cut more flakes in the tangential direction to have flakes with higher bending properties but this is not yet practical. This idea may lead to better panels due to better bending properties of raw materials. Variability in properties between and within species causes variabilities in raw material properties but this is unavoidable. The only way to reduce the effect of variability is to spread out the materials within the panel.

Taking a closer look at the variables that affect bending properties, drying temperature is the most important parameter that radically affects the bending stiffness and strength of flakes. This is also the only parameter that can be easily controlled and monitored. Lower drying temperature definitely assures higher MOE, MOR, and SPL for dried flakes.

REFERENCES

- AMERICAN SOCIETY OF TESTING MATERIALS (ASTM). 1994. Methods of testing small clear specimens of timber D 143-94. 1994 Annual Book of ASTM Standards Vol. 04.10. Philadelphia, PA.
- AMERICAN SOCIETY OF TESTING MATERIALS (ASTM). 1994. Standard test methods for specific gravity of wood and wood-base materials D 2395-93. 1994 Annual Book of ASTM Standards Vol. 04.10. Philadelphia, PA.
- AMERICAN SOCIETY OF TESTING MATERIALS (ASTM). 1994. Standard test methods for direct moisture content measurement of wood and wood-base materials D 4442-92. 1994 Annual Book of ASTM Standards Vol. 04.10. Philadelphia, PA.
- AMERICAN SOCIETY OF TESTING MATERIALS (ASTM). 1994. Standard guide for moisture conditioning of wood and wood-base materials D 4933-91. 1994 Annual Book of ASTM Standards Vol. 04.10. Philadelphia, PA.
- BODIG, J. and B.A. JAYNE. 1982. Mechanics of Wood and Wood Composites. Van Nostrand Reinhold Co.

FOREST PRODUCTS SOCIETY (FPS). 1999. Wood Handbook: Wood as an Engineering Material. Reprinted from USDA Forest Service Forest Products Laboratory General Technical Report FPL-GTR 113.

GERHARDS, C.C. 1982. Effect of moisture content and temperature on the mechanical properties of wood: An analysis of immediate effects. Wood and Fiber 14(1): 4-36.

HAYGREEN, J.G. and J.L. BOWYER. 1996. Forest Products and Wood Science: An Introduction. 3rd ed. Iowa State University Press, Ames, Iowa.

OTT, R.L. 1992. An Introduction to Statistical Methods and Data Analysis. 4th ed. Wadsworth Publishing Co., Belmont, CA.

PLAGEMANN, W.L., E.W. PRICE and W.E. JOHNS. 1984. The response of hardwood flakes and flakeboard to high temperature drying. J. Adhesion 16:311-338.

PLAGEMANN, W.L. 1982. . The response of hardwood flakes and flakeboard to high temperature drying. Master's thesis. Washington State University, Pullman, WA.

SALAMAN, M. 1969. High-temperature drying and its effect on wood properties. For. Prod. J. 19(3): 27-34.

SNEDECOR, G.W. and W.G. COCHRAN. 1980. Statistical Methods. 7th ed. Iowa State University Press, Ames, Iowa.

STEELE, R.G.D. and J.H. TORRIE. 1980. Principles and Procedures of Statistics: A Biometrical Approach. 2nd ed. McGraw Hill, New York.

ATTACHMENT 4

MECHANISM OF FLAKE DRYING*

Edgar C. Deomano
Research Assistant

and

Audrey Zink-Sharp
Associate Professor
Department of Wood Science and Forest Products
Virginia Polytechnic Institute and State University
Blacksburg, Virginia 24061

* The authors wish to acknowledge the financial support of U.S. Department of Energy (DOE) project –DE–FC07–97ID13537– Moisture distribution and flow during drying of wood and fiber.

ABSTRACT

This research focuses on experimental investigations of the drying properties of wood flakes. Three species (southern yellow pine, sweetgum, and yellow-poplar) were tested. Experiments on flake drying and effect of flake properties (cutting direction and dimension) and an external factor (temperature) were used to evaluate the flake drying process. Observation on drying and drying rate curves revealed that the rate of moisture loss consists of two falling rate periods; no constant rate drying period was observed. First falling rate drying period is controlled by convective heat transfer. Bound water diffusion controls the second falling rate drying period. Species, cutting direction, dimension, and temperature were found to have significant effect on drying rate of wood flakes.

INTRODUCTION

OSB is manufactured through a simple process. First, logs are debarked then crosscut into short bolts. These bolts are passed through flaking machines to reduce them into flakes and dried to desired moisture content. Resin is applied and the furnish is spread evenly forming a mat to be pressed to its final thickness. For the flake drying process, dryers (rotary or conveyor) that employ high temperature convective drying and short residence/dwell time are used to achieve drying of large volumes of flakes. These dryers use a significant amount of energy and so an optimized process is essential in order to save energy. The industry currently relies on high temperature to drive the drying process. The challenge is to optimize residual heat of gas while maintaining acceptable drying rate and quality of dried materials. Spurred by the rising cost and shortage of energy, the industry needs innovative technology to conserve energy. To attain these goals, it is first necessary to gain the fundamental understanding of the drying mechanism of wood flakes.

Despite the increasing use of OSB, very few studies have been reported on the mechanism of flake drying. Drying of flakes is done in a different manner than conventional wood drying. Lumber drying must be done gradually to avoid defects and can take days or even weeks. In contrast, drying of flakes can take only seconds or minutes at high temperature. The lack of data on drying rate and experimentally derived insight into the mechanism that control the drying of flakes were the motivating factors for this research.

BACKGROUND

Convective drying of wood flakes is a continuous process with changes in moisture content and temperature of the material. These changes occur simultaneously and vary for different conditions and methods. A series of experiments was undertaken to achieve the following objectives: 1) to determine the moisture content and surface temperature of flakes during drying; 2) to develop a regression model that fits the flake drying curve; and 3) to determine the effect of several parameters on drying rate. This information will be the basis for understanding the flake drying process and to supplement the knowledge obtained from the literature.

The drying curve can be characterized by an equation that is differentiated to obtain the drying rate curve. Various equations have been used to characterize the drying of wood. A simple analytical approach has been the assumption that the drying rate is proportional to the average moisture content. This can be expressed as:

$$E = \exp(-kt) \quad (1)$$

where: E is relative moisture content

k is an empirical constant

t is time

This equation was used by Tschernitz and Simpson (1979) in determining the drying rate of northern red oak lumber but they added an empirical thickness coefficient to account for the effect of thickness. Rosen (1978, 1980a) presented a two-parameter model based on the exponential relationship of relative moisture content and time. The model fits the drying of wood and wood-based materials very well (Rosen, 1980b). Linearized transformation of the analytical equation (Eq. 1) was used by Silitonga (1983) in describing the drying curve of wood chips. His equation was in the form:

$$\ln E = -kt \quad (2)$$

Polynomials are also used in describing curvilinear relationships. These types of models are useful in situations where curvilinear effects are present in the response function. They are also useful in approximating functions to unknown and possibly very complex nonlinear relationships. Laytner (1989) used a 5th order polynomial equation to describe the drying of wafers:

$$M = b_0 + b_1t + b_2t^2 + b_3t^3 + b_4t^4 + b_5t^5 \quad (3)$$

where: M is moisture content

$b_0, b_1, b_2, b_3, b_4, b_5$ are regression coefficients

Another form of describing the drying of wood is piecewise linear regression. Comstock (1971) described the drying of veneer as a linear function of moisture content comprised of two falling rate periods. The same approach was done by Pang et al. (1997) to express the three drying periods (constant rate followed by two falling rate periods) of veneer based on simulations.

There are many variables that affect the drying properties of wood flakes. These can be categorized as process and material variables. The process variable of primary interest from the standpoint of drying mechanism is temperature. Material variables considered were wood species, cutting direction, and flake dimensions. This study incorporates these variables because of their effect on flake drying behavior. Southern yellow pine, sweetgum, and yellow poplar were used in the experiments based on their wide use in the OSB industry. Flakes were cut along two directions (radial and tangential). Four flake sizes were cut: 15x117, 15x152, 25x117, and 25x152 mm. Drying temperatures were at 150, 200, and 250°C.

MATERIALS AND METHODS

Fresh, green bolts, 1.5 m and around 30 cm in diameter of southern yellow pine (Pinus spp.) and sweetgum (Liquidambar styraciflua) were cut into 50 mm boards using a portable sawmill. Freshly-cut yellow-poplar (Liriodendron tulipifera) boards 50 mm in thickness were also obtained.

Sound boards from each species were segregated according to type of cut: flatsawn or quartersawn. Radially-cut specimens were taken from the flatsawn boards while tangentially-cut specimens were taken from quartersawn boards (Figure 1). Four block dimension (15x117, 15x152, 25x117, and 25x152 mm) were then randomly selected from the boards. Each block was properly labeled for easy identification. The blocks were placed in plastic bags segregated according to species and cutting direction and stored in a refrigerated room maintained at 2°C.

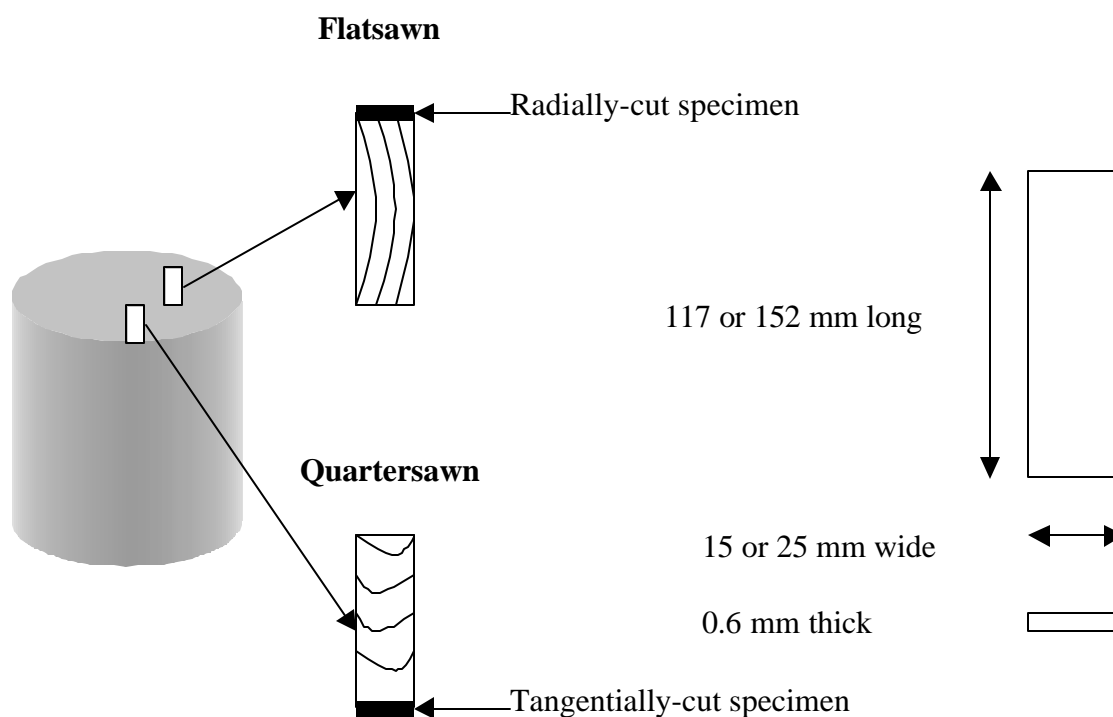


Figure 1 Cutting Diagram of Flake Drying Specimens

Drying Apparatus for Single Wafer Drying

An experimental drying apparatus was assembled so that a single flake could be dried at constant temperature and airflow while monitoring weight loss and surface temperature. It consisted of the following sub-assemblies as shown in Figure 2:

- A drying chamber with temperature control and uniform unidirectional flow;
- Balance for measuring weight loss;
- Infrared (IR) thermometer and thermocouple for measuring flake and air temperatures, respectively; and
- Automated data acquisition systems for monitoring of flake weight and temperature, and air temperature during drying.

The drying chamber was a mechanical convection oven (Lindberg/Blue MO 1440SA) with modifications particularly on the door. The door was installed with a double-walled glass panel and a zinc crystal to allow measurement of flake temperature.



Figure 2 Flake Drying Apparatus

A balance (Mettler PR1203) connected to an automated data acquisition system was placed on top center of the oven to measure the weight loss of the flake during drying. A wire that passes through the ceiling of the oven through a small hole was connected to the bottom weighing hook of the balance. An alligator clip was connected at the other end of the wire (inside the oven) where a single flake was suspended.

Flake temperature was measured using the IR thermometer (Omega OS552-MA-1). The IR thermometer was mounted right in front of the oven door. Temperature of the circulating air inside

the oven was monitored using a Type K fiberglass insulated thermocouple probe connected to a thermocouple thermometer (Cole-Parmer Digi-Sense 91100-50). The thermocouple was positioned right beside the flake. Both flake and air temperatures were monitored using automated data acquisition systems.

Flake Drying Experiments

Prior to drying, a block was randomly selected. Seven flakes with a target thickness of 0.6 mm were cut from each block using a CAE flaker. Six out of seven flakes cut from the block were used for drying experiments and the other one for moisture content and specific gravity determination. The first and second flakes were dried at 150°C, one at a time. The third and fourth flakes were dried at 200°C and the last two flakes were dried at 250°C. All flakes dried at the end of the day were placed inside the oven overnight at $102 \pm 3^\circ\text{C}$ for determination of oven-dry weight. Oven-dry weight was used for calculating the moisture content of the flake. Five replicates were done for every flake dimension. Total number of flakes dried in this experiment was 720. The extra flake was used for determination of moisture content and specific gravity. Table 1 shows the average initial moisture content and specific gravity of the flakes.

Table 1 Average Initial Moisture Content and Specific Gravity of the Flakes

SPECIES	MOISTURE CONTENT (%)	SPECIFIC GRAVITY
SYP	138.6	0.46
Sweetgum	96.6	0.55
Yellow-poplar	78.3	0.49

The drying oven was turned on and allowed to reach the desired drying temperature. Balance, IR thermometer, thermocouple thermometer, and data acquisition systems were also switched on prior to any drying experiment. Balance was tared and the IR thermometer was aimed

correctly at the wire rod. Once the temperature reading inside the oven had stabilized, balance and both thermometers started to acquire data. The oven door was opened and the wafer attached to the alligator clip quickly and the door closed immediately. The flake weight and temperature, and air temperature inside the oven were collected by the data acquisition systems every five seconds. Data logging was terminated when no significant weight loss was observed. The wafer was then taken out of the oven and then measured for thickness and labeled properly.

Statistical Analyses

The experimental data were analyzed. Experimental values of moisture content were plotted against time. This resulted in the drying curve of each flake. Each curve was fitted into equation 1 and 2). The equation that best fit the experimental data was selected to describe the flake drying curve. General Linear Model (GLM) and Nonlinear (NLIN) procedures of SAS were used in the regression analyses of the drying curve. Several criteria were used in testing validity of the regression model. Test for significance of the regression model was performed. Mean square error (MSE) and mean square regression (MSR) were checked. Tests on the parameter coefficients were also performed. Coefficient of determination (R^2) was also checked. Plots of observed versus fitted values and residuals were observed.

The drying rate was obtained by differentiating the drying curve model. Drying rates at specified moisture content levels were calculated. Multiple comparisons of drying rates between the several parameters were done using analyses of variance (ANOVA) and Tukey's test. Drying rate at specified moisture content levels was compared between species, flake dimension, cutting direction, and drying temperature using the split-plot design (Snedecor and Cochran, 1980; Steele and Torrie,

1980). Species represented the whole plots. Cutting direction, flake dimension, and temperature represented the sub-plots. The linear model considered for the analysis of drying rate is shown next:

$$\begin{aligned}
 y_{ijklm} = & \mu + S_i + C_j + SC_{ij} + D_k + SD_{ik} + CD_{jk} + SCD_{ijk} + \varepsilon_{ijkl}^{(A)} + \\
 & T_m + ST_{im} + CT_{jm} + SCT_{ijm} + DT_{km} + SDT_{ikm} + CDT_{jkm} + SCDT_{ijkm} + \\
 & \varepsilon_{ijklm}^{(B)} + \varepsilon_{ijklmp}
 \end{aligned} \tag{4}$$

where: y_{ijklm} is calculated drying rate

μ is mean

S_i is species effect

C_j is effect of cutting direction

SC_{ij} is interaction effect of species and cutting direction

D_k is effect of flake dimension

SD_{ik} is interaction effect of species and flake dimension

CD_{jk} is interaction effect of cutting direction and flake dimension

SCD_{ijk} is interaction effect of species, cutting direction, and flake dimension

$\varepsilon_{ijkl}^{(A)}$ is whole-plot error

T_m is temperature effect

ST_{im} is interaction effect of species and temperature

CT_{jm} is interaction effect of cutting direction and temperature

SCT_{ijm} is interaction effect of species, cutting direction, and temperature

DT_{km} is interaction effect of flake dimension and temperature

SDT_{ikm} is interaction effect of species, flake dimension, and temperature

CDT_{jkm} is interaction effect of cutting direction, flake dimension, and temperature

$SCDT_{ijkm}$ is interaction effect of species, cutting direction, flake dimension, and temperature

$\varepsilon_{ijklm}^{(B)}$ is split-plot error

ε_{ijklmp} is sampling error

RESULTS AND DISCUSSION

Drying Curve

A typical flake drying curve (Figure 3) indicates a non-linear relationship throughout the entire drying period. A continuous falling rate period was observed right from the start of every drying test. A linear trend reflecting a constant rate period typical of wood drying was not observed in all cases. Just like any other curve, the drying curve can be characterized by an equation. However, the mathematical relation between moisture content versus time of wood flakes is not well documented.

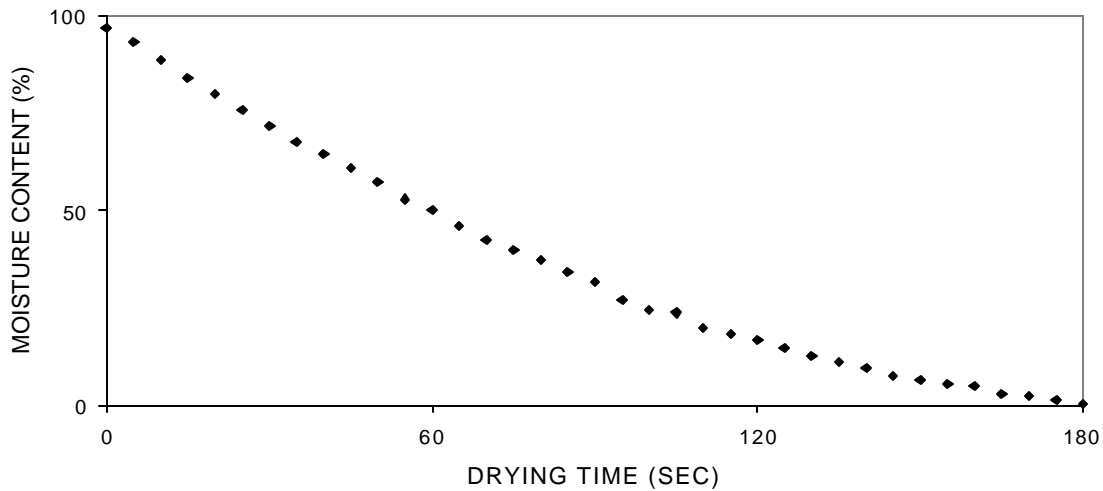


Figure 3 Typical Flake Drying Curve

Transformation of the data to get a linear fit was first tested. Logarithmic transformation of the relative moisture content (Eq. 2) still resulted in a curvilinear trend. The same logarithmic transformation was used by Silitonga (1983) in describing the drying of wood chips. However, his data transformation resulted in a near perfect linear fit. Various statistical tests suggested that his transformation was appropriate.

Since the logarithmic transformation was not appropriate to describe the drying of flakes, the data were fitted using the analytical relation (Eq. 1) between moisture content and drying time. The fit was not perfect with the exponential curve overestimating the early part of drying. Even with the addition of another parameter [i.e. bend factor (Rosen, 1978)], the exponential model was still not a good fit.

Since the logarithmic and exponential relationship of relative moisture content versus time was not good enough in describing the drying of flakes, the use of a polynomial equation was tested. Polynomial models are useful where a curvilinear effect is present in the true response function and

for approximating functions to unknown and possibly very complex nonlinear relationships (Montgomery and Peck, 1992).

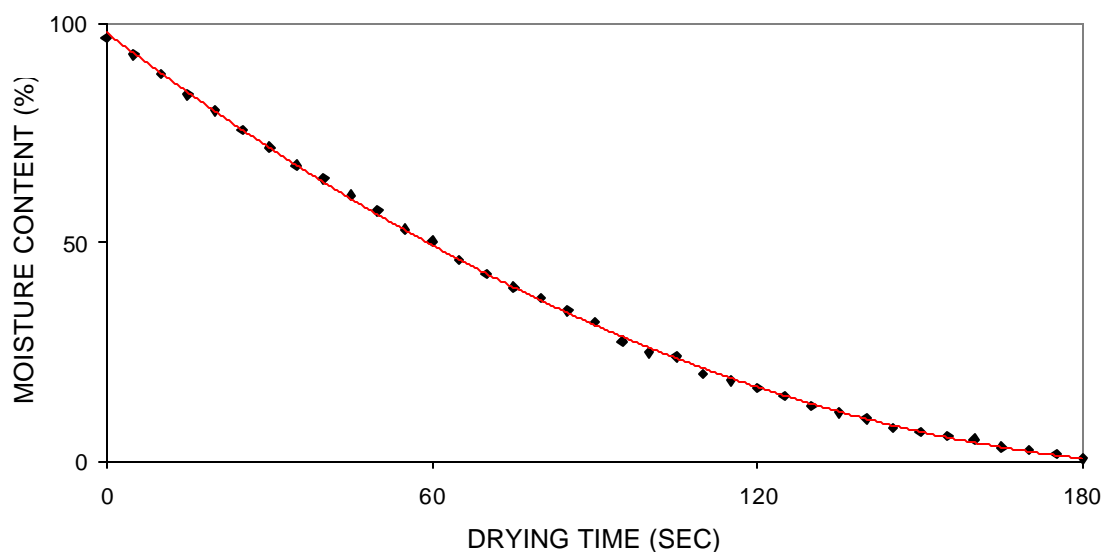


Figure 4 Plot of Experimental Data and Fitted Quadratic Model

A near perfect fit was obtained for a second-order/quadratic model (Figure 4). The order of the model was kept as low as possible. The use of higher-order polynomials should be avoided unless they are justified (Montgomery and Peck, 1992). A low-order model is always preferable to a high-order model. According to them, arbitrary fitting of high-order polynomials is a serious abuse of regression analysis.

The quadratic model was highly significant based on its ANOVA. MSE for every case was very small compared to the MSR. All three parameter coefficients (β_0 , β_1 , and β_2) in every case were significant. Standard error of the coefficients was very small. R^2 was at least 0.9900 for all cases. Observed values were very close to fitted values. As observed values of moisture content increased, the predicted value also increased. Residual plots showed random distribution of residuals above

and below the zero reference line. No distinct distribution pattern of residuals was observed indicating no obvious model defect.

The drying curve of flakes can now be modeled as:

$$E(y) = \beta_0 + \beta_1 X + \beta_2 X^2 \quad (4.)$$

where: $E(y)$ is estimated moisture content

β_0 is the intercept

β_1 is the linear effect coefficient

β_2 is the quadratic effect coefficient

x is time.

β_0 is related to initial moisture content. β_1 and β_2 are both related to the properties of the flakes and drying conditions. The quadratic model is adequate to describe the convective drying of wood flakes. This model can also be used to estimate the drying time needed to reach a given moisture content.

Initial moisture contents of the flakes were different. Therefore, the actual drying times were inappropriate for comparing the influence of flake properties and drying temperature on drying time. The drying rates at certain moisture content levels were calculated and used as a variable to measure the drying property of the flakes.

Drying Rate

The drying rate of each flake at prescribed moisture content was determined by differentiating the quadratic model that described the drying curve accurately. This approach gave the advantage of analyzing the data with the use of a single equation. Since the quadratic equation

fitted the data very well, the resulting drying curve should also be accurate. The drying rate curve is smooth having the same basic shape of the drying curve. Figure 5 shows the drying rate curve of the moisture content versus time plot shown in Table 3. The curve is based on the drying data of a sweetgum flake measuring 15x117 mm cut radially and dried at 150°C.

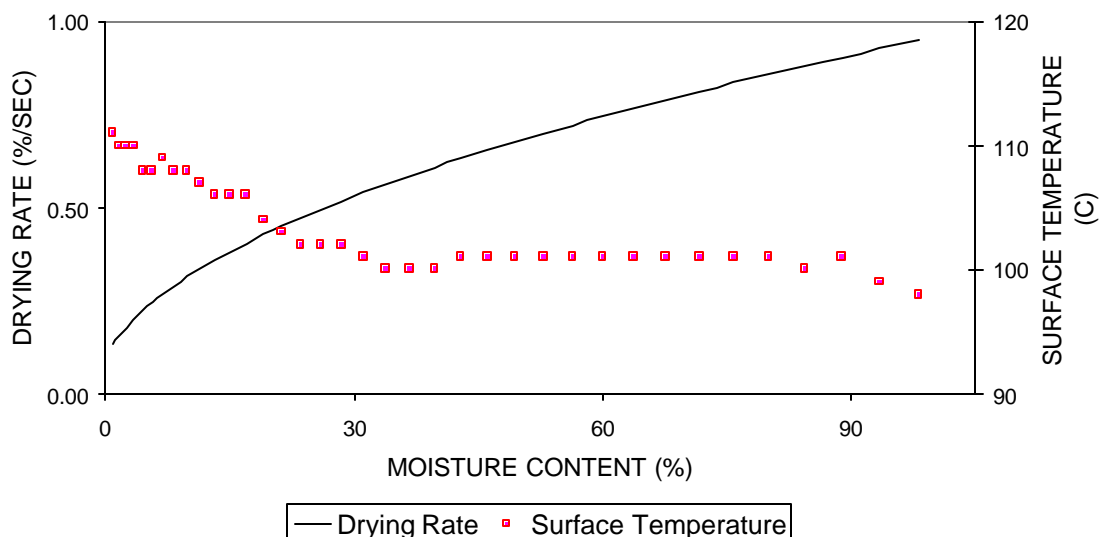


Figure 5 Typical Drying Rate Curve

Observations on drying rate curves revealed two drying regimes: first falling rate period followed by a second falling rate period. None of the specimens produced a constant rate drying period in the range of moisture contents under investigation, which is typical in the drying of wood. Similar observations were made on drying of wafers (Laytner, 1989), veneer (Comstock, 1971), and wood particles (Alves and Figueiredo, 1989; Di Blasi, 1998; Saastamoinen and Impola, 1995; Silitonga, 1983). This means that decreasing rate can occur in the presence of free water in the flakes.

All the drying rate curves have similar parabolic decrease in drying rate with decreasing moisture content. The decreasing rate begins right at the very start of the drying process. The

severeness of the drying conditions caused the decreasing rate to occur immediately in the drying period. At more severe drying conditions, the flake surface was probably not completely wetted. Some areas drop below the fsp before others. The free evaporation of liquid water occurs over a decreasing wetted surface area thus, a falling rate rather than a constant rate drying period. The presence of moisture gradient in small and thin wood have been observed based on experiments and simulations by several authors (Di Blasi, 1998; Laytner, 1989; Melaaen, 1996; Pang et al. 1997; Silitonga, 1983; Souza and Nebra, 2000). The extent of the gradient has significant bearing on the drying rate curve. At this stage of drying, convective heat transfer is the controlling mechanism. Same controlling mechanism was postulated for wafer (Laytner, 1989), veneer (Comstock, 1971; Pang et al. 1997), and wood particles (Alves and Figueiredo, 1989; Di Blasi, 1998; Melaaen, 1995; Saastamoinen and Impola, 1995; Silitonga, 1983; Souza and Nebra, 2000).

At about 30% moisture content, the rate of moisture loss indicates another decreasing rate. The drying rate curves have no abrupt deflection at this moisture content indicative of gradual switch from one drying mechanism to another. Temperature of the flake starts to increase. Surface moisture content reaches its maximum sorptive value. No free water exists. The moisture flow is produced by bound water only. The rate of moisture transport is limited by the ability of bound water to diffuse through the wood to its surface (Comstock, 1971; Fyhr and Rasmuson, 1996; Kayihan and Stanish, 1984; Laytner, 1989; Malte et al. 1976; Pang et al. 1997; Silitonga, 1983).

Drying rates at every 5% (below fsp) or 10% (above fsp) change in moisture content of each flake were determined. The succeeding subsections discuss the effect of several parameters on the drying rate of wood flakes. These parameters include species, cutting direction, dimensions, and drying temperature. ANOVA indicates that there were variations in drying rates between the main

parameters. The analyses showed that there were highly significant differences in drying rates between species, cutting direction, dimensions, and drying temperature.

EFFECT OF SPECIES

Analyses of the whole data set were limited to the 50 to 5% moisture content range. This was constrained by the data of yellow-poplar which had a low range of initial moisture content (50-101%). Analyses from 80 to 60% were between southern yellow pine and sweetgum only. Statistical analyses indicates that there were highly significant differences in drying rates from 80 to 60% between southern yellow pine and sweetgum and from 50 to 5% moisture content between the three species (Table 2). This is expected since wood has been established to have variations in drying properties between species (FPS, 1997 and 1999).

Table 2. Average Drying Rate of the Three Species.

MC (%)	SYP	SG	YP
120	1.498		
110	1.438		
100	1.378		
90	1.312		
80	1.244	1.193	
	a	b	
70	1.172	1.121	
	a	b	
60	1.095	1.044	
	a	b	
50	1.012	0.960	0.981
	a	b	b
40	0.922	0.885	0.869
	a	b	b
30	0.823	0.771	0.767
	a	b	b
25	0.768	0.710	0.707
	a	b	b
20	0.709	0.648	0.636
	a	b	b
15	0.644	0.580	0.557

10	a	b	c
	0.571	0.502	0.464
5	a	b	c
	0.488	0.408	0.345
	a	b	c

SYP - southern yellow pine

SG - sweetgum

YP - yellow-poplar

Means with the same letter are not significantly different at $p=0.05$

Drying rates are presented Table 2 and Figure 6 shows the drying rate curves of the three species. Among the three species, southern yellow pine had the fastest drying rate. This was followed by sweetgum, and yellow-poplar had the slowest drying rate except at 50%. From 80 to 60% moisture content, drying rates of southern yellow pine and sweetgum were statistically different. Drying rate of southern yellow pine remained significantly different from sweetgum and yellow-poplar from 50 to 5% moisture content. Higher drying rate of southern yellow pine can be attributed primarily to its specific gravity. Southern yellow pine had the lowest average (0.46) compared to the two other species (sweetgum had 0.55 and yellow-poplar had 0.49). Faster drying is expected as specific gravity decreases due to less water present in wood for a given moisture content. Also, drying rate increases with decreasing specific gravity because of a larger proportion of voids that promotes bulk flow and vapor diffusion. These are faster mechanisms than bound water diffusion that affect the drying rate.

Differences in drying rates of sweetgum and yellow-poplar were not significantly different at 50 to 20% but were significant at 15, 10, and 5%. According to Comstock (1971), veneer of the same density and thickness will follow the same drying curve. In this experiment, sweetgum and yellow-poplar have different average specific gravity and almost equal thickness but followed the same drying rate curve within a certain moisture content range. This may be explained by other factors such as permeability, porosity, and cell morphology, among others.

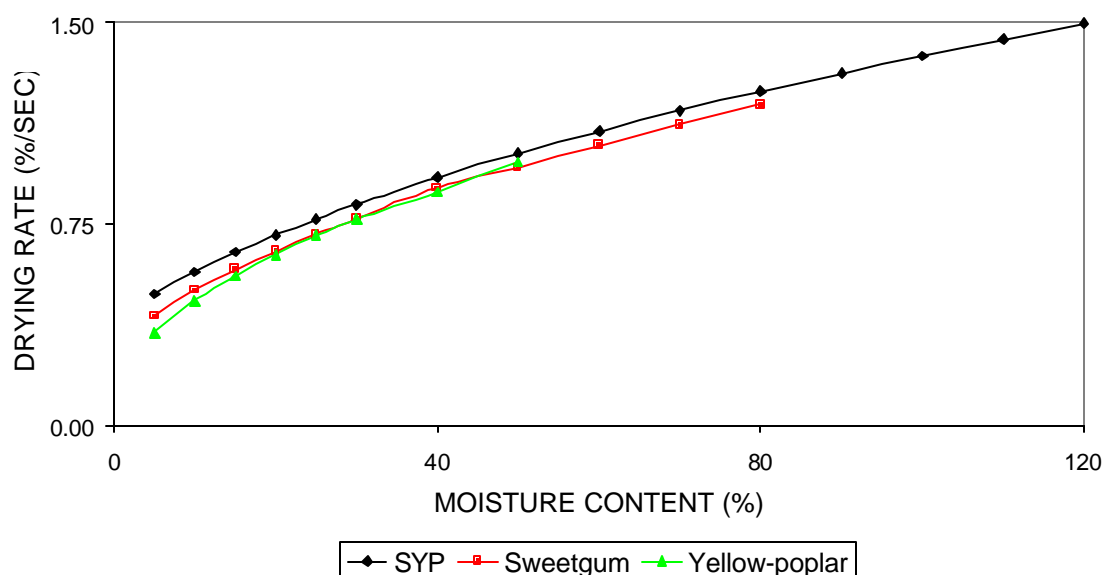


Figure 6 Drying Rate Curves of the three species

EFFECT OF CUTTING DIRECTION

Cutting direction was found to have an effect on the drying rates of flakes at all moisture content levels (Table 3). Drying rates between the two cutting directions are presented in Table 3 and the drying rate curves in Figure 7. Radially-cut specimens consistently have slower drying rates than tangentially-cut specimens at all moisture content levels. This may be explained by the exposure of wood rays on the wide surface of tangentially-cut specimens that provide passageways for water coming out of the flakes. Thus, faster drying rates for tangentially-cut specimens.

Table 3 Average Drying Rate of the Two Cutting Directions

MC (%)	R	T
80	1.186	1.251
	a	b
70	1.115	1.177
	a	b
60	1.040	1.099
	a	b
50	0.945	1.024
	a	b

40	0.855	0.929
	a	b
30	0.753	0.820
	a	b
25	0.697	0.759
	a	b
20	0.636	0.693
	a	b
15	0.567	0.619
	a	b
10	0.489	0.535
	a	b
5	0.394	0.433
	a	b

R - Radially-cut specimen

T - Tangentially-cut specimen

Means with the same letter are not significantly different at $p=0.05$

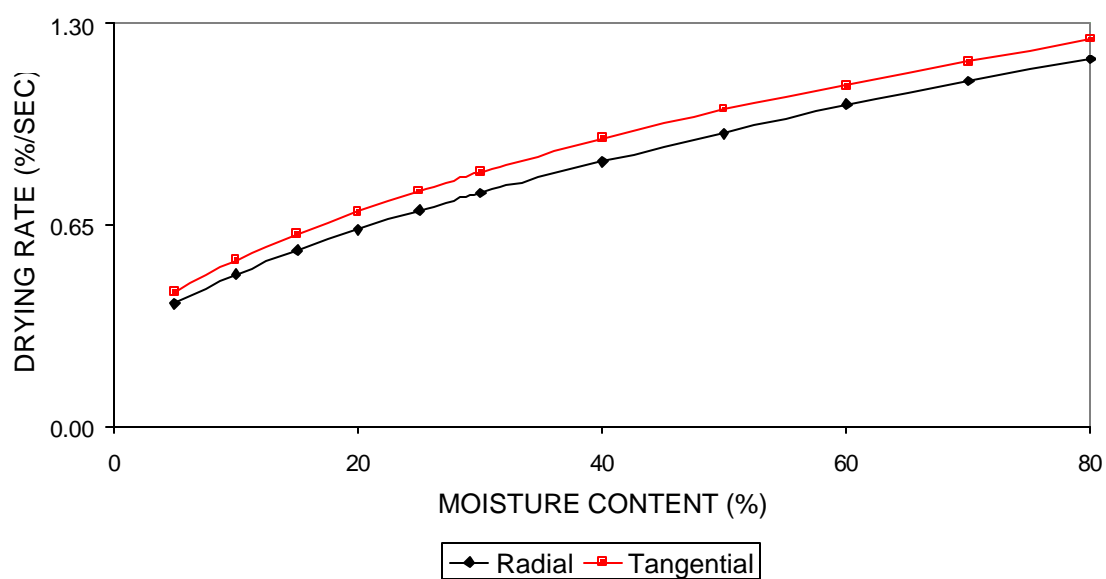


Figure 7 Drying Rate Curves of the Two Cutting Directions

EFFECT OF DIMENSION

Differences in drying rate between the four flake dimensions were found to be significant at all moisture content levels (Table 4). Drying rates of the four dimensions are shown in Table 4. Drying rate curves of the four dimensions are presented in Figure 8. Narrow flakes (15x117 and 15x152 mm) have faster drying rates than the wide flakes (25x117 and 25x152 mm). Width effect is caused by moisture transport along the transverse pathways (perpendicular to the wide surface) that serve as additional moisture passageways. Shorter width translates to lesser resistance thus, faster drying rate.

Table 4. Average Drying Rate of the Four Dimensions.

MC (%)	15x117	15x152	25x117	25x152
80	1.231 ab	1.301 a	1.174 b	1.167 b
70	1.157 ab	1.225 a	1.105 b	1.100 b
60	1.077 ab	1.143 a	1.030 b	1.027 b
50	0.977 a	1.041 b	0.953 a	0.965 a
40	0.881 a	0.944 b	0.865 a	0.878 a
30	0.774 a	0.833 b	0.764 a	0.776 a
25	0.715 a	0.772 b	0.706 a	0.720 a
20	0.650 a	0.705 b	0.644 a	0.659 a
15	0.577 a	0.630 b	0.575 a	0.591 a
10	0.493 a	0.545 b	0.497 a	0.514 a
5	0.390 a	0.442 c	0.401 ab	0.421 bc

Dimensions in mm

Means with the same letter are not significantly different at $p=0.05$

However, long flakes (15x152 and 25x152 mm) have faster drying rates than short flakes (15x117 and 25x117 mm). This can be explained by the lower average thickness of long flakes (0.68 mm) than the short flakes (0.72 mm). Drying rate of wood is generally more sensitive to thickness. Using the argument for the width effect, the short flakes should have faster drying rate than long flakes. This was consistent with the findings of Laytner (1989) on length effect on the drying of wafers.

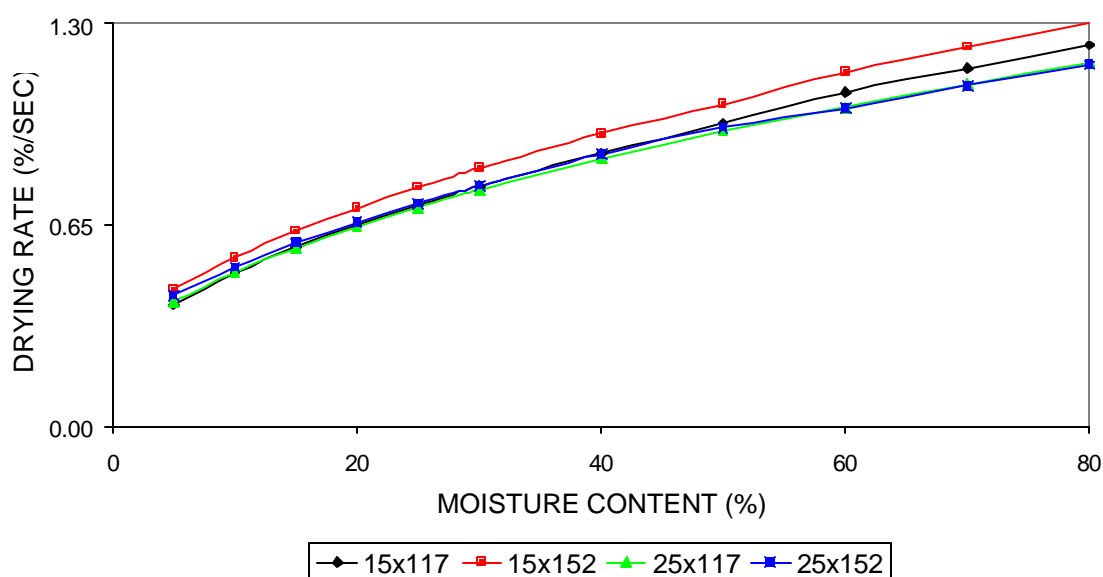


Figure 8 Drying Rate Curves of the Four Dimensions

EFFECT OF TEMPERATURE

Effect of temperature was found to be significant at all moisture content levels (Table 5). Influence of temperature on the drying rates is shown in Table 5 and Figure 9. Higher temperature has an effect on drying rate by virtue of higher thermal energy and mass transfer. An increase in temperature resulted in a roughly linear increase in drying rate of flakes. According to Comstock (1971), linear relationship between veneer drying rate and temperature holds true for temperatures

above 100°C. The linear increase in drying rate with increase in temperature is caused by the dependence of diffusivity, partial pressure and vapor pressure on temperature.

Table 5 Average Drying Rate of the Three Temperatures

MC (%)	150	200	250
80	0.850	1.208	1.597
	a	b	c
70	0.799	1.137	1.503
	a	b	c
60	0.744	1.060	1.403
	a	b	c
50	0.682	0.973	1.301
	a	b	c
40	0.616	0.880	1.180
	a	b	c
30	0.541	0.776	1.042
	a	b	c
25	0.499	0.719	0.966
	a	b	c
20	0.454	0.656	0.883
	a	b	c
15	0.403	0.586	0.791
	a	b	c
10	0.345	0.506	0.687
	a	b	c
5	0.272	0.409	0.560
	a	b	c

Temperature in °C

Means with the same letter are not significantly different at $p=0.05$

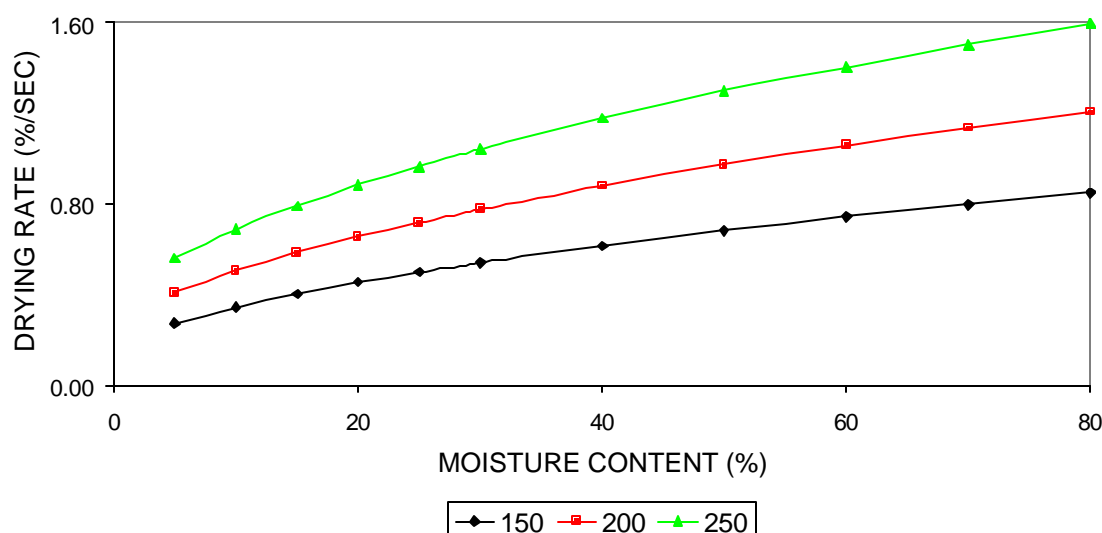


Figure 9 Drying Rate Curves of the Three Temperatures

Conclusions

The drying curve of flakes can be accurately described by a second-order/quadratic model. The validity of the model was tested using several criteria (i.e. test of significance of the model and parameter coefficients, MSE, MSR, R^2 , and plots of observed values versus fitted values and residuals).

Drying rate of the flakes was calculated by differentiating the quadratic model. Observation of drying rate curves revealed two falling rate drying periods. No constant rate drying was observed. The first falling rate period at the start of drying is attributed to the decreasing wetted surface area caused by severe drying conditions. Free evaporation of liquid occurs over a decreasing wetted surface area thus, no constant rate drying period. This period is predominantly controlled by convective heat transfer. At about 30% moisture content, the drying rate indicates a second falling rate. Temperature of the flake starts to rise. This period is controlled by internal bound water diffusion. The drying rate curve has no deflection indicative of a gradual switch from one mechanism to another.

Drying rates were found to vary between species. Southern yellow pine had the fastest drying rate at all moisture content levels followed by sweetgum. Yellow-poplar had the slowest drying rate. Difference in drying rates between species is attributed to specific gravity. Other factors such as permeability, porosity, and cell morphology may also play a role in affecting drying rates of flakes.

Cutting direction was found to have an effect on drying rates. Radially-cut specimens have slower drying rates than tangentially-cut specimens. This is due to the exposure of wood rays on the wide surface of tangentially-cut specimens that provide passageways for moisture coming out of the flakes.

Dimension of the flakes also had an effect on the drying rate. Narrow flakes have faster drying rates than wider flakes. Width effect is caused by moisture transport along the transverse direction that serves as additional passageways. Shorter distance means less resistance thus, higher drying rate. Following the same argument, short flakes should have higher drying rate than long flakes. However, long thinner flakes were found to have faster drying rates than the short thicker flakes. This brings the effect of thickness which is more sensitive to drying properties of flakes.

Temperature was found to have a highly significant effect on drying rate. An increase in temperature resulted in an approximately linear increase in drying rate at all moisture content levels. Same trend holds true for all three species. This is caused by the temperature dependence of moisture transport parameters.

It is apparent that flake properties and drying temperature have significant effects on drying rates. Therefore, these properties and conditions can be altered to optimize the drying rate of flakes. Flake properties were found to have an effect on drying rate. Thin, narrow, short, and tangentially-cut flakes are ideal to increase the drying rate. However, both cutting directions and flake

dimensions can be very difficult to control in the actual flaking process in OSB manufacture.

Given also the variability of properties (i.e. specific gravity, initial moisture content) that is usual in wood-based materials, flake properties may not be the variable to be controlled.

Drying condition (i.e. temperature) may be the better alternative since this parameter can be easily controlled and monitored to increase the drying rate. Since the early part of drying is controlled by heat transfer, temperature plays an important role in the flake drying process.

REFERENCES

- ALVES, S.S. and J.L. FIGUEIREDO. 1989. A model for pyrolysis of wet wood. *Chem. Engg. Sci.* 44(12): 2861-2869.
- COMSTOCK, G.L. 1971. The kinetics of veneer jet drying. *For. Prod. J.* 21(9): 104-111.
- Di BLASI, C. 1998. Multi-phase moisture transfer in the high-temperature drying of wood particles. *Chem. Engg. Sci.* 53(2): 353-366.
- FHYR, C. and A. RASMUSON. 1996. Mathematical model of steam drying on wood chips and other hygroscopic porous media. *AIChE J.* 42(9): 2491-2502.
- FOREST PRODUCTS SOCIETY (FPS). 1999. *Wood Handbook: Wood as an Engineering Material*. Reprinted from USDA Forest Service Forest Products Laboratory General Technical Report FPL-GTR 113.
- FOREST PRODUCTS SOCIETY (FPS). 1997. *Dry Kiln Operator's Manual*. Reprinted from USDA Agricultural Handbook No. 188.
- KAYIHAN, F. and M.A. STANISH. 1984. Wood particle drying: A mathematical model with experimental evaluation. In *Drying '84*. pp. 330-347.
- LAYTNER, F., N. EIPSTEIN, J.R. GRACE and K.L. PINDER. 1991. Kinetics of wood wafer drying. *Drying '92*. pp. 1135-1144.
- LAYTNER, F. 1989. *Fundamentals and Technology of Wafer Drying*. Ph. D dissertation. University of British Columbia.
- MALTE, P.C., R.W. COX, W.J. KENNISH, S.C. SCHMIDT, R.J. ROBERTUS, G.R. MESSINGER and M.D. STRICKLER. 1976. Experiments on the kinetics and mechanisms of drying small wood particles. Research Report TEL-76-8. Thermal Energy Laboratory, College of Engineering, Washington State University, Pullman, WA.

- MELAAEN, M.C. 1996. Numerical analysis of heat and mass transfer in drying and pyrolysis of porous media. *Numerical Heat Transfer, Part A* 29(4): 331-355.
- MONTGOMERY, D.C. and E.A. PECK. 1992. *Introduction to Linear Regression Analysis*. 2nd ed. Wiley-Interscience.
- PANG, S., S.G. RILEY and A.N. HASLETT. 1997. Simulation of Pinus radiata veneer drying: Moisture content and temperature profiles. *For. Prod. J.* 47(8): 51-58.
- ROSEN, H.N. 1980a. Wood behavior during impingement drying. *Dying '80* pp. 413-421.
- ROSEN, H.N. 1980b. Empirical model for characterizing wood drying curves. *Wood Sci.* 12 (4): 201-206.
- ROSEN, H.N. 1978. Evaluation of drying time, drying rates, and evaporative fluxes when drying with impinging jets. *Proc. First International Symposium on Drying*. McGill Univ, Science Press, Princeton, NJ. pp. 192-200.
- SAASTAMOINEN, J.J. and R.K. IMPOLA. 1995. Drying of solid fuel particles in hot gases. *Drying Tech.* 13(5-7): 1305-1315.
- SILITONGA, T.M. 1983. Moisture transport rate and energy consumption for convective drying of fuelwood chips. PhD dissertation. University of Minnesota.
- SNEDECOR, G.W. and W.G. COCHRAN. 1980. *Statistical Methods*. 7th ed. Iowa State University Press, Ames, Iowa.
- SOUZA, M.E.P. and S.A. NEBRA. 2000. Heat and mass transfer model in wood chip drying. *Wood and Fiber Sci.* 32(2): 156-163.
- STEELE, R.G.D. and J.H. TORRIE. 1980. *Principles and Procedures of Statistics: A Biometrical Approach*. 2nd ed. McGraw Hill, New York.
- TSCHERNITZ, J.L. and W.T. SIMPSON. 1979. Drying rate of northern red oak lumber as an analytical function of temperature, relative humidity, and thickness. *Wood Sci.* 11(4): 202-208.

Attachment 5

GEOMETRIC MODELING OF WOOD TRANSVERSE THERMAL CONDUCTIVITY FOR
SOFTWOOD SPECIES*

Hongmei Gu, *Ph.D*
Dr. Audrey Zink-Sharp, *Associate Professor*

Wood Sci. & Forest Products,
Virginia Polytechnic Institute & State University,
Blacksburg, VA 24060

* The authors wish to acknowledge the financial support of U.S. Department of Energy (DOE) project –DE–FC07–97ID13537– Moisture distribution and flow during drying of wood and fiber.

Abstract

Thermal conductivity of wood is the important parameter for measuring heat transfer rate in wood. The accuracy and consistency for the values of thermal conductivity of wood with a wide range of moisture content are required for the drying model development and industry operations. Wood material properties are structure dependent. Geometric models for predicting softwood thermal conductivity in radial and tangential directions were proposed and examined. The models were generated from wood anatomical structure observation and measurements. Structure observation was made under the Scanning Electron Microscope and Environmental Scanning Electron Microscope and measurements were performed with the help of image analysis. Modeling the effective thermal conductivity in radial and tangential direction is helpful to understand the heat transfer mechanism in the two directions and predict the values in a wide range when the practical experiments for obtaining those values are hard to make.

Model estimations provide insights for changes of the heat transfer parameters -- thermal conductivity, with the independent variables used in the model. Theoretical estimations for the radial thermal conductivity of softwood species is greater than the tangential thermal conductivity for moisture content below FSP due to the structure difference in the two directions. A linear relationship was found between moisture content (in the range of 0%-30%) and the radial thermal conductivity, while a less significant linear

relationship is between moisture content and the tangential thermal conductivity. Both radial and tangential thermal conductivity are increasing with the increase of latewood percentage in wood. When MC is above FSP with free water appears in wood samples, tangential and radial thermal conductivity increase dramatically and nonlinearly with the moisture content increase. No significant difference was found between the radial and tangential thermal conductivity above FPS. The geometric difference in the two directions has little affect on the model estimated thermal conductivities when free water takes part of the cell lumen.

1. INTRODUCTION

Wood is a typical porous material. The porosity and free of electrons give wood and wood-based materials the good insulating properties. The low thermal conductivity and good strength make them of special interest for building construction, refrigerators, cars and beer barrels, etc. (Ward 1960). The structure of wood is complicated and direction dependent. For instance, there are thick-walled latewood tracheids and thin-walled earlywood tracheids in the softwood species. Most of the cells are in the longitudinal direction as the tree's grain direction. Some of wood cells, such as ray cells, are arranged in the radial-transverse direction, perpendicular to the grain direction. It is the structure of wood that makes it an anisotropic material. Wood material properties, such as thermal conductivity, are structure dependent. Thermal conductivity of wood varies with the direction of heat flow with respect to the grain, varies with specific gravity, defects, extractives, and also the moisture content in wood and temperature (MacLean 1941). The theoretical models for examining the relationship between wood structure and thermal conductivity have been studied for years (Kollmann & Malmquist 1956, Siau et al. 1968, Couturier 1996). But no theoretical values for wood thermal conductivity in three directions ---- longitudinal, radial and tangential ---- have been given and compared with experiments. And, no theoretical prediction for the thermal conductivity change with structure and moisture content change is available.

Thermal conductivity of wood is usually measured by the steady-state method, which usually requires some time for wood samples to reach equilibrium. If the wood samples contain high moisture content, it will take a fairly long time for the moisture distribution in wood to reach the equilibrium state. It is not quite realistic to measure the thermal conductivity of high moisture wood samples with the current experiment method. With the help of theoretical modeling of the wood thermal conductivity, it will be possible to predict the change of this property in an extended range of moisture content. Knowledge of thermal conductivity of wood in a large range of moisture content is important for kiln-drying operations, preservation impregnation, hot pressing of wood based composites, wood thermal degradation and other process in which wood is subjected to a temperature change.

2. BACKGROUND

The anatomical structure difference of softwood species in the three orthogonal directions has been studied for a long time (Haygreen & Bowyer 1982, Hoadley 1980). The majority component of softwood species is long slender cells called longitudinal tracheids, which occupy about 90-95% of the total wood volume. On the cross section of a tree, they are close to rectangular shape with different cell wall thickness. Tracheids that are formed early in a growing season are thin-walled cells with greater diameters, while those formed later in the year are thick-walled cells with smaller diameters. Tracheids give softwood the mechanical strength required (especially the thick-walled latewood tracheids) and provide for heat and mass transport. The heat transfer in wood is mainly by conduction through the cell walls, and partly by the convection of air in the cell lumens. Another important type of cells in softwood is ray cell, which include ray tracheids and ray parenchyma arranging in radial strands perpendicular to the grain direction. Ray cells are small compared to the longitudinal tracheids

The ability of a material to conduct heat as a result of transmitting molecular vibrations from one atom or molecule to another varies greatly depending upon the chemical nature of the material and its gross structure. Thermal conductivity, k , is expressed in terms of quantity of heat, Q , that flows across unit thickness, x , of a material with a unit cross section, A , under unit temperature difference between the two faces, T , in unit time, t :

$$k = \frac{Q * x}{A * T * t}$$

Equa. (1)

Thermal conductivity of wood has been showed related to the structure of wood and moisture content in wood. Wangaard (1940, 1943) tried to predict thermal conductivities on the basis of specific gravity and moisture content from his experimental results with several wood species. The linear relationship between thermal conductivity and density of wood was also found by Van Dusen (1920), Rowley (1933), MacLean (1941), Urakami and Fukuyama (1981). The significant variables affecting the rate of heat flow in wood are concluded as: 1).density of wood; 2).moisture content of wood; 3).direction of heat flow with respect to the grain; 4).relative density of latewood and earlywood and proportion of latewood and earlywood in the lumber; 5).extractives or chemical substances in the wood, and defects, etc. MacLean (1941) gave two explicit expressions for estimating thermal conductivity as a faction of moisture content and specific gravity of wood. Moisture content's significant influence on wood thermal conductivity is easy to understand. Since wood is a porous material, its insulating nature results from the dead air in cell lumens. According to Jay (1957), water vapor in these spaces has little effect, but free water in the spaces increases the conductivity considerably.

The wood structure influence, such as the grain orientation, on thermal conductivity has been proved by several scientists (Griffiths and Kaye 1923, Wangaard 1940, MacLean 1941, Hendricks 1962, and Suleiman 1999). The conductivity in wood longitudinal direction is found to be about 2.25 to 2.75 times the conductivity in transverse direction. Griffiths and Kaye (1923) found the thermal conductivity of wood in the radial direction to be about 5% to 10% greater than in the tangential direction. Rowley (1933) found that in species with strongly marked springwood and summerwood, tangential conductivity was somewhat greater than radial conductivity, but no appreciable differences exists between conductivities in radial and tangential direction in woods which possess uniformity of structure throughout the annual ring. However, Wangaard (1940) found that in hardwoods radial conductivity exceeds tangential conductivity by a comparatively small but significant amount. He attributed this difference to the influence of the significant amount of wood rays in hardwoods. The ray volume in hardwoods is about 17 to 20%, while in softwoods the ray volume is only about 7%. This is why he found there was no significant difference between radial and tangential conductivity in softwoods. According to Steinhagen's (1977) review, it appears that the ratio of the tangential to radial conductivity is primarily determined by the volume of the ray cell in hardwoods and by the latewood volume in softwood.

Investigations on wood thermal conductivity for the past 80 years have provided us with the empirical models for predicting thermal conductivity from its influences, such as density or specific gravity, moisture content, and temperature, etc. Some theoretical models were studied based on the understanding of heat transfer mechanism, but all were based on single cell's structure (Kollmann and Malmquist 1956, Siau et al. 1968, 1995, and Couturier et al. 1996), without taking the macro-structure of wood into the consideration, such as cell arrangement and earlywood/latewood interaction. Also the models were not differentiated for different directions of wood structure.

3. EXPERIMENTAL RESEARCH ON WOOD ANATOMICAL STRUCTURE

3.1 MATERIALS AND METHODS

The purpose of this test is to observe the general structure difference in the radial and tangential directions. Two softwood species -- southern yellow pine (*Pinus spp.*) and Scots pine (*P. sylvestris*) were selected in this study, which are the most popular construction lumber used species in America and Europe.

Southern yellow pine were collected and examined at Virginia Tech, Blacksburg, Virginia. Scots pine materials were collected and examined at the EMPA (The Swiss Federal Institute for Material Testing), Switzerland. Approximate 6×6×6 mm cubes were cut from each species. One clear, smooth surface of the cube was cut by a razor blade for the Scanning Electron Microscope (SEM) observation. All the cubes were fully saturated in a special vacuum container before they were surfaced. After cut, the sample cubes were

subjected to the drying process to get rid of all of moisture in the samples because the Scanning Electron Microscope requires completely dry samples to work in a vacuum environment. The dried samples were mounted on the SEM sample holders and sputter coated with platinum or gold and then inserted into the Scanning Electron Microscope for observation. Southern yellow pine samples were observed with the AMRAY 1800 Scanning Electron Microscope at Forest Products Brooks Center of Virginia Tech, and Scots pine samples were observed in the field emission scanning electron microscope (FE-SEM) JEOL-6300-F at EMPA, Switzerland. In order to compare the cell wall percentage on the cross section between dried and wet wood samples, Scots pine saturated samples were examined under the Philips XL30-FEG Environmental Scanning Electronic Microscope with field emission cathode (FE-ESEM) at the University of Basel, Switzerland. This ESEM equipment eliminates the high vacuum in the microscope chamber of conventional SEMs, and uses a high-pressure gaseous atmosphere for study of wet or oily samples. This allows the observation in a normal environment, i.e. in a humid atmosphere with normal air pressure. So, the cell wall thickness of the radial and tangential wall could be measured under the 'original' wet condition to compare with the dry sample cell wall amount.

Transverse sections of the two species were examined under the Scanning Electron Microscope (SEM) and Environmental Scanning Electron Microscope (ESEM). Twenty clear images were collected from southern yellow pine, 10 of which were from the earlywood area (Figure 1), and the other 10 were from the latewood area (Figure 2).

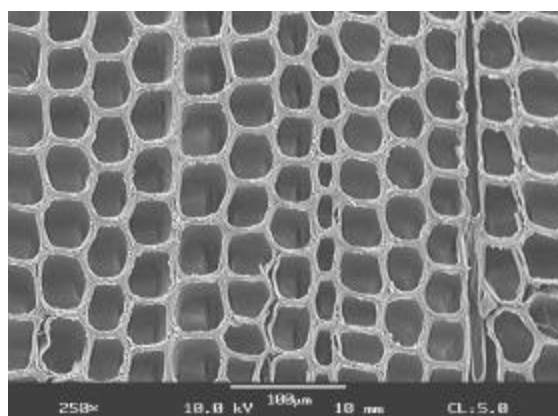


Figure 1 Southern yellow pine earlywood image.

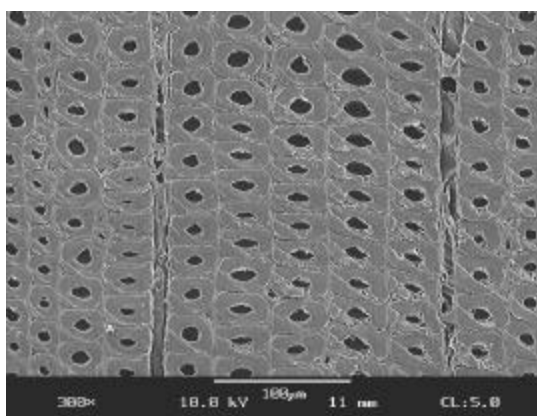


Figure 2 Southern yellow pine latewood image.

Ten images of dry earlywood and latewood structure were collected from the Scots pine sample cubes, five of which were latewood images (Figure 3), and the other five images were latewood structure (Figure 4). The same amount of images was collected from the Scots pine saturated samples by the ESEM (Figure 5, 6).

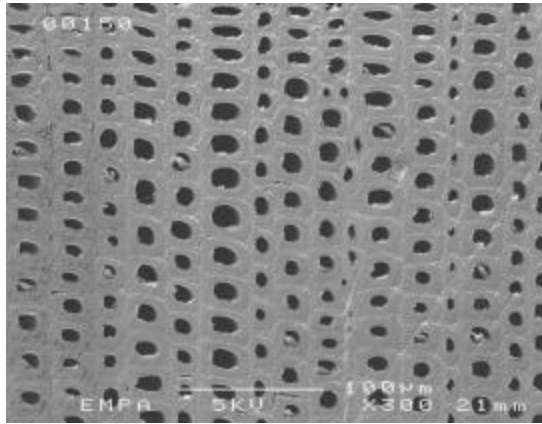


Figure 3 Scots pine latewood image (dry condition).

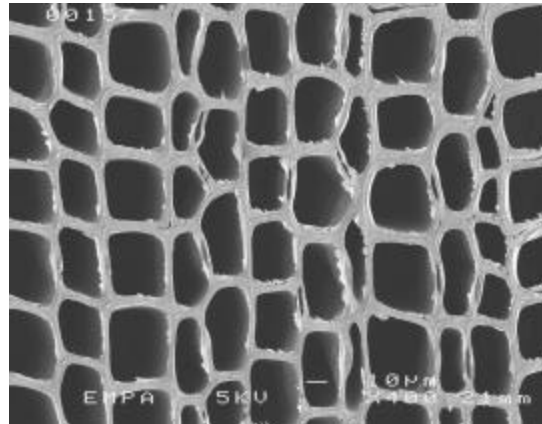


Figure 4 Scots pine earlywood image (dry condition).

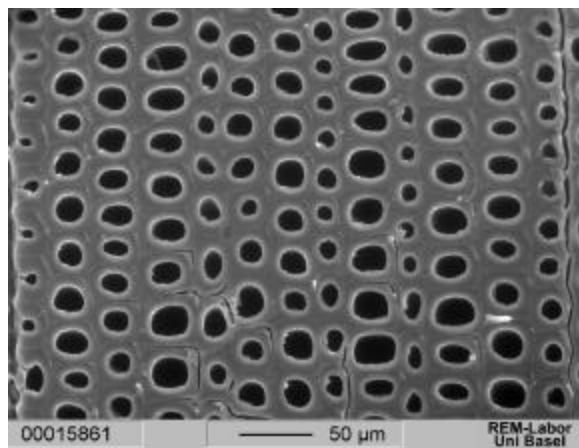


Figure 5 Scots pine latewood image (green condition)

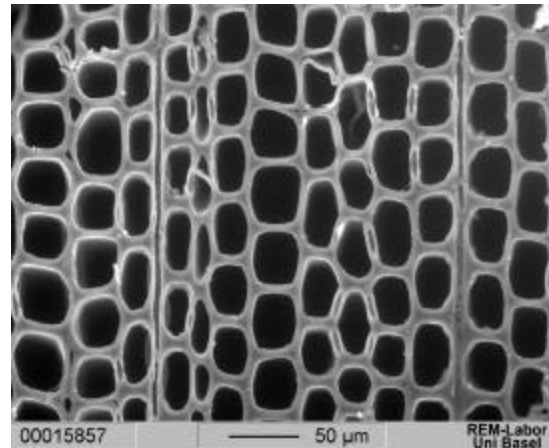


Figure 6 Scots pine earlywood image (green condition).

After all the required images were collected, they were loaded into the image analysis software for measurement. Ten random lines were drawn on each image horizontally and vertically. (Horizontal direction

on the image correspond to the tangential direction of wood structure, and vertical direction corresponds to the radial direction). Cell wall percent on each line were measured and calculated.

3.2 RESULTS AND DISCUSSION

One obvious gross structure on the cross section of wood is the growth ring. Tree growth is characterized as fast growing in early spring and slowing down in late summer before ceasing in the fall. This growing style gives wood structure an alternating arrangement of earlywood and latewood on the cross section. In earlywood, cells are big with thin cell walls and large lumens, while in latewood cells are relatively small with very thick walls and small lumens. Due to this structure difference between the earlywood cells and latewood cells, the physical and mechanical properties of earlywood and latewood are very different. The amount of earlywood and latewood on the cross section of wood varies from ring to ring and from sample to sample. The overall wood physical and mechanical properties are related to the amount of earlywood and latewood contained in wood. The simplified structure for the softwoods can be displayed as shown in Figure 7. The earlywood and latewood are in parallel arrangement in the tangential direction, and in series arrangement for the radial direction. It can be further modified or simplified by moving all the latewood together on the top, and all the earlywood together at the bottom. The geometric models will be based on this simplified structure of softwood species.

From the images of the two softwood species ---- southern yellow pine (Figure 1 and 2) and Scots pine (Figure 3 and 4), it was observed that the arrangement of individual cells (most of them are longitudinal tracheids) is neat for both earlywood and latewood. They are aligned perfectly in the radial direction with several small rays between the aligned tracheids. The cells are arranged alternately in the tangential direction. Among all the randomly drawn lines in the tangential direction across the image, there was no one single line with all the cell wall occupied. It was always cell wall and cell lumen alternately arranged. But in the radial direction, there was a part of the image with full cell wall running through the whole radial lines (vertical lines on the image). This part is the side walls of radially aligned cells. The effective thermal conductivity of wood represents the resultant thermal conductivity of the major components in wood ----cell wall substance and air in cell lumen. Therefore the arrangement and the amount of the cell wall in the two directions are the basis for setting up the wood thermal conductivity geometric models.

The averaged cell wall percent in the radial and tangential direction for the two softwood species were measured, calculated and concluded in Table 1 and 2. The side-wall percentage in the radial direction were also measured and shown in the tables.

These measurements were obtained by using image analysis software. Each result was averaged from 50 (for Scots pine) or 100 (for SYP) measurements. The large number of the data measured provides confidence to assume a normal distribution of these data. Based on the normal distribution assumption, the statistical ANOVA can be applied on these data to examine the significant difference between the species, between the earlywood and latewood, and between the radial and tangential direction.

The *generalized random block design (GRBD)* statistical model analysis results showed that the cell wall percentages in the tangential direction were significantly greater than the cell wall percentages in the radial direction for both earlywood and latewood in the two softwood species. If there is a difference for the cell wall substance in the radial and tangential directions, the heat transfer property – thermal conductivity, may show differences in the two directions too, because heat transportation in wood mainly goes through the cell wall part. No significant difference of the cell wall substance between the two softwood species was found for both earlywood and latewood.

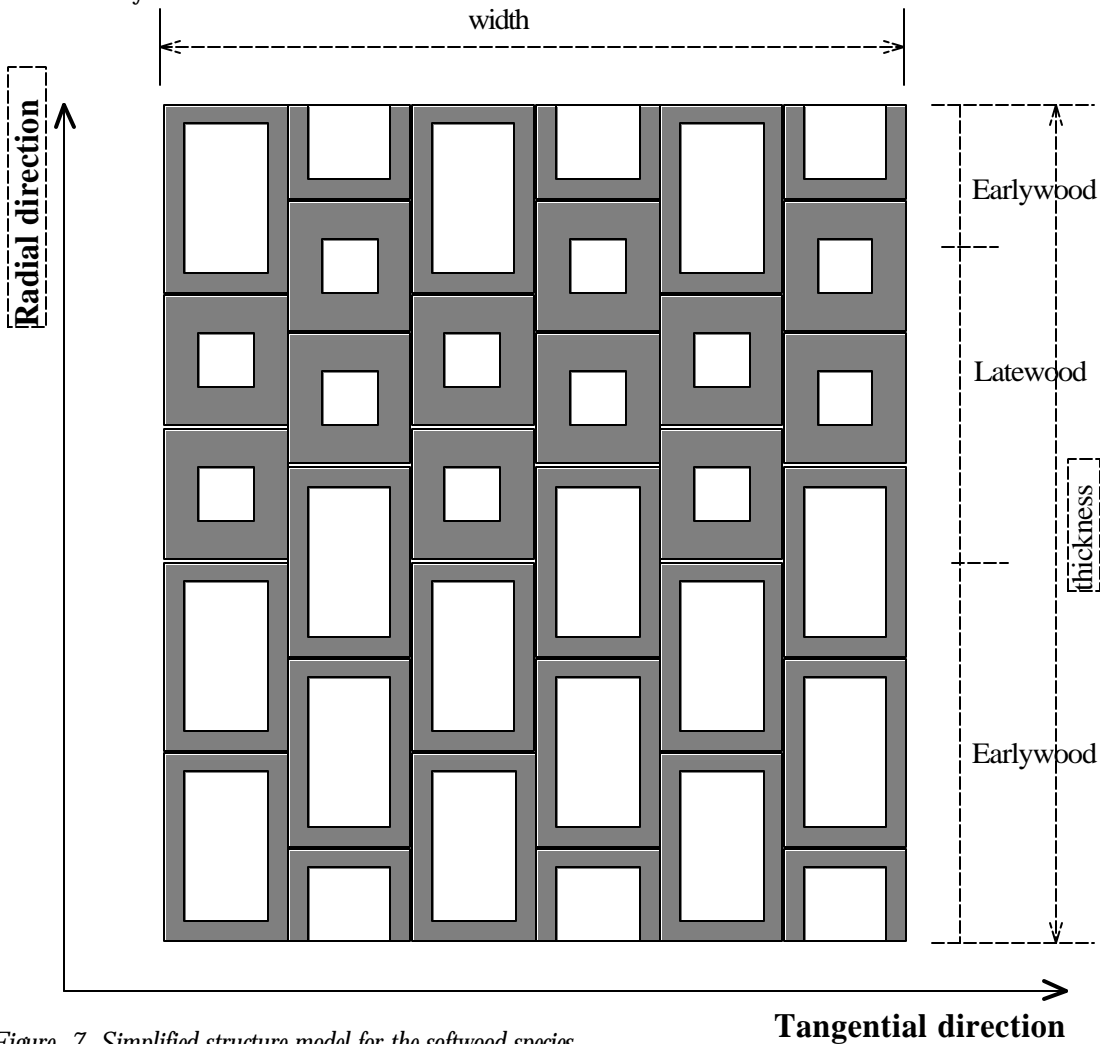


Figure 7 Simplified structure model for the softwood species.

Table 1 The anatomical structure measurement result for southern yellow pine

	Earlywood			Latewood		
	radial	tangential	side wall	radial	tangential	side wall
cell wall percent	16.49%	31.50%	15.94%	44.37%	66.94%	50.77%

Table 2 The anatomical structure measurement result for Scots pine.

	Earlywood			Latewood		
	radial	tangential	side wall	radial	tangential	side wall
cell wall percent	13.69%	31.46%	13.50%	52.98%	71.51%	50.83%

All the data examined so far are the ones obtained from the dry wood samples of the two species. Cell wall substance will be swollen if there is moisture in wood. So the cell wall percentage in the two directions obtained from the wet samples was suspected to be different from the values obtained from the dry samples. Only Scots pine cell wall percentage under the wet condition was measured by the help of the Environmental Scanning Electron Microscope. The *randomized complete block design (with subsamplings)* model was used to examine the significant difference of cell wall percentages between the dry and green samples. No significant difference between the dry and wet samples for the cell wall percentage in latewood area was found. But there is significant difference between the two sets of data for the earlywood cell wall percentage. This is explained by the fact that latewood cells are small with thick walls and small lumens, while the earlywood cells are big with very thin walls and much bigger lumens. Although thick walls may give latewood cells more swelling than the thin-walled cells, the less void or lumen space in the latewood area prevents the swelling, while the thinner cell walls of the earlywood tracheids may not be able to swell by themselves as much as the latewood tracheids, they can be forced to swell with their neighbors --latewood tracheids, to certain extent. And the large lumens provide the space for the cell walls to swell. So the cell walls in the earlywood significantly increased for the wet samples. Next in the model estimation process, the cell wall percentage parameters required in the model inputs have to be distinguished for the dry wood model and the wet wood model since they are significantly different.

4. ANALYTICAL RESEARCH ON WOOD TRANSVERSE THERMAL CONDUCTIVITY MODELING

The geometric models for the thermal conductivity in the radial and tangential directions proposed in this study are based on the consideration of earlywood/latewood percentage and arrangement, cell wall percentage and arrangement in the two directions. The latewood percentage and cell wall percentage are the two major contributing factors to the specific gravity of wood species and individual samples. The inclusion of these two components in the model made it a closer representation of the wood structure influence on the properties than the previous models proposed by Kollmann (1956) and Siau (1968) before, in which, only single cells were chosen as the structure basis for the geometric model.

Since the microscope structure of softwoods doesn't vary significantly from species to species, except for the specific gravity, which came from the different amount of cell wall percentage and latewood percentage in the samples, the geometric model proposed for deriving the thermal conductivity is the same for all the softwood species, only with parameters (such as cell wall percentage) modified for different species in the model.

4.1 MODEL DEVELOPMENT

Geometric models were set up based on the microscopic observations. Assumptions made for the models are:

- cell wall, cell lumen arrangement and amount percentage in the radial and tangential direction represent the heat transfer path in the two directions;
- shrinkage/swelling in the cell wall is not considered in the model before reaching the FSP. Cell wall percentage is assumed constant below FSP. When FSP (MC of 30%) is reached, cell wall percentages are increased to new values for both radial and tangential directions due to the fully saturation of bound water in the cell wall;
- Earlywood/Latewood are separated for the heat transportation in the geometric models developed due to the different cell wall amount in earlywood and latewood;

Model development was based on the simplified and modified structure of softwoods shown in Figure 7. Earlywood and latewood were arranged in parallel for the tangential direction and in series for the radial direction. The total cell wall percentage in the radial and tangential direction for both earlywood and latewood were given by microscopic measurement tests. The structure can be further simplified by moving all the cell walls together, and all the lumens together. Within each earlywood and latewood, cell wall and cell lumen were arranged in series for tangential direction. The geometric model for softwood tangential structure is shown in Figure 8. In radial direction, side walls were arranged in parallel with the series layout of the cross

walls (top and bottom walls of cells) and cell lumen. Therefore the geometric model for softwood radial structure is shown in Figure 9.

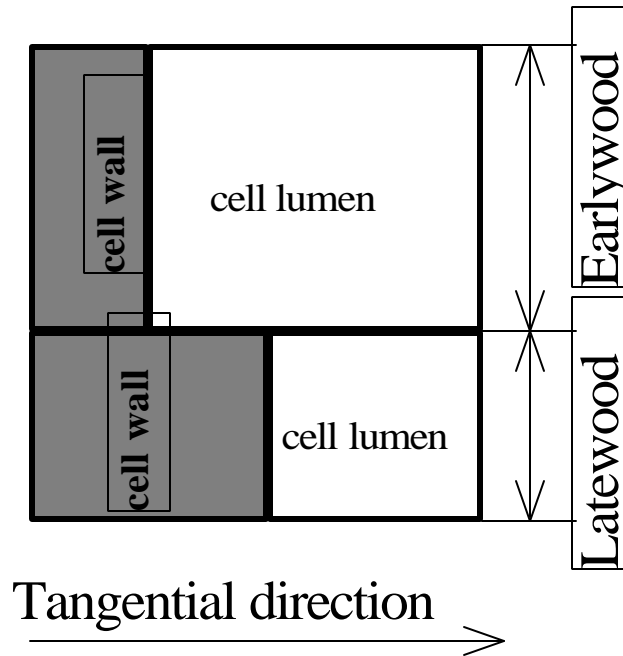


Figure 8 Tangential geometric model for softwood species

These two geometrical models were for the dry sample or the samples with moisture content (MC) below the fiber saturation point (FSP, usually 30%MC). Fiber saturation point is the special moisture content point at which wood contains no liquid water in the cell cavities but fully saturated cell walls with bound water attached to the hydrogen-bonding sites. An example illustration of the moisture change in a single cell is shown in Figure 10. There are 3 states for water existing in wood: bound water, water vapor and free water. When wood is under oven-dry condition, there is no moisture at all in wood. Below FSP, moisture in wood exists as bound water in the cell walls and vapors in the cell lumens. FSP is when bound water are taken all the possible hydrogen-bonding sites in the cell wall and cell lumens are full of saturated water vapor, but no free water in the lumen. When MC is over the FSP, some free water will appear in the lumens. The amount of free water in the lumen depends on the total MC of wood. When the lumen is filled up with all the free water, the fully saturation state of wood is reached. At this

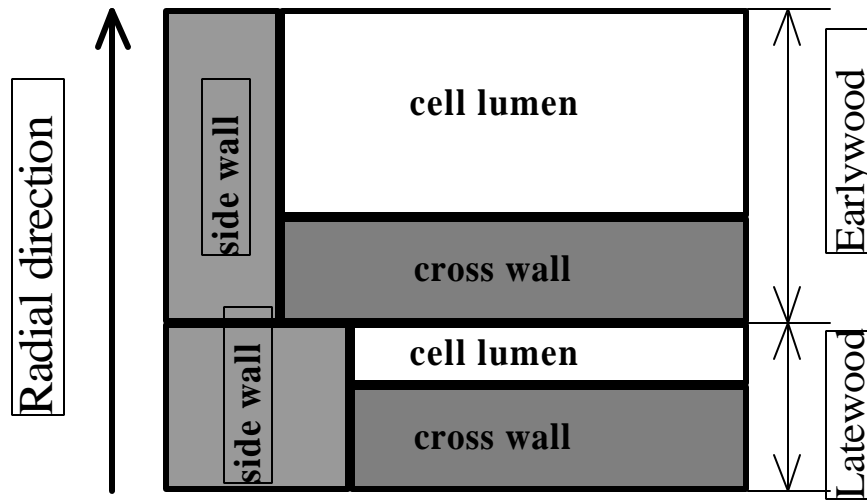


Figure 9 Radial geometric model for softwood species.

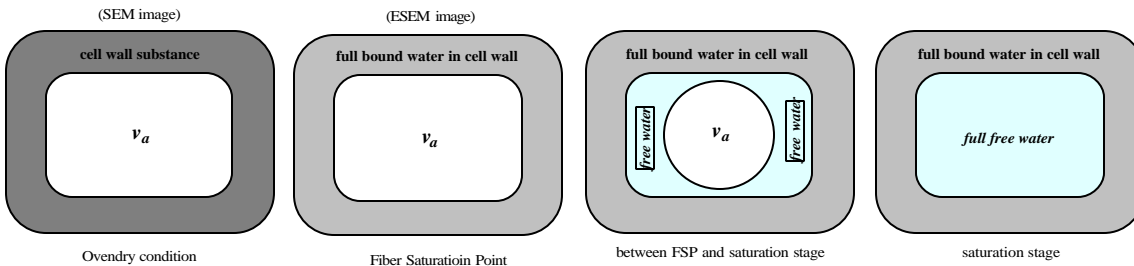


Figure 10 Single cell structure change from dry to fully saturated condition.

state, wood has the maximum MC. When free water takes part of the cell lumens, there will be significant change in the estimated effective thermal conductivity in both directions because water has much greater thermal conductivity value than air and vapor. Since the arrangement of free water and vapor in the cell lumen is hard to model due to the surface tension between free water and vapor, a mixture of free water and vapor is assumed to exist in the cell lumen. The weighed average of the free water thermal conductivity and air/vapor conductivity values in the lumen is used in the geometric models for the MC over the FSP. Geometric models for wet softwood samples (with MC above the FSP) are the same as the ones for MC below FSP, only replacing the pure vapor thermal conductivity by the weight average thermal conductivity in the cell lumen.

The percentage of air and/or vapor in the cell lumen can be calculated based on Siau's (1995) wood porosity (V_a) definition:

$$V_a = 1 - G \left(\frac{1}{G_0^w} + 0.01MC \right)$$

Equa. (2)

Where, G ---- specific gravity;

G_0^w ---- oven-dry cell wall specific gravity, =1.53;

MC ---- moisture content (%);

V_a is calculated based on total volume V of wood. According to Gong (1992), in order base it on the volume of cell lumen, it needs to be multiplied by V/V_{lumen} , which is the inverse of V_a at $MC=0$. So,

$$V_1 = \frac{1 - G \left(\frac{1}{G_0^w} + 0.01MC \right)}{1 - G \frac{1}{G_0^w}}$$

Equa. (3)

This V_1 is the percentage of porosity (contains air and vapor) in the cell lumen at certain MC above FSP. The fraction for the free water in the lumen will be:

$$V_{fw} = 1 - V_1$$

Equa. (4)

The weighed average of thermal conductivity for vapor and free water in the cell lumen can be calculated as:

$$k_{aw} = V_1 * k_a + (1 - V_1) * k_w$$

Equa. (5)

4.2 THEORETICAL DERIVATION OF THERMAL CONDUCTIVITY

4.2.1 Thermal resistance model

The analogous electrical resistance system can be applied here in order to derive the overall thermal conductivity as a resultant value from the known thermal conductivities of its substances. The thermal resistance models for radial and tangential directions generated from the geometric models are shown in Figure 11.

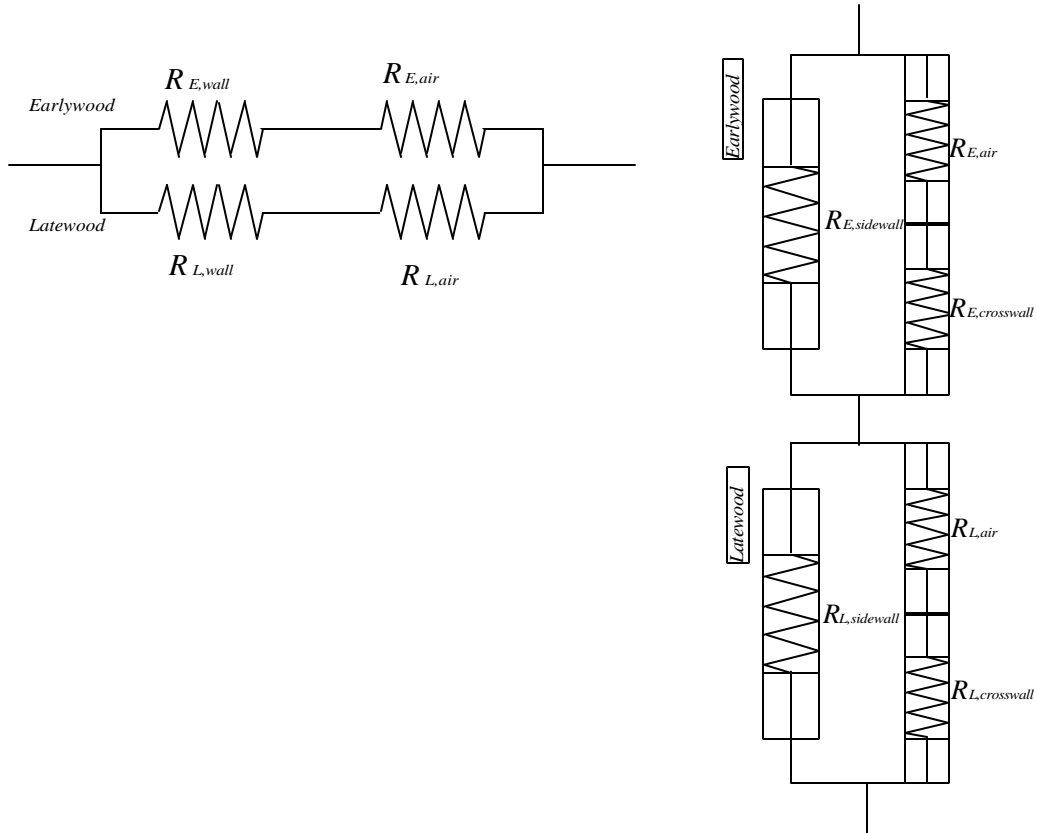


Figure 11 Thermal resistance model for softwood species tangential (left) and radial (right) direction when MC is below FSP.

Introducing the electrical conductance definition into the thermal system gives the thermal conductance defined as:

$$g = k \frac{A}{L}$$

Equa. (6)

Where, g ---- thermal conductance, W/K;

k ---- thermal conductivity, W/m·K;

A ---- cross section of the heat flow, m²;

L ---- length of the heat flow, m;

Thermal resistance (R) is the inverse of the thermal conductance:

$$R = \frac{1}{g} = \frac{L}{kA}$$

Equa. (7)

4.2.2 Tangential thermal conductivity derivation

According to the electrical resistance calculation in parallel systems, the effective thermal conductivity in tangential direction is obtained by:

$$\frac{1}{R_{T,eff}} = \frac{1}{R_E} + \frac{1}{R_L}$$

Equa. (8)

Where, $R_{T,eff}$ ---- total effective thermal resistance in tangential direction;

R_E ---- total thermal resistance from the earlywood part;

R_L ---- total thermal resistance from the latewood part;

Equation (8) is based on the parallel arrangement of the earlywood and latewood in the tangential direction. Within the earlywood or latewood area, cell wall substance and air in the lumens are arranged in series. So,

$$R_E = R_{E,wall} + R_{E,air}$$

$$R_L = R_{L,wall} + R_{L,air}$$

Equa. (9)

Where, $R_{E,wall}$ ---- resistance from earlywood cell wall substance;

$R_{E,air}$ ---- resistance from air in earlywood cell lumen;

$R_{L,wall}$ ---- resistance from latewood cell wall substance;

$R_{L,air}$ ---- resistance from air in latewood cell lumen;

By the definition and anatomical measurement results, each of these resistances can be calculated by:

$$R_{E,wall} = \frac{TED\% * L}{k_c * E\% * A};$$

$$R_{E,air} = \frac{(1 - TED\%) * L}{k_a * E\% * A};$$

$$R_{L,wall} = \frac{TLD\% * L}{k_c * L\% * A};$$

$$R_{L,air} = \frac{(1 - TLD\%) * L}{k_a * L\% * A}$$

$$R_{T,eff} = \frac{L}{k_{T,eff} * A}$$

Where, $TED\%$ ---- cell wall percentage in Tangential direction of Earlywood Dry sample;

$E\%$ ---- Earlywood percentage measured in wood samples;

$TLD\%$ ---- cell wall percentage in Tangential direction of Latewood Dry sample;

$L\%$ ---- Latewood percentage measured in wood samples;

By plugging all these resistances into the *Equation 9* then *Equation 8*, the effective tangential thermal conductivity for the dry softwood samples can be calculated. The detailed calculation is implemented in *Mathematica* software. All the percentage parameters required in the calculation were obtained from the anatomical test above. The thermal conductivity values for cell wall substance and air in the lumen were taken from Maku (1954):

$$k_c = 0.41 \text{ W/m}\cdot\text{K};$$

$$k_a = 0.046 \text{ W/m}\cdot\text{K};$$

For the wet sample model (MC above FSP), the thermal resistance in cell lumen is assumed to be the mixture of vapor and free water. The total thermal resistance in the tangential direction is calculated by the same as derived above. Only the difference is the thermal resistance from cell lumen is the weighed average

thermal conductivity of vapor and water instead of pure air/vapor thermal conductivity value. The cell wall percentages in earlywood and latewood are different, too.

The thermal conductivity for pure water is taken:

$$k_{water} = 0.59 \text{ W/m}\cdot\text{K}; \text{ (Siau 1995)}$$

4.2.3 RADIAL THERMAL CONDUCTIVITY DERIVATION

With the series arrangement of earlywood and latewood in the radial direction (see Figure 9 and Figure 11 right), the total effective thermal resistance in the radial direction is:

$$R_{R,eff} = R_E + R_L$$

Equa. (10)

Where, $R_{R,eff}$ ---- the total effective thermal resistance in radial direction;

Within earlywood or latewood area, the thermal resistance arrangement is more complicated than in the tangential direction. Part of the cell walls (side walls) are arranged in parallel with the series arrangement of the other part of cell wall (cross walls) and air in cell lumen. So the resistances from earlywood and latewood are:

$$\frac{1}{R_E} = \frac{1}{R_{E,side\,wall}} + \frac{1}{R_{E,air} + R_{E,cross\,wall}}$$

$$\frac{1}{R_L} = \frac{1}{R_{L,side\,wall}} + \frac{1}{R_{L,air} + R_{L,cross\,wall}}$$

Equa. (11)

Where, $R_{E,side\,wall}$ ---- resistance from earlywood side walls;

$R_{E,air}$ ---- resistance from air in earlywood cell lumens;

$R_{E,cross\,wall}$ ---- resistance from earlywood cross walls;

$R_{L,side\,wall}$ ---- resistance from latewood side walls;

$R_{L,air}$ ---- resistance from air in latewood cell lumens;

$R_{L,cross\,wall}$ ---- resistance from latewood cross walls;

By definition and anatomical measurement results, each of these resistances can be calculated:

$$R_{E,side\,wall} = \frac{E\% * L}{k_c * SERD\% * A};$$

$$R_{E,air} = \frac{E\% * (1 - CERD\%) * L}{k_a * (1 - SERD\%) * A};$$

$$R_{E,cross\,wall} = \frac{E\% * CERD\% * L}{k_c * (1 - SERD\%) * A};$$

$$R_{L,side\,wall} = \frac{L\% * L}{k_c * SLRD\% * A};$$

$$R_{L,air} = \frac{L\% * (1 - CLRD\%) * L}{k_a * (1 - SLRD\%) * A};$$

$$R_{L,cross\,wall} = \frac{L\% * CLRD\% * L}{k_a * (1 - SLRD\%) * A};$$

$$R_{R,eff} = \frac{L}{k_{R,eff} * A}$$

Where, *SERD%* ---- Side wall percentage in *Earlywood Radial* direction of *Dry* sample;

CERD% ---- Cross wall percentage in *Earlywood Radial* direction of *Dry* sample;

SLRD% ---- Side wall percentage in *Latewood Radial* direction of *Dry* sample;

CLRD% ---- Cross wall percentage in *Latewood Radial* direction of *Dry* sample;

All these parameters were obtained from the anatomical tests in the previous section. By plugging these resistances into *Equation 11* then *Equation 10*, the effective radial thermal conductivity for the dry softwood samples can be calculated. For MC above FSP, the derivation is the same, except with the thermal resistance from cell lumen is taken from the mixture of vapor and water instead of pure air/vapor.

4.3 NUMERICAL RESULTS FOR THE MODEL ESTIMATION

4.3.1. Estimation results for southern yellow pine

Model estimations for southern yellow pine thermal conductivities in the two directions were performed in *Mathematica* software based on the resistance models and derivations described above. Since the latewood (or earlywood) percent on the cross section may vary from sample to sample, the program

estimated k values for latewood% ranging from 1% to 99%. The thermal conductivity value for air (k_a) in the lumen is set as a constant of 0.046 W/m·K, while the thermal conductivity value for the cell wall substance k_c is defined as a function of moisture content based on the relationship given by Siau (1995):

$$k_{qT} = G(0.2 + 0.0038 * MC) + 0.024 \quad [W / m \cdot K] \quad \text{for } MC < 40\% \quad \text{Equa. (12)}$$

where, k_{qT} ---- the transverse thermal conductivity;

G ---- specific gravity;

If $k_c = 0.41$ W/m.K is the assumed value (Maku 1954) at the oven dry condition (MC=0%), and the specific gravity of the cell wall at the oven dry condition is 1.45 (Kellogg & Wangaard 1969), then the k_c as a function of MC can be simplified as:

$$k_c = 0.41 + 0.0055 * MC \quad \text{for } MC \leq 30\% \quad \text{Equa. (13)}$$

Above the FSP (30%), k_c values will stay constant because cell wall composition does not change when MC is over FSP.

The estimation values for thermal conductivity of southern yellow pine are shown in Table 3 and Table 4. The two-dimensional plots for the radial and tangential thermal conductivity changes with MC and latewood percent in the sample are shown in Figure 12 and 13.

From the tables and figures, it can be seen that there is significant difference for model-predicted thermal conductivity values between the radial and tangential directions. Radial thermal conductivity is higher than the tangential values. From the model prediction, latewood volume in the sample has a substantial effect on the transverse thermal conductivities. This is consistent with previous literature results. It has been known for a long time that thermal conductivity is a positive linear function of specific gravity, and latewood percentage is the main contributor to the wood specific gravity. The more the thick-cell-walled latewood in the samples, the higher the specific gravity is.

Table 3 Southern yellow pine model predicted tangential thermal conductivity values in the range of latewood percentage from 10% to 99% and MC from 0% to 30%.

Latewood percentage	Moisture content									
	0%	5%	10%	11%	12%	13%	14%	15%	20%	30%
10%	0.0688	0.0691	0.0694	0.0695	0.0695	0.0696	0.0696	0.0697	0.0699	0.0703
20%	0.0738	0.0742	0.0746	0.0747	0.0747	0.0748	0.0749	0.0749	0.0753	0.0758
30%	0.0788	0.0793	0.0798	0.0799	0.0800	0.0801	0.0801	0.0802	0.0806	0.0813
40%	0.0837	0.0844	0.0850	0.0851	0.0852	0.0853	0.0854	0.0855	0.0860	0.0868
45%	0.0862	0.0869	0.0876	0.0877	0.0878	0.0879	0.0880	0.0881	0.0887	0.0896
50%	0.0887	0.0895	0.0902	0.0903	0.0904	0.0905	0.0907	0.0908	0.0913	0.0923
55%	0.0912	0.0920	0.0927	0.0929	0.0930	0.0932	0.0933	0.0934	0.0940	0.0951
60%	0.0937	0.0945	0.0953	0.0955	0.0956	0.0958	0.0959	0.0961	0.0967	0.0979
70%	0.0986	0.0996	0.1005	0.1007	0.1009	0.1010	0.1012	0.1013	0.1021	0.1034
80%	0.1036	0.1047	0.1057	0.1059	0.1061	0.1063	0.1064	0.1066	0.1074	0.1089
90%	0.1086	0.1098	0.1109	0.1111	0.1113	0.1115	0.1117	0.1119	0.1128	0.1144
99%	0.1130	0.1144	0.1156	0.1158	0.1160	0.1162	0.1164	0.1166	0.1176	0.1194

Table 4 Southern yellow pine model predicted radial thermal conductivity values in the range of latewood percentage from 10% to 99% and MC from 0% to 30%.

Latewood percentage	Moisture content									
	0%	5%	10%	11%	12%	13%	14%	15%	20%	30%
10%	0.1171	0.1219	0.1267	0.1276	0.1286	0.1295	0.1305	0.1315	0.1362	0.1458
20%	0.1243	0.1295	0.1347	0.1358	0.1368	0.1378	0.1389	0.1399	0.1451	0.1554
30%	0.1325	0.1382	0.1439	0.1450	0.1461	0.1472	0.1484	0.1495	0.1552	0.1664
35%	0.1370	0.1430	0.1489	0.1501	0.1513	0.1525	0.1536	0.1548	0.1607	0.1725
40%	0.1418	0.1481	0.1543	0.1556	0.1568	0.1580	0.1593	0.1605	0.1667	0.1791
45%	0.1470	0.1536	0.1601	0.1614	0.1628	0.1641	0.1654	0.1667	0.1732	0.1862
50%	0.1525	0.1595	0.1664	0.1678	0.1692	0.1706	0.1719	0.1733	0.1802	0.1939
55%	0.1586	0.1659	0.1732	0.1747	0.1761	0.1776	0.1790	0.1805	0.1878	0.2022
60%	0.1650	0.1728	0.1806	0.1821	0.1837	0.1852	0.1868	0.1883	0.1960	0.2113
70%	0.1798	0.1886	0.1974	0.1991	0.2009	0.2026	0.2044	0.2061	0.2149	0.2322
80%	0.1974	0.2075	0.2176	0.2196	0.2217	0.2237	0.2257	0.2277	0.2377	0.2577
90%	0.2188	0.2307	0.2425	0.2449	0.2472	0.2496	0.2519	0.2543	0.2660	0.2895
99%	0.2425	0.2564	0.2703	0.2731	0.2758	0.2786	0.2814	0.2841	0.2980	0.3256

Tangential thermal conductivity (TTC) of southern yellow pine is predicted to change linearly with LW percent, but insignificantly changed with MC in the samples. Radial thermal conductivity (RTC) changes linearly with moisture content, and non-linearly with LW percentage. RTC is an inverse function of earlywood percentage ($\text{earlywood}\% = 1 - \text{latewood}\%$), which gives the trend as the lower the earlywood percentage (higher latewood percentage), the higher the RTC, and the increase of RTC is greater with the decrease of earlywood percentage (corresponding to the increase of latewood percentage). The ratio for RTC over TTC is basically controlled by the RTC because RTC is much greater than and changes more significantly than TTC. The ratio ranges from 1.2 to 2.5 for the whole range shown in Figure 14.

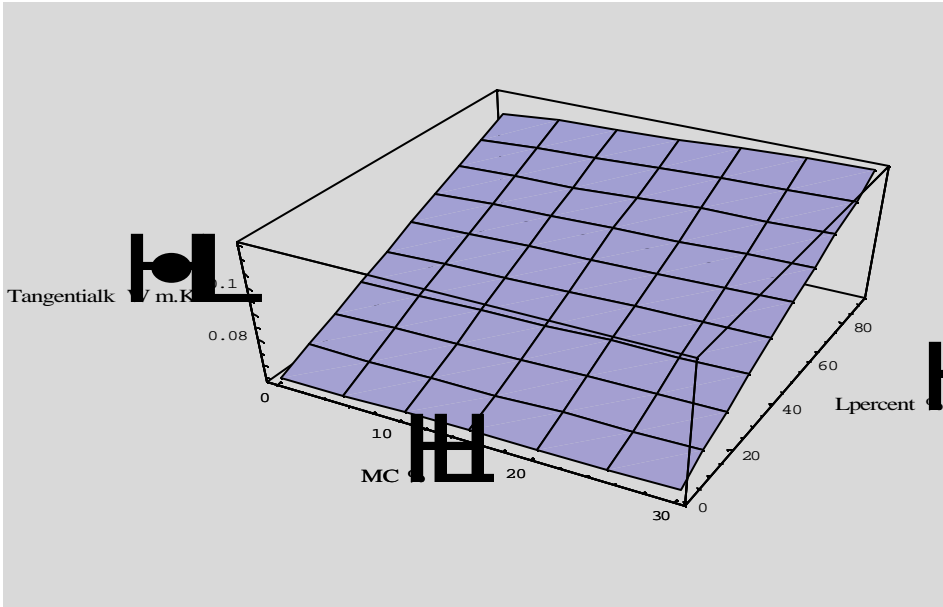


Figure 12 Southern yellow pine model predicted tangential thermal conductivity values change with the latewood percentage on the cross section and moisture content change in the sample.

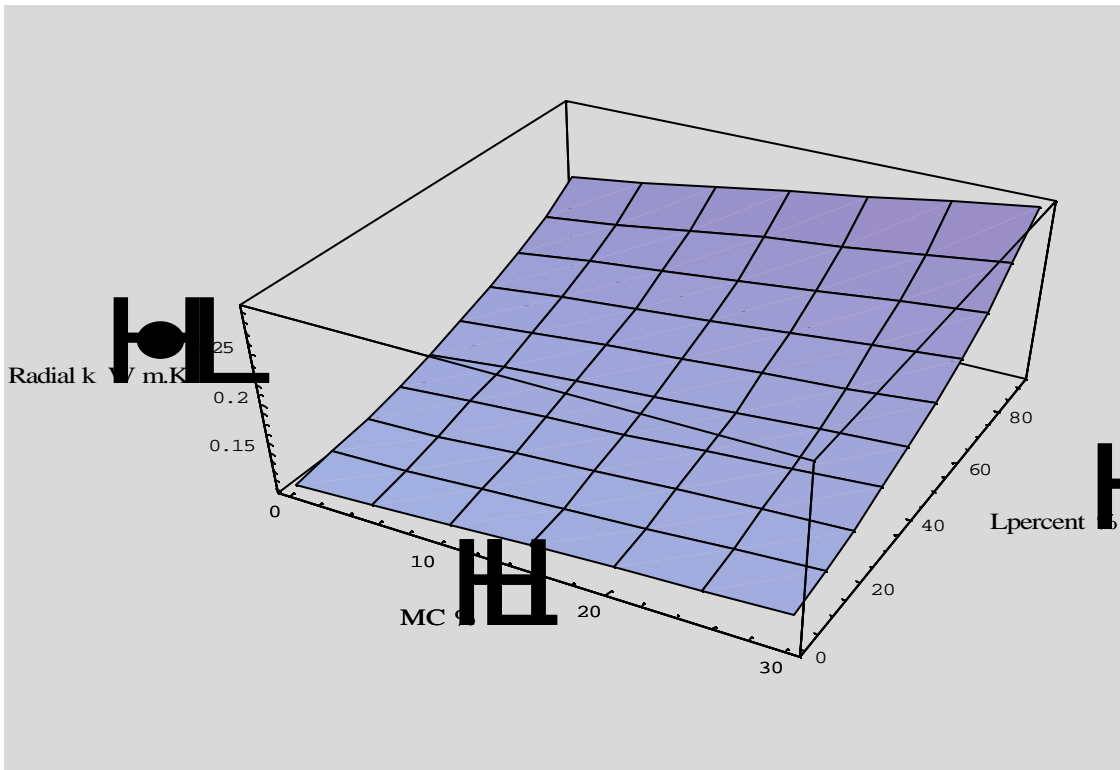


Figure 13 Southern yellow pine model predicted radial thermal conductivity values change with the latewood percentage on the cross section and moisture content in the sample.

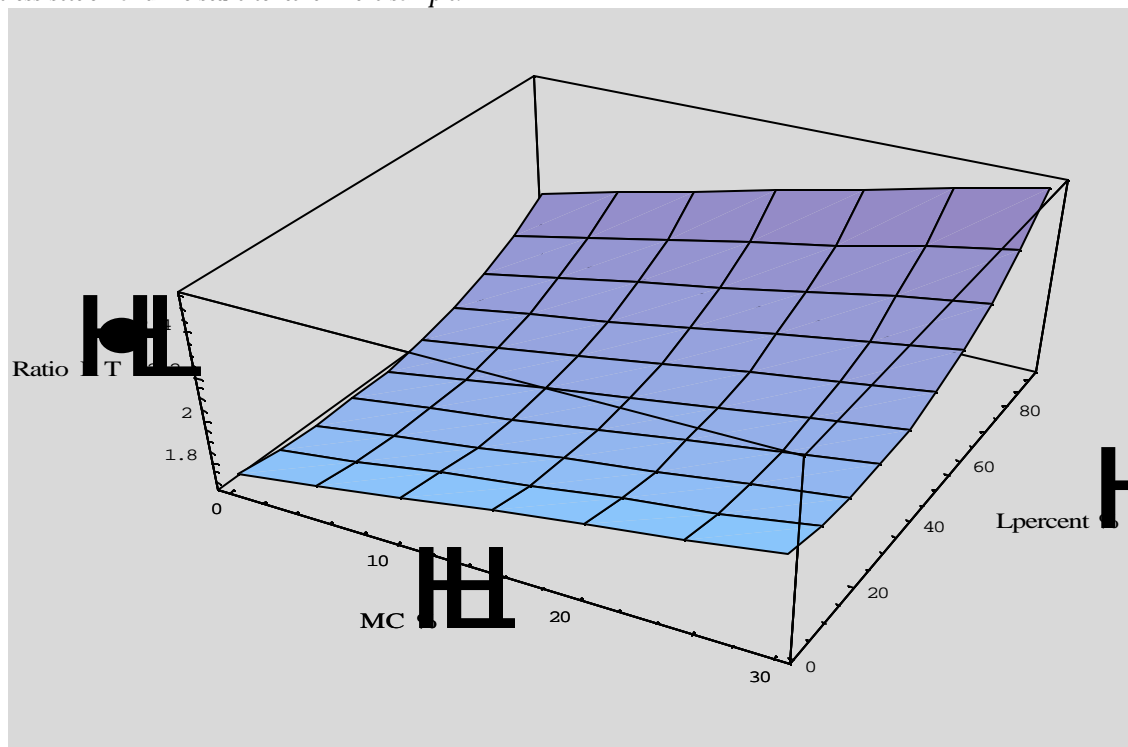


Figure 14 Southern yellow pine model predicted ratio of radial vs. tangential thermal conductivity with the change of latewood percentage on the cross section and moisture content in the sample.

4.3.2 *Estimation results for Scots pine*

The estimations for Scots pine radial and tangential k values performed by the same program. Since the two species have the same geometric models and the anatomical structure parameters are similar too, the theoretical model results are very close, too.

The geometric and thermal resistance models for softwood species with MC above FSP are the same as the models for MC below FSP. Only the parameter of thermal conductivity from cell lumen is different from MC over FSP. Also the anatomical structure parameters obtained from wet samples are different from the ones obtained from the dry samples.

The maximum moisture content that Scots pine can have under the fully saturated condition was calculated by the equation given by Siau (1995):

$$MC_{\max} = \frac{100}{G_{\text{dry}}} - 65.3$$

Equa. (14)

MC_{\max} of 178%, was used in the program as the upper limit.

The model outputs are shown in Tables 7, 8 and Figures 15-17.

Table 5 Scots pine model predicted tangential thermal conductivity values in the range of latewood percentage from 5% to 99% and MC from 0% to maximum 178%.

Latewood percent	Moisture content (%)											
	0%	5%	15%	30%	40%	60%	80%	100%	120%	140%	160%	178%
5%	0.0669	0.0672	0.0677	0.0682	0.2023	0.2789	0.3465	0.4066	0.4606	0.5093	0.5535	0.5900
10%	0.0700	0.0704	0.0710	0.0717	0.2083	0.2848	0.3516	0.4108	0.4636	0.5111	0.5541	0.5895
20%	0.0763	0.0768	0.0776	0.0787	0.2202	0.2966	0.3620	0.4192	0.4697	0.5148	0.5554	0.5886
30%	0.0825	0.0831	0.0843	0.0857	0.2321	0.3083	0.3724	0.4275	0.4757	0.5184	0.5566	0.5877
40%	0.0887	0.0895	0.0909	0.0926	0.2440	0.3201	0.3827	0.4359	0.4818	0.5221	0.5579	0.5868
50%	0.0949	0.0959	0.0976	0.0996	0.2559	0.3318	0.3931	0.4442	0.4879	0.5258	0.5591	0.5859
60%	0.1011	0.1023	0.1042	0.1066	0.2678	0.3436	0.4035	0.4526	0.4939	0.5294	0.5604	0.5850
70%	0.1073	0.1086	0.1109	0.1135	0.2797	0.3553	0.4138	0.4610	0.5000	0.5331	0.5616	0.5842
80%	0.1136	0.1150	0.1175	0.1205	0.2916	0.3671	0.4242	0.4693	0.5061	0.5368	0.5629	0.5833
90%	0.1198	0.1214	0.1242	0.1275	0.3035	0.3789	0.4346	0.4777	0.5121	0.5404	0.5641	0.5824
99%	0.1254	0.1271	0.1301	0.1338	0.3142	0.3894	0.4439	0.4852	0.5176	0.5437	0.5652	0.5816

Table 6 Scots pine model predicted radial thermal conductivity values in the range of latewood percentage from 5% to 99% and MC from 0% to maximum 178%.

Latewood percent	Moisture content (%)											
	0%	5%	15%	30%	40%	60%	80%	100%	120%	140%	160%	178%
5%	0.1038	0.1077	0.1155	0.1272	0.2410	0.2998	0.3555	0.4084	0.4587	0.5065	0.5521	0.5913
10%	0.1071	0.1111	0.1193	0.1315	0.2464	0.3052	0.3605	0.4127	0.4620	0.5086	0.5528	0.5907
20%	0.1143	0.1188	0.1277	0.1410	0.2580	0.3166	0.3709	0.4215	0.4687	0.5129	0.5544	0.5895
30%	0.1227	0.1276	0.1374	0.1521	0.2707	0.3288	0.3819	0.4307	0.4756	0.5173	0.5559	0.5884
40%	0.1324	0.1379	0.1488	0.1650	0.2847	0.3420	0.3936	0.4403	0.4828	0.5217	0.5575	0.5873
50%	0.1437	0.1499	0.1621	0.1803	0.3003	0.3564	0.4060	0.4503	0.4902	0.5262	0.5590	0.5861
60%	0.1571	0.1642	0.1781	0.1987	0.3177	0.3720	0.4192	0.4608	0.4978	0.5308	0.5606	0.5850
70%	0.1734	0.1815	0.1975	0.2214	0.3372	0.3890	0.4333	0.4718	0.5056	0.5355	0.5622	0.5839
80%	0.1933	0.2028	0.2218	0.2499	0.3593	0.4076	0.4484	0.4834	0.5137	0.5403	0.5638	0.5827
90%	0.2184	0.2299	0.2528	0.2867	0.3844	0.4281	0.4646	0.4955	0.5220	0.5451	0.5654	0.5816
99%	0.2474	0.2614	0.2892	0.3307	0.4102	0.4485	0.4802	0.5069	0.5298	0.5496	0.5668	0.5806

From results shown in the table, we found that tangential thermal conductivity increases dramatically when free water appears in wood ($MC > 30\%$). And above the FSP, the moisture content shows much more affects on the tangential thermal conductivity than it does below the FSP. Before the free water appears, air in the lumen has very low conductance, which contributes very little to the total effective conductance in the tangential direction (with series arrangement of the cell wall and cell lumen). The thermal conductivity of free water ($k_c = 0.59$) is much higher than that of air, and even higher than thermal conductivity of cell wall substance. The appearance of free water in the lumen increases the total effective conductance in the tangential direction, and with its volume increase, the conductance will increase more. Moisture content or free water appearance also has a same positive affect on the total effective conductance in the radial direction, but not as significant as the tangential direction. The thermal conductivity increases nonlinearly with moisture content above the FSP in both radial and tangential directions (Figure 18). The thermal conductivities in the two directions were predicted to be close with the ratio near 1 for MC above FSP (Figure 19).

The ratio of the two thermal conductivities predicted by the model in the whole range changed dramatically at the FSP. Below the FSP, the ratio is tend to follow the radial thermal conductivity change because radial values and changes are much more significant than the tangential ones. At the FSP, the ratio (R/T) dropped straight down to near 1.0, which means that the tangential thermal conductivity jumps close to the radial thermal conductivity when free water appears in the sample according to the model's prediction. The thermal conductivities in the two directions are not significantly different from each other.

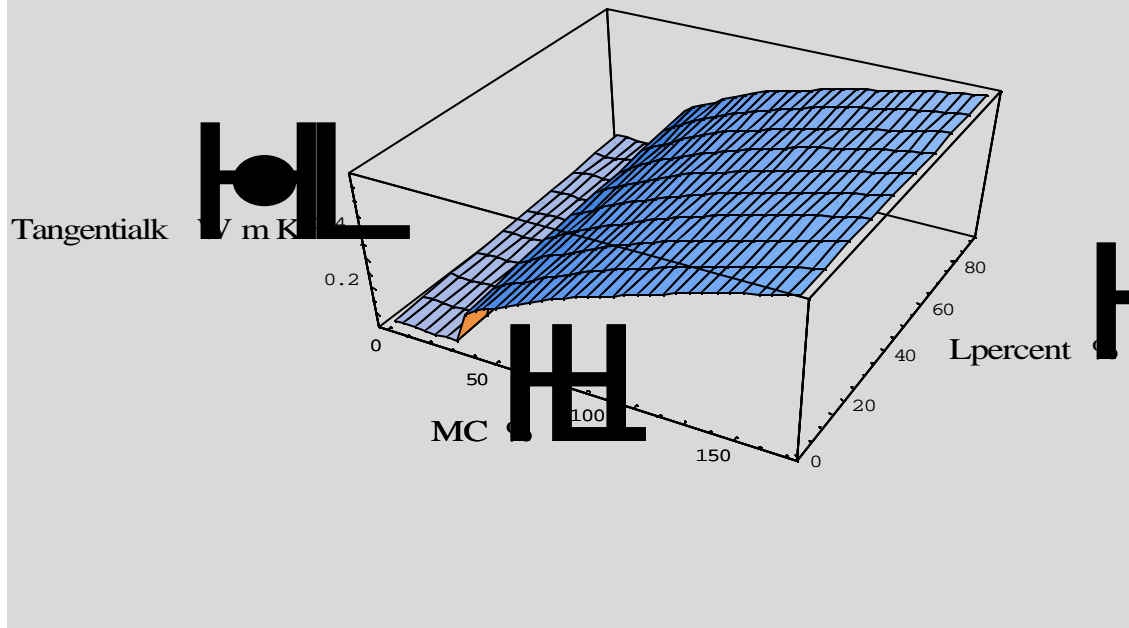


Figure 15 Scots pine model predicted tangential thermal conductivity values change with the latewood percentage on the cross section and moisture content change (the whole range) in the sample.

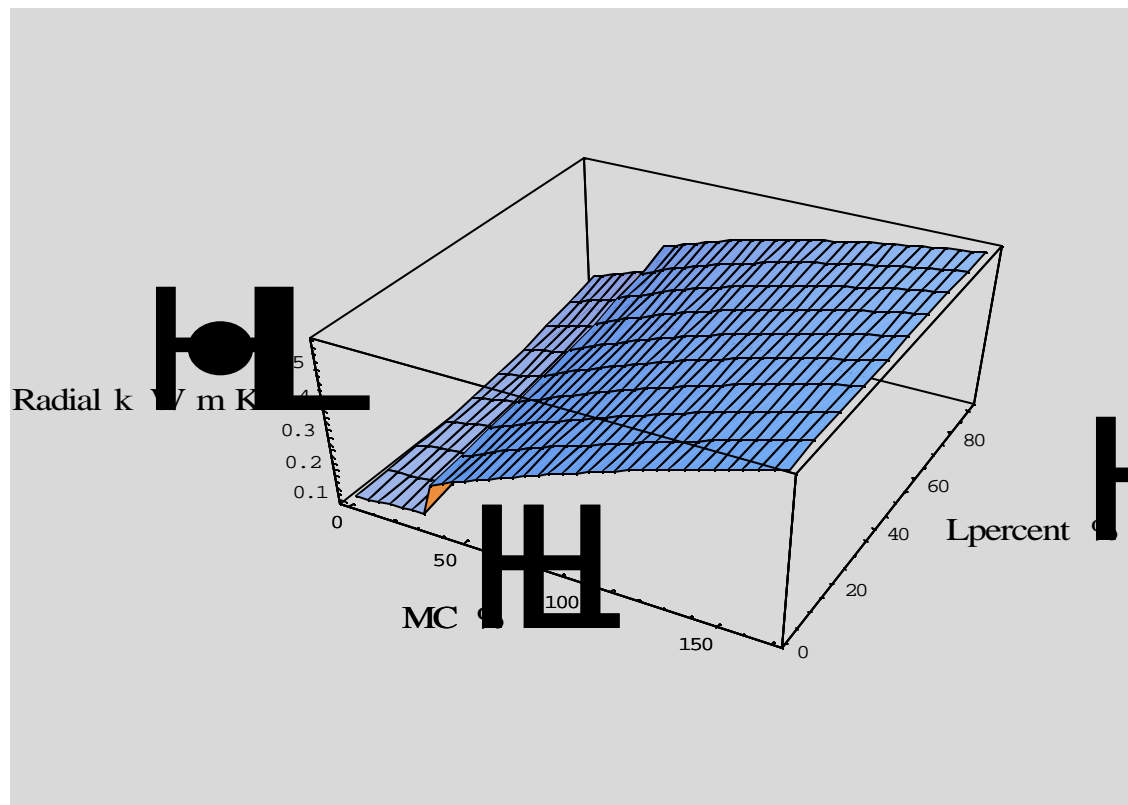


Figure 16 Scots pine model predicted radial thermal conductivity values change with the latewood percentage on the cross section and moisture content change (the whole range) in the sample.

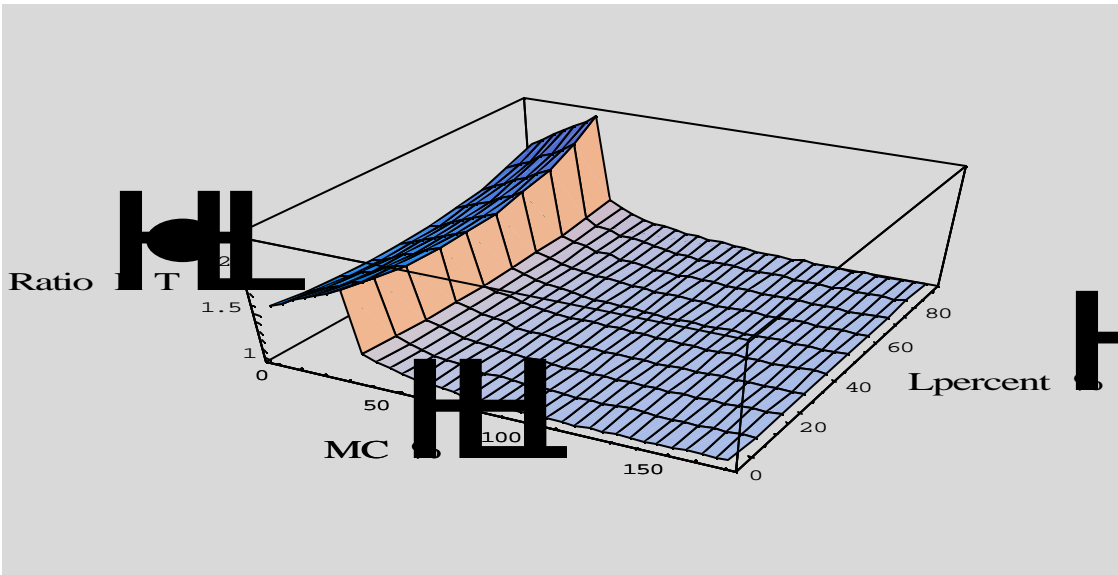


Figure 17 Scots pine model predicted ratio of radial vs. tangential thermal conductivity with the change of latewood percentage on the cross section and moisture content (the whole range) in the sample.

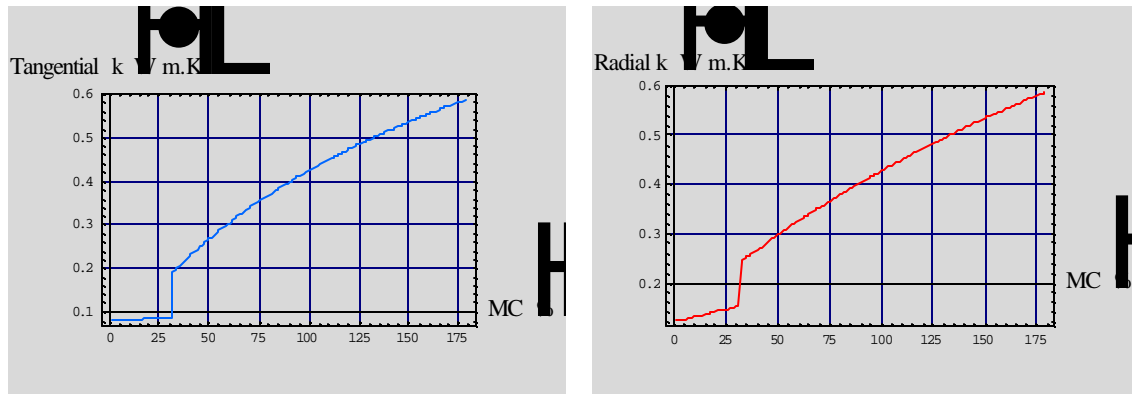


Figure 18 Scots pine tangential and radial thermal conductivity change in the whole moisture range (from 0% to fully saturated) for a fixed latewood percent on the sample (LW=30%).

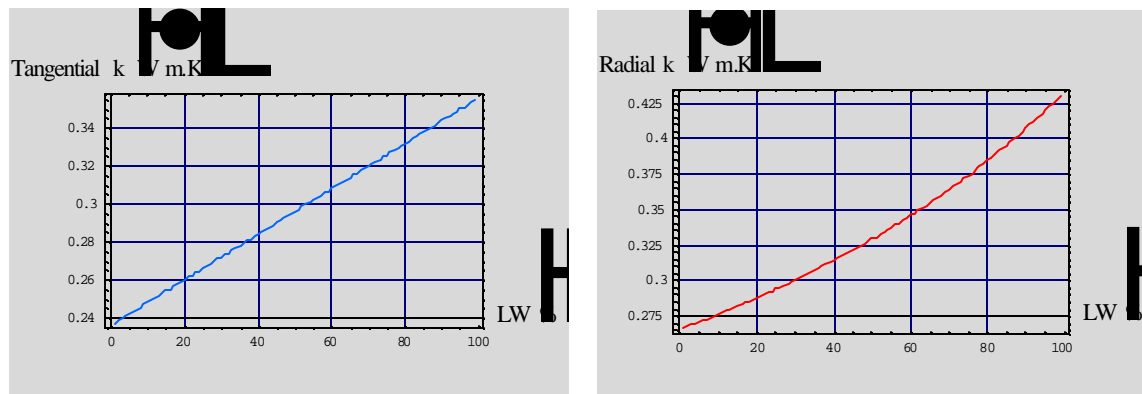


Figure 19 Scots pine tangential and radial thermal conductivity change with latewood percent on the samples for a fixed moisture content in the sample (MC=50%).

5 CONCLUSIONS

Observation of wood anatomical structure of two softwood species gave the basis and requisite parameters to develop the geometric and thermal resistance models for the radial and tangential thermal conductivities. Results from the observation and image analysis measurements showed the structure differences between the radial and tangential direction on wood cross section. Regular (close to square) shaped cells aligned in the radial direction gave a different arrangement for the cell wall and cell lumen in the radial and tangential direction as described in the models. There is more cell wall substance in the tangential direction than in the radial direction. The different percentage of cell wall substance in the radial and tangential direction between the dry and wet condition was examined on Scots pine samples. Statistical analysis showed that cell wall percentage in the latewood area does not change significantly from dry condition to wet condition, but in the earlywood area, cell wall percentage in the radial and tangential direction both change significantly from dry to wet condition. This was explained by the different lumen space and wall thickness between the earlywood cells and latewood cells.

The geometric models for theoretically deriving thermal conductivities in the radial and tangential direction for softwood species were developed based on the anatomical structure measurements. The models were based on the wood structure observed on the cross section instead of a single cell structure. The current models included the earlywood-latewood interaction and cell wall percentage and arrangement in the two transverse directions. The analogous electrical resistance circuit was applied to generate the thermal resistance models. Model-estimated thermal conductivities were calculated by a program written in *Mathematica* software and plotted as a function of latewood percentage in the heat transfer direction and moisture content in the samples.

Theoretical estimations for the thermal conductivities of two softwood species are very close because they have similar anatomical structures and same models (geometric and resistance models). Radial thermal conductivity is greater than tangential thermal conductivity for moisture content below FSP due to the structure difference in the two directions, which result in the different geometric models for the two directions. Radial thermal conductivity is about 1.2 to 2.5 times of tangential thermal conductivity in the moisture range from 0% to 30% and latewood percent range from 1% to 99%. A linear relationship was found between moisture content (in the range of 0%-30%) and the radial thermal conductivity. A less significant linear relationship is shown between moisture content and the tangential thermal conductivity.

There is also a linear relationship between the tangential thermal conductivity (TTC) of softwood species and the LW percentage in the samples. The higher the LW% is, the higher the TTC. An inverse

relationship between the radial thermal conductivity and (1-LW%) on softwood species was found, which gives an increase of RTC with the increase of LW percentage. These relationships are resulted from the different arrangement of earlywood-latewood in the radial and tangential geometric models.

Two-direction thermal conductivity values in the large MC range from oven-dry to saturation state were estimated by the Scots pine models. Above the FSP, when free water appears in the wood sample, TTC and RTC increase dramatically with moisture content changes. No significant difference was found between TTC and RTC. The geometric difference in the two directions has little effect on the resulted thermal conductivities when free water takes part of the cell lumen.

All these conclusions were based on the theoretical model estimations. Although the geometric models and thermal resistance models were set up based on the wood anatomical structure and numerous microscopic measurements on the major thermal conductivity influenced structures -- cell wall percent and latewood percent in wood, the theoretical models are always idealized by certain assumptions. So the theoretical model outputs have to be compared with experimental results to evaluate the capability of model predictions. Validation tests for thermal conductivity measurement had been done on the two softwood species modeled in this study but not included in this paper.

References:

- Couturier, M.F., K. George, M.H. Schneider. 1996. Thermophysical properties of wood-polymer composites. *Wood Science and Technology* Vol.30:179-196.
- Gong, L. 1992. A theoretical numerical and experimental study of heat and mass transfer in wood during drying. Ph.D. Thesis, Washington State University, Dept. of Mechanical and Material Engineering, U.S.
- Griffiths, E. and G.W.C. Kaye. 1923. *Proc. Roy. Soc. Lond. Ser. A* 104:71.
- Grober, H. 1910. *Wärmeleitfähigkeit von Isolier- und Baustoffen*. A. Ver deutsch. Ing. 54:1319-1324.
- Haygreen, J.G. and J.L. Bowyer. 1982. *Forest Products and Wood Science, an introduction*. 3rd Ed. Iowa State University Press/ Ames.
- Hendricks, L. 1962. Thermal conductivity of wood as a function of temperature and moisture content. Thesis. State University College of Forestry at Syracuse University, Syracuse, NY 12310.
- Hoadley, B.R. 1980. *Identifying Wood, An accurate results with simple tools*. The Taunton Press, Newtown, Connecticut 06470-5506.

- Incropera, F.P. and D.P. DeWitt. 1981. Fundamentals of Heat and Mass Transfer. 4th Ed. School of Mechanical Engineering, Purdue University. John Wiley & Sons.
- Kellog, R.M. and F.F. Wangaard. 1969. Variation in the cell density of wood. Wood Fiber, Vol.1:180-204.
- Kollmann, F. 1934. Über die waimetechischen Eigneschaften der Holzer. Gesundheits Ing. 57:224-227.
- Kollmann, F. 1951. Technologie des Holzes und der Holzwerkstoffe 2nd Ed., Vol. 1, Springer-Verlag, Berlin-Gottingen-Heidelberg
- Kollmann, F. and L. Malmquist. 1956. Über die Waimeleitzahl von Holz und Holzwerkstoffen. Holz als Roh- und Werkstoff. Vol.14:201-204.
- MacLean, J.D. 1941. Thermal conductivity of wood. Heating, Piping and Air Conditioning. Vol.13:380-391.
- Maku, T. 1954. Studies on the heat conduction in wood. Wood Res. Bull. Vol.13:1-80. Kyoto Univ.
- Nicolls, J.W.P. 1984. Tracheid cell dimensions and density relationships for normal and abnormal wood of *Pinus radiata* D. Don. Australian Forest Research. Vol.14(2):85-98.
- Nobuchi, T. T. Fujisawa, and H. Saiki. 1995. An application of the pinning method to the marking of the differentiating zone and to the estimation of the time course of annual ring formation in sugi. Journal of the Japan Wood Research Society. Vol.39(6):716-723.
- Quirk, J.T. 1984. Shrinkage and related properties of Douglas-fir cell walls. Wood and Fiber Science, Vol.16(1):115-133.
- Rayleigh, L. 1892. Phil. Mag., Vol.34:481.
- Rowley, F.B. 1933. The heat conductivity of wood at climatic temperature differences. Heating, Piping, and Air Conditioning. Vol. 5:313-323.
- Siau, J.F., R.W. Davidson, J.A. Meyer, and C. Skaar. 1968. A geometrical model for wood-polymer composites. Wood Science Vol. 1(2):116-128.
- Siau, J.F. 1995. Wood: Influence of Moisture on Physical Properties. Department of Wood Science and Forest Products, Virginia Tech.

- Steihagen, H.P. 1977. Thermal properties of wood, green or dry, from -40°C to +100°C: A literature review. USDA Forest Service General Technical Report FPL-9, Forest Products laboratory, Madison, WI
- Suleiman, B.M., J.B. Largeldt, and M. Gustavsson. 1999. Thermal conductivity and diffusivity of wood. *Wood Science and Tehnology* 33:465-473.
- Trenard, Y. and P.Gueneau. 1977. Relation between anatomical structure and extent of shrinkage of wood. *Holzforschung*, Vol.31(6):194-200.
- Urakami, H. and M. Kuyuyama. 1981. The influence of specific gravity on thermal conductivity of wood. *Bull. Kyoto Prefect Univ. For.* Vol. 25:38-45.
- Van Dusen, M.S. 1920. The thermal conductivity of heat insulators. *J. Am. Soc. Heat. Vent. Eng.* Vol.26:625-656.
- Wangaard, F.F. 1940. Transverse heat conductivity of wood. *Heating, Piping and Air Conditioning*. Vol. 12:459-464.
- Wangaard, F.F. 1943. The effect of wood structure upon heat conductivity. *Transactions of the A.S.M.E.* February, 1943:127-135.
- Wangaard, F.F. 1969. Heat transmissivity of southern yellow pine wood, plywood, fiberboard, and particleboard. *Wood Science*. Vol.2(1):54-60.
- Ward, R.J. 1960. A dynamic method for determining specific heat and thermal conductivity of wood based materials as a function of temperature. Thesis. State University College of Forestry at Syracuse University, Syracuse, NY 12310.

Attachment 6

Energy Consumption Worksheet for single OSB Flake, 3 species

ENERGY WORKSHEET

Energy required to dry a single flake can be divided into two parts:

Total energy required (Q) = sensible heat (Q_s) + latent heat (Q_l)

1. Sensible heat (Q_s) is the energy required to change the temperature of the wood. It is expressed as:

$$Q_s = C_m W_o (1 + (IMC/100))(T_o - T_f)$$

where:

C_m is specific heat (kJ/kg*°C) = $0.268 + 0.0011 * T_{ave} + (IMC/100)/(0.239 * (1 + (IMC/100)))$

W_o is overdry weight (kg)

IMC is initial moisture content (%)

T_o is drying temperature (°C)

T_f is flake temperature (°C)

2. Latent heat (Q_l) is the energy required to change the phase of water inside wood expressed empirically as:

$$Q_l = W_o [Q_o ((IMC/100) - (FMC/100)) + 83.7 (\exp(-14 * (FMC/100)) - \exp(-14 * (IMC/100)))]$$

where:

Q_o is heat of vaporization (kJ/kg) = $3072 - (2.09 * T_o)$ Note: T_o in °K

IMC is initial moisture content (%)

FMC is final moisture content (%)

Computation of energy consumed in drying of a single flake:

$$\text{TOTAL ENERGY CONSUMED (Q)} = Q * T$$

where:

q is drying rate (W=J/sec)

t is drying time (sec)

Only convection is included in the computation. Radiation and other forms of energy consumption (air generation) are not included. Analysis was done on forced air convection on a flat plate.

$$q = hA (T_o - T_f)$$

$$h = \text{Nu} * k / L$$

$$\text{Nu} = 0.664 \text{Re}^{0.5} \text{Pr}^{0.33}$$

$$\text{Re} = \rho V L / \mu$$

$$\text{Pr} = C_p \mu / K$$

h is convection coefficient (W/m²*°K)

A is flake area (m²)

T_o is drying temperature (°C)

T_f is flake temperature (°C)

Nu is Nusselt number for a flat plate

Re is Reynolds number

ρ is air density (kg/m³)

V is air velocity (m/sec)

L is boundary length (m)

μ is air viscosity (N*s/m²)

Pr is Prandtl number

C_p is specific heat of air (J/kg*°C)

K is thermal conductivity of air (W/m*°C)

Southern yellow pine

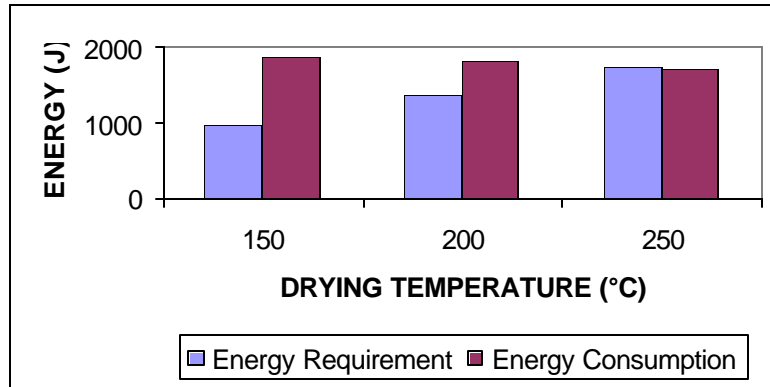
PARAMETER	SYMBOL	UNITS	TEMPERATURE LEVEL		
Drying Temperature	To	°C	150	200	250
Average Temperature	Tave	°C	83	108	133
Flake Temperature	Tf	°C	15	15	15
Initial MC	IMC	%	136	136	136
Final MC	FMC	%	0	0	0
Ovendry Weight	Wo	kg	0.001	0.001	0.001
Specific Heat	Cm	kJ/kg*°C	3	3	3
Heat of vaporization	Qo	kJ/kg	2188	2083	1979
Sensible Heat	Qs	J	971	1352	1744
Latent Heat	Ql	J	3	3	3
Energy Requirement	Q	J	974	1355	1747
PARAMETER	SYMBOL	UNITS	TEMPERATURE LEVEL		
Drying Temperature	To	°C	150	200	250
Flake Temperature	Tf	°C	15	15	15
Boundary Length	L	m	0.020	0.020	0.020
Boundary Width	W	m	0.135	0.135	0.135
Velocity	V	m/s	0.8	0.8	0.8
Density	p	kg/m ³	0.8264	0.7383	0.6672
Viscosity	u	N*s/m ²	2.40E-05	2.60E-05	2.79E-05
Reynolds Number	Re		551.9	455.0	383.3
Specific Heat	Cp	J/kg*°C	1017	1025	1035
Thermal conductivity	K	W/m*°C	0.0354	0.0389	0.0422
Prandtl Number	Pr		0.6883	0.6840	0.6831
Nusselt Number	Nu		13.79	12.50	11.46
Convection coefficient	h	W/m ² *K	24.4	24.3	24.2
Heat Rate	q	W	9	12	15
Drying Time	t	sec	210	150	112
Energy Consumption	Q	J	1868	1821	1719

Sweetgum

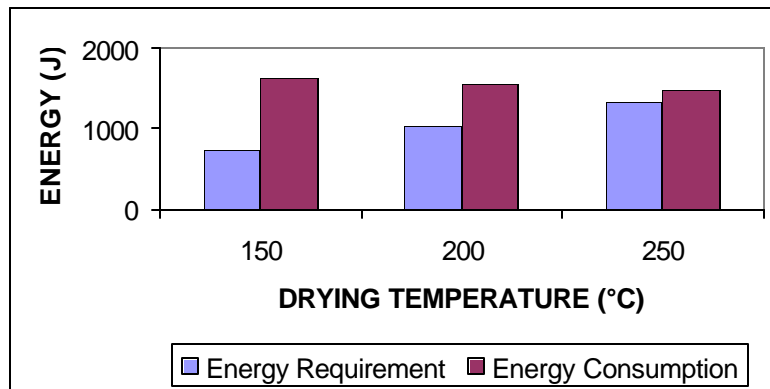
PARAMETER	SYMBOL	UNITS	TEMPERATURE LEVEL		
Drying Temperature	To	°C	150	200	250
Average Temperature	Tave	°C	83	108	133
Flake Temperature	Tf	°C	15	15	15
Initial MC	IMC	%	95	95	95
Final MC	FMC	%	0	0	0
Ovendry Weight	Wo	kg	0.001	0.001	0.001
Specific Heat	Cm	kJ/kg*°C	3	3	3
Heat of vaporization	Qo	kJ/kg	2188	2083	1979
Sensible Heat	Qs	J	739	1034	1341
Latent Heat	Ql	J	2	2	2
Energy Requirement	Q	J	741	1036	1343
PARAMETER	SYMBOL	UNITS	TEMPERATURE LEVEL		
Drying Temperature	To	°C	150	200	250
Flake Temperature	Tf	°C	15	15	15
Boundary Length	L	m	0.02	0.02	0.02
Boundary Width	W	m	0.135	0.135	0.135
Velocity	V	m/s	0.8	0.8	0.8
Density	p	kg/m ³	0.8264	0.7383	0.6672
Viscosity	u	N*s/m ²	2.40E-05	2.60E-05	2.79E-05
Reynolds Number	Re		551.9	455.0	383.3
Specific Heat	Cp	J/kg*°C	1017	1025	1035
Thermal conductivity	K	W/m*°C	0.0354	0.0389	0.0422
Prandtl Number	Pr		0.6883	0.6840	0.6831
Nusselt Number	Nu		13.79	12.50	11.46
Convection coefficient	h	W/m ² *K	24.4	24.3	24.2
Heat Rate	q	W	9	12	15
Drying Time	t	sec	184	128	96
Energy Consumption	Q	J	1637	1554	1473

Yellow-poplar

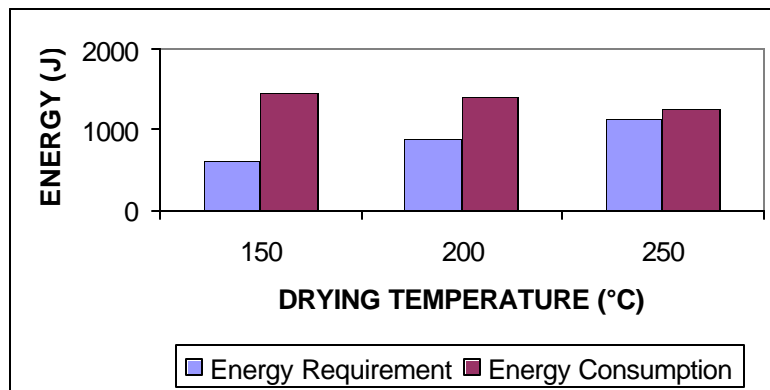
PARAMETER	SYMBOL	UNITS	TEMPERATURE LEVEL		
Drying Temperature	To	°C	150	200	250
Average Temperature	Tave	°C	83	108	133
Flake Temperature	Tf	°C	15	15	15
Initial MC	IMC	%	75	75	75
Final MC	FMC	%	0	0	0
Ovendry Weight	Wo	kg	0.001	0.001	0.001
Specific Heat	Cm	kJ/kg*°C	3	3	3
Heat of vaporization	Qo	kJ/kg	2188	2083	1979
Sensible Heat	Qs	J	626	880	1144
Latent Heat	Ql	J	2	2	2
Energy Requirement	Q	J	628	881	1146
PARAMETER	SYMBOL	UNITS	TEMPERATURE LEVEL		
Drying Temperature	To	°C	150	200	250
Flake Temperature	Tf	°C	15	15	15
Boundary Length	L	m	0.02	0.02	0.02
Boundary Width	W	m	0.135	0.135	0.135
Velocity	V	m/s	0.8	0.8	0.8
Density	p	kg/m ³	0.8264	0.7383	0.6672
Viscosity	u	N*s/m ²	2.40E-05	2.60E-05	2.79E-05
Reynolds Number	Re		551.9	455.0	383.3
Specific Heat	Cp	J/kg*°C	1017	1025	1035
Thermal conductivity	K	W/m*°C	0.0354	0.0389	0.0422
Prandtl Number	Pr		0.6883	0.6840	0.6831
Nusselt Number	Nu		13.79	12.50	11.46
Convection coefficient	h	W/m ² *K	24.4	24.3	24.2
Heat Rate	q	W	9	12	15
Drying Time	t	sec	165	115	82
Energy Consumption	Q	J	1468	1396	1258



southern yellow pine



sweetgum



yellow-poplar